REPORT DOCUMENTATION PAGE

READ INSTRUCTIONS BEFORE COMPLETING FORM

1. REPORT NUMBER: NAVENVPREDRSCHFAC Contractor Report CR 84-11
2. GOVT ACCESSION NO.:
3. RECIPIENT'S CATALOG NUMBER:

4. TITLE (and Subtitle): Characteristics of North Indian Ocean Tropical Cyclone Activity

5. TYPE OF REPORT & PERIOD COVERED: Final

6. PERFORMING ORG. REPORT NUMBER:

7. AUTHOR(s): Cheng-Shang Lee and William M. Gray

8. CONTRACT OR GRANT NUMBER(s): N00228-83-C-3122

9. PERFORMING ORGANIZATION NAME AND ADDRESS
Department of Atmospheric Science
Colorado State University
Fort Collins, CO 80523

10. PROGRAM ELEMENT, PROJECT, TASK AREA & WORK UNIT NUMBERS: PE 62759N NEPRF WU 6.2-22

11. CONTROLLING OFFICE NAME AND ADDRESS
Naval Air Systems Command
Department of the Navy
Washington, DC 20361

12. REPORT DATE: December 1984

13. NUMBER OF PAGES: 110

14. MONITORING AGENCY NAME & ADDRESS (if different from Controlling Office)
Naval Environmental Prediction Research Facility
Monterey, CA 93943-5106

15. SECURITY CLASS. (of this report): UNCLASSIFIED

15a. DECLASSIFICATION/DOWNGRADING SCHEDULE:

16. DISTRIBUTION STATEMENT (of this Report)

Approved for public release; distribution is unlimited.

17. DISTRIBUTION STATEMENT (of the abstract entered in Block 20, if different from Report)

18. SUPPLEMENTARY NOTES

19. KEY WORDS (Continue on reverse side if necessary and identify by block number)
North Indian Ocean
Tropical cyclone
Tropical cyclone climatology
Tropical cyclone structure

20. ABSTRACT (Continue on reverse side if necessary and identify by block number)

Characteristics of North Indian Ocean tropical cyclones are discussed from a combined climatological, composite, and individual-case perspective. Presented are both a general discussion of the monthly climatology of these spring/autumn tropical cyclones and a comparison of their structure, genesis, intensity, and movement with these qualities of northwest Pacific Ocean tropical cyclones.

((continued on reverse))

DD FORM 1 JAN 73 1473 EDITION OF 1 NOV 65 IS OBSOLETE
S/N 0102-014-6601

Block 20, Abstract, continued.

Detailed individual case analyses are made of each North Indian Ocean tropical cyclone that occurred during the First Global GARP Experiment (FGGE) period. Each tropical cyclone's characteristics from genesis to decay are discussed. All data sources of the FGGE year period were consulted, including the analysis of the European Centre for Medium Range Weather Forecasts (ECMWF).

AN (1) AD-A153 085
FG (2) 040200
CI (3) (U)
CA (6) COLORADO STATE UNIV FORT COLLINS DEPT OF ATMOSPHERIC SCIENCE
TI (6) Characteristics of North Indian Ocean Tropical Cyclone Activity.
TC (8) (U)
DN (9) Final contractor rept.,
AU (10) Lee,C. S.
AU (10) Gray,W. M.
RD (11) Dec 1984
PG (12) 114p
CT (15) N00228-83-C-3122
RN (18) NEPRF-CR-84-11
RC (20) Unclassified report
DE (25) *TROPICAL CYCLONES, INDIAN OCEAN, NORTH(DIRECTION), CLIMATE
DC (24) (U)
ID (25) FGGE(First Global GARP Experiment), PE62759N, WU6222
IC (26) (U)
AB (27) Characteristics of North Indian Ocean tropical cyclones are discussed from a combined climatological, composite, and individual-case perspective. Presented are both a general discussion of the monthly climatology of these spring/autumn tropical cyclones and a comparison of their strucutre, genesis, intensity, and movement with these qualities of northwest Pacific Ocean tropical cyclones. Detailed individual case analyses are made of each North Indian Ocean tropical cyclone that occurred during the First Global GARP Experiment (FGGE) period. Each tropical cyclone's characteristics from genesis to decay are discussed. All data sources of the FGGE year period were consulted, including the analysis of the European Centre for Medium Range Weather Forecasts (ECMWF).
AC (28) (U)
DL (33) 01
SE (34) F
CC (35) 088310

NAVENVPREDRSCHFAC
CONTRACTOR REPORT
CR 84-11

NAVENVPREDRSCHFAC CR 84-11

CHARACTERISTICS OF NORTH INDIAN OCEAN TROPICAL CYCLONE ACTIVITY

Prepared By:

Cheng-Shang Lee and William M. Gray
Colorado State University
Fort Collins, CO 80523

Contract No. N00228-83-C-3122

DECEMBER 1984

Prepared For:

NAVAL ENVIRONMENTAL PREDICTION RESEARCH FACILITY
MONTEREY, CALIFORNIA 93943-5106

TABLE OF CONTENTS

LIST OF ACRONYMS AND SYMBOLS

ATR	Annual Typhoon Report
ECMWF	European Center for Medium-range Weather Forecasts
FGGE	First Global GARP Experiment
ITCZ	Inter Tropical Convergence Zone
JTWC	Joint Typhoon Warning Center, Guam
NCAR	National Center for Atmospheric Research, Boulder, CO
NEPRF	Naval Environmental Prediction Research Facility
NHC	National Hurricane Center, Miami, FL
N.I.O.	North Indian Ocean
NOAA	National Oceanic and Atmospheric Administration
NMC	National Meteorological Center, Washington, D.C.
SMS	Synchronous Meteorological Satellite
V_t	tangential wind
V_r	radial wind
V_{max}	maximum low-level sustained wind in a cyclone
TC	tropical cyclone
$\bar{V}_t$	mean tangential wind at 6° radius about a tropical disturbance of storms between 1000-700 mb levels
$\bar{V}_r$	mean radius outflow at 6° radius about a tropical disturbance or storm between 150 and 250 mb

1. INTRODUCTION

Growing international tensions over the Arabian Sea shipping routes and the recent acceleration of US-Indian research activity on the Indian sub-continent monsoon circulations have heightened the interest in the characteristics of North Indian Ocean (N.I.O.) tropical cyclones. How do tropical cyclones of the N.I.O. compare with the tropical cyclones of other global basins as to their genesis, intensification, structure, movement, and decay characteristics? What influence do N.I.O. tropical cyclones have on the onset and retreat of the monsoon? These are difficult questions to answer because the tropical cyclones of this region have not been as well observed as the tropical cyclones of the northwest Pacific or those of the western Atlantic for the following reasons:

1. Although routinely done in the Atlantic and the northwest Pacific for the last 35 years, there have been no aircraft reconnaissance flights into N.I.O. tropical cyclones. To obtain intensity or maximum wind estimates of N.I.O. cyclones one must rely on the Dvorak (1975) satellite technique for estimation. Before the satellite era one estimated cyclone strength as best he could from the surrounding wind and surface pressure information. When the Dvorak scheme is used by inexperienced meteorologists and when cyclones have a-typical structural features that do not well fit the Dvorak intensity curve, this very excellent technique can lead to errors in estimates of maximum wind (as occurred when the

technique was tested in other ocean basins). In addition, as will be discussed later, a maximum wind determination in a cyclone may not be a very good estimate of the net damage or flooding potential of the cyclone. Damage and flooding can, in many instances, be more related to the cyclone's outer wind strength than to its maximum wind or minimum central pressure. Weatherford and Gray (1984) have recently been making special studies of the relationships between tropical cyclone intensity (maximum wind) and cyclone strength (mean tangential wind over $1-3^{\circ}$ radius about the cyclone) from analysis of western Pacific US Air Force weather reconnaissance flights. As will be discussed, we found that cyclone intensity and strength are often times not well related to each other.

Despite these difficulties, we have no other choice but to use the Dvorak satellite technique for an estimate of N.I.O. cyclone intensity. In a general sense, this technique, as it has been applied over the last 7-8 years, has proven itself to be quite reliable, especially in the qualitative sense concerning change in cyclone intensity.

2. Synchronous meteorological satellite (SMS) data have not been available over the Indian Ocean. In the Atlantic we have had SMS data since 1967 and in the western Pacific since 1978. SMS satellite data have been a very valuable source of tropical cyclone information. We are fortunate that SMS data were available for a portion of the FGGE year in which we analyzed individual N.I.O. tropical cyclones. This is one of the reasons we chose the FGGE year for our individual case tropical cyclone analysis.

3. Island and land stations to the equatorial side of tropical cyclones in the N.I.O are mostly absent as compared with the western Pacific and the western Atlantic. This hinders the proper analysis of Southern Hemisphere influences, which later in this study will be shown to be very important for the formation and/or intensity change of many N.I.O. tropical cyclones.

Although a number of climatological studies and other individual case studies of tropical cyclones in the N.I.O have been made, there have not been, to our knowledge, any comprehensive studies of the combined climatological, synoptic setting and structure of individual tropical cyclones in the region, or a comparison of N.I.O tropical cyclones with the better documented tropical cyclones of other ocean basins. This report attempts to make this more comprehensive study of N.I.O. tropical cyclones. We have made a detailed analysis of all the tropical cyclones that formed in the N.I.O. during the FGGE year. More reliable information exists on N.I.O cyclones during the 1979 FGGE year than at any other time because of the special observing systems and analysis procedures which were established for that year alone. This included the very unique and well archived European Center for Medium-Range Forecasts (ECMWF) FGGE year analysis of this region. We are also making much use of the ECMWF analysis to study tropical cyclones in the other global storm basins (see Lee, 1984; Chen and Gray, 1984; and Askue and Lee, 1984). We have found the ECMWF objective analysis to be very reliable and most useful for the understanding of tropical cyclones in the northwest Pacific and Atlantic. Comparisons using independent rawinsonde analysis (to be shown later) have shown the ECMWF analysis to

be quite reliable -- especially the large-scale rotational or tangential component of the wind fields and the general wind analyses at lower and upper tropospheric levels where SMS satellite wind vectors and/or aircraft data are available in large numbers.

This study does not treat the more numerous tropical depressions that form in the Bay of Bengal during the summer season (Saha et al., 1981).

We hope that this report will give the reader a better overall understanding of N.I.O. tropical cyclones that form almost exclusively in the late spring and autumn seasons.

We will first discuss the long-term climatology of N.I.O. tropical cyclones, then discuss the typical environmental flow features in which these cyclone systems typically form. A detailed analysis of each cyclone system by itself will then be given. We will also compare N.I.O. cyclones with northwest Pacific tropical cyclones and discuss the distinctive features of N.I.O. tropical cyclones.

2. TROPICAL CYCLONE CLIMATOLOGY

2.1 Yearly, Seasonal and Monthly Frequency

Unlike tropical cyclone formation in the other ocean basins tropical cyclones of the N.I.O. form in the late spring and autumn seasons. The summer is mostly devoid of tropical cyclones although many monsoon depressions form in the northern part of the Bay of Bengal during the summer period of June through September. But very few of these monsoon depressions ever intensify to cyclones of tropical storm strength. This report deals mainly with tropical cyclones that develop sustained low-level wind velocities and were reported as significant tropical cyclones by JTWC or Indian Meteorological Agency.

Table 1 gives a yearly listing of the number of N.I.O. tropical cyclones and hurricanes that have been reported since 1958. Generally, the yearly variation of cyclone number is not large. N.I.O. tropical cyclones represent about 7-8% of the 80 or so tropical cyclones and hurricanes that form per year about the globe. Figure 1 gives the tracks of N.I.O. tropical cyclones during the 10-year period of 1968-1977.

Earlier Climatology. A study by Bansal and Datta (1972) has shown that from 1891 to 1970 there were 362 cyclonic storms ($\geq$ 17 m/s) that originated in the Bay of Bengal, or about 4.5 storms per year. Another study by Mooley (1980) indicates 453 cyclonic storm systems in the 101-year period of 1877-1977. These figures are higher than that obtained

TABLE 1

Yearly number of reported tropical cyclones in the North Indian Ocean from Indian Meteorological Agency and JTWC.

Year	Number of reported tropical cyclones from Indian Meteorological Agency
1958	5
1959	6
1960	4
1961	6
1962	5
1963	6
1964	7
1965	6
1966	9
1967	6
1968	7
1969	6
1970	7
1971	6
1972	6
1973	6
1974	7
Average	6.2

Year	Number of reported tropical cyclones from JTWC ATR
1975	6
1976	5
1977	5
1978	4
1979	7
1980	2
1981	3
1982	5
1983	3
Average	4.4

from the JTWC ATR (Annual Typhoon Report) 1975-1983 average of 3.0 significant tropical cyclones per year in the Bay of Bengal. The differences between these figures appear to be due to the use of different data sources and the uncertainty in determining the cyclone intensity. The previous two studies utilized the data collected by the Indian Meteorological Agency, which uses different definitions for the intensity of tropical cyclones (see Table 2). On the other hand, JTWC uses different criteria for issuing tropical cyclone warning. For example, Typhoon Hope (1979) moved westward across the south China Sea and SE Asian Peninsula and into northeast Bay of Bengal in August, 1979.

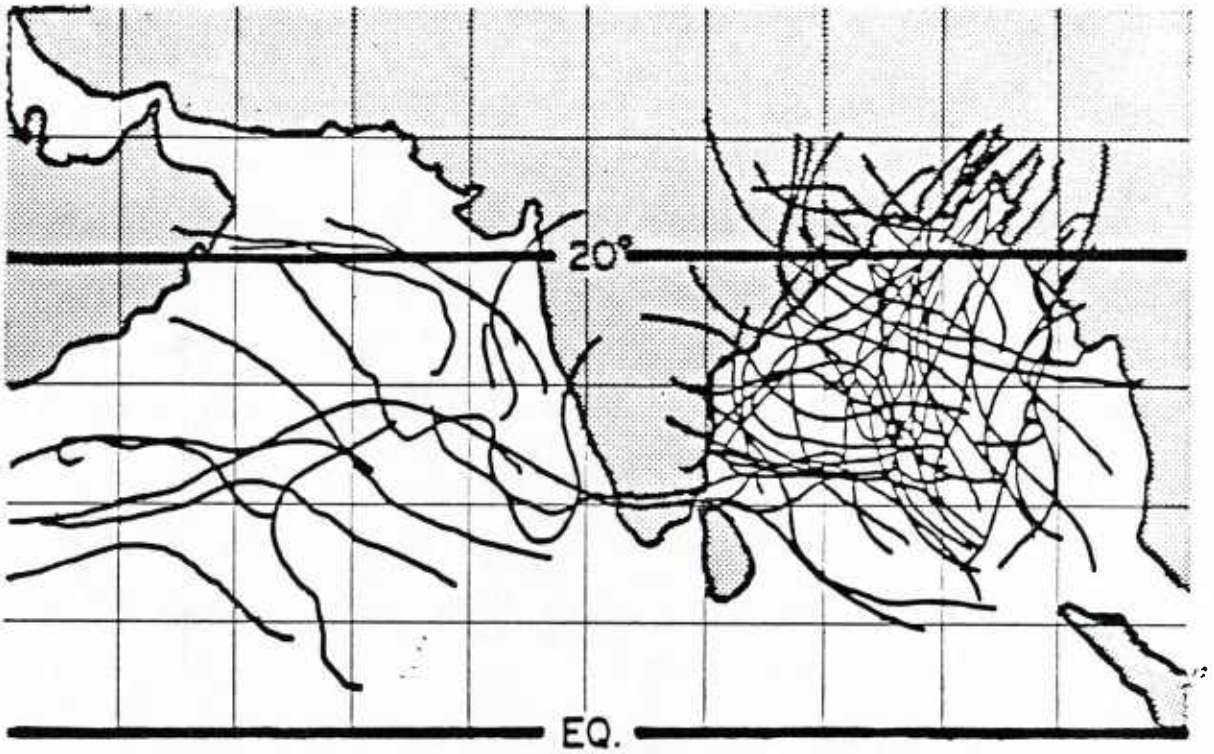

Fig. 1. Typical tropical cyclone tracks in the North Indian Ocean for the 10-year period 1968-1977.

TABLE 2

Indian Meteorological Department classification of tropical disturbances in the Bay of Bengal.

Classification	Range of Wind Speeds (m/s)
Low	< 8.5
Depression	8.5 - 13.5
Deep depression	14.0 - 16.5
Cyclonic Storm	17.0 - 23.5
Severe Cyclonic Storm	24.0 - 31.5
Severe Cyclonic Storm (Hurricane)	≥ 32

The JTWC ATR did not report it as a tropical cyclone in the N.I.O., but the Indian Meteorological Agency (as discussed by De Angelis, 1980c) did.

We believe that the Indian Meteorological Office sometimes listed Bay of Bengal monsoon disturbances as tropical cyclones when (by JTWC criteria) they were not. In other words, JTWC rarely warned on systems that originated in the northern Bay of Bengal and could possibly be interpreted as monsoon depressions. A comparison of the monthly frequencies of tropical cyclones reported by JTWC and the Indian Meteorological Agency (Tables 3 and 5) reveal that the largest difference occurs during summer (June-August) or the most active period for monsoon depression.

Bansal and Datta's (1972) tabulations indicated that there were 98 cyclonic storms in the Arabian Sea region during the 80-year period of 1891-1970. The average number was 1.2 storms per year. This is not much different from the recent year value of 1.4 cyclones per year which have occurred over the last nine years (as monitored by JTWC). The difference between the number of tropical cyclones in the Bay of Bengal and Arabian Sea by Bansal and Datta's estimate was 3.75 to 1. Recent year information places the figure at about 2 to 1. These differences are due to the new case count of tropical cyclones in the Bay of Bengal being decreased.

Among the 362 cyclonic storms (or systems with $V_{max} \geq 17$ m/s) in the Bay of Bengal as listed by Bansal and Datta, 132 or 36% were reported to be of severe cyclonic storm strength ($V_{max} \geq 24$ m/s). In the Arabian Sea 53 of 98 or 54% were so classified. These numbers agree qualitatively with those reported by JTWC, in terms of the numbers,

Arabian Sea tropical cyclones (although fewer in number) are, in general, somewhat stronger than Bay of Bengal tropical cyclones.

Table 3 gives a summary by month of the distribution of tropical cyclones ($V_{max} \geq 17$ m/s, and $V_{max} \geq 24$ m/s), in the N.I.O. during this 80-year period. November and October are the most active and second most active tropical cyclone months in both the Bay of Bengal and Arabian Sea. May is the second most active month for the more intense Arabian Sea cyclones, however. The large numbers of storm systems in the Bay of Bengal in July and August are believed by us to be mostly monsoon depressions that occurred in the northern Bay of Bengal.

TABLE 3

Number of cyclonic storms in the N.I.O. during 1891-1970 with intensity ($V_{max} > 17$ m/s) and the number (in parentheses) that were estimated to be severe storms ($V_{max} > 24$ m/s). Data from Bansal and Datta, 1972.

	JAN	FEB	MAR	APR	MAY	JUN	JUL	AUG	SEP	OCT	NOV	DEC	TOTAL
Bay of Bengal													
All Storms	5	1	4	19	39	35	38	26	32	62	68	34	362
(Severe Storms)	(2)	(1)	(2)	(8)	(26)	(4)	(7)	(1)	(10)	(26)	(32)	(13)	(132) (36%)*
Yearly Average of All Storms	0.1	0.0	0.1	0.2	0.5	0.4	0.5	0.3	0.4	0.8	0.9	0.4	4.5
Arabian Sea													
All Storms	2	0	0	5	16	15	3	2	5	19	26	5	98
(Severe Storms)	(0)	(0)	(0)	(4)	(13)	(9)	(0)	(0)	(1)	(7)	(18)	(1)	(53) (54%)*
Yearly Average of All Storms	0.0	0.0	0.0	0.1	0.2	0.2	0.0	0.0	0.1	0.2	0.3	0.1	1.2

*Percentage of the number of all storms that are severe.

In the Arabian Sea regions, only 5 systems formed in the July-August period and none of them attained severe storm intensity. In the spring active period (April-June), only 28% of the storm systems reported by Bansal and Datta (36 out of 129) formed in Arabian Sea region. But of this 28% of systems which formed in the Arabian Sea, 72% (or 26 out of 36) attained severe cyclonic storm intensity. A summary of storm numbers during these two active seasonal periods in both basins is shown in Table 4. It is also interesting to note that depressions can form in the Bay of Bengal in almost every month but only those depressions that form in the active monsoon transitional periods intensify into severe storms and hurricanes.

TABLE 4

Number of tropical storms (1891-1970) during each of the two active season periods and the percent that are severe cyclonic storms (i.e., systems of tropical cyclone or greater intensity).

	Apr-Jun	Sep-Dec
Bay of Bengal		
All Cyclones (V_{max} > 17 m/s)	93	196
All Cyclones (V_{max} > 24 m/s)	38 (41%)	111 (57%)
Arabian Sea		
All Cyclones (V_{max} > 17 m/s)	36	55
All Cyclones (V_{max} > 24 m/s)	26 (72%)	27 (49%)

Figure 2 shows, by three month intervals, 20 years of origin points of significant tropical cyclones. Note the concentration of formation in the spring (April-May-June) and autumn (October-November-December) months. In comparison with the western North Pacific region, the N.I.O. has as high or higher number of tropical cyclone formations per unit

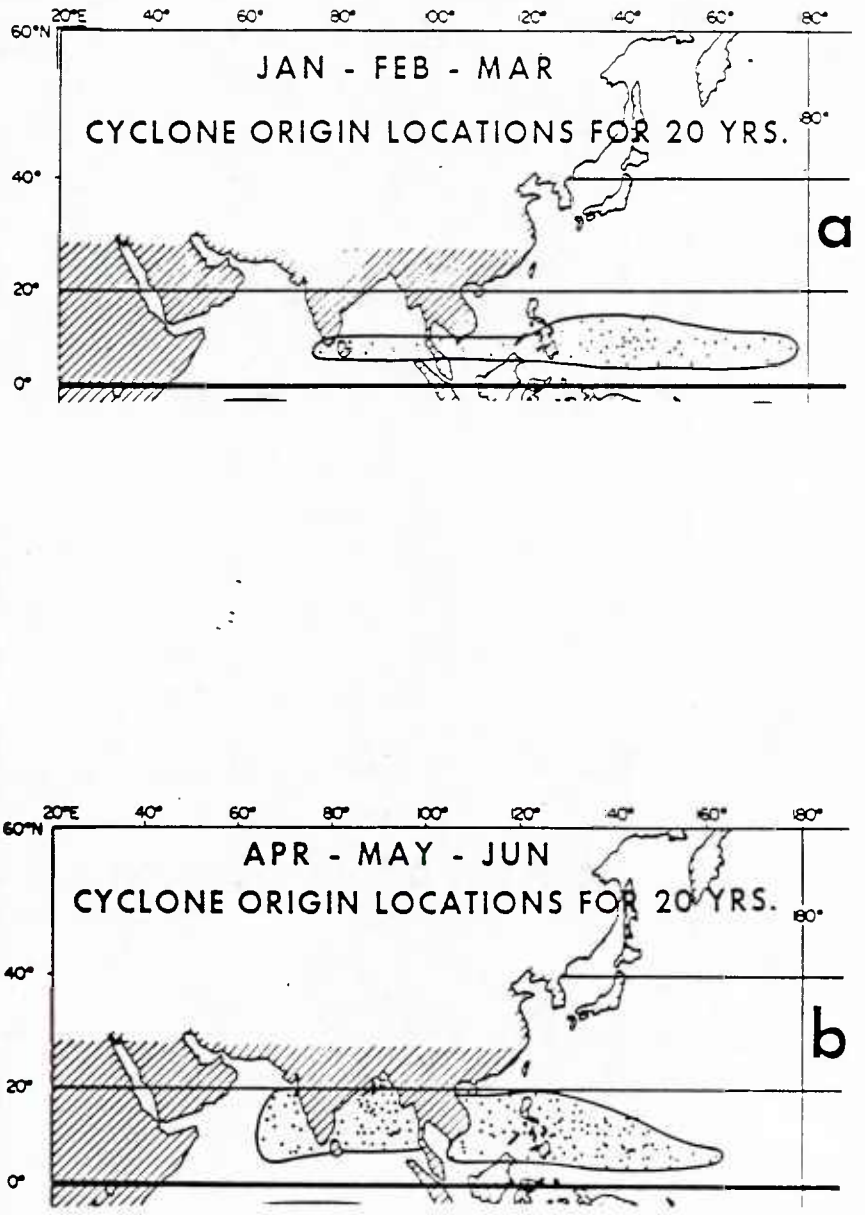

Fig. 2. Origin points by three month intervals for a 20-year period of significant tropical cyclones. Some of the original locations in the northern Bay of Bengal during July-August-September can be classified as monsoon depressions.

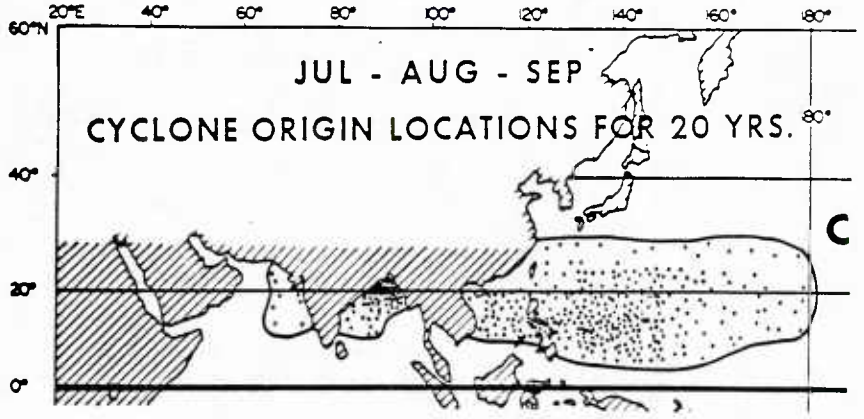

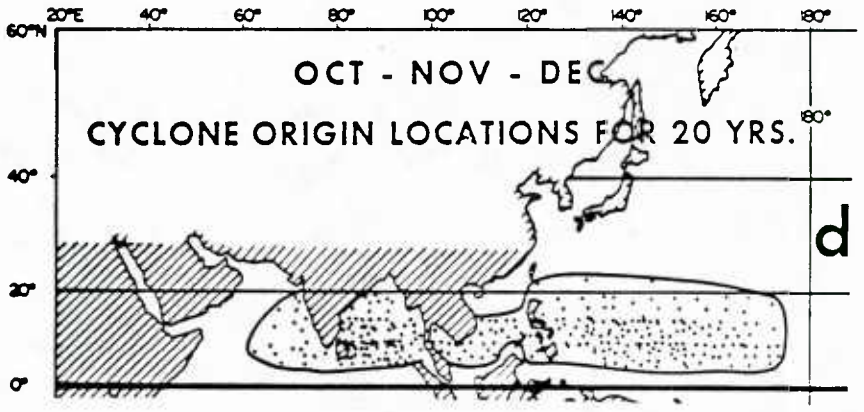

Fig. 2. Continued.

area as the Pacific. Differences in total numbers of storms are more a result of the larger Pacific formation area.

N.I.O. Tropical Cyclones Monitored by JTWC in Recent Years. Before 1974 the Guam Joint Typhoon Warning Center (JTWC) area of responsibility did not include the Arabian Sea region. Valid statistics using satellite information and the Dvorak intensity classification (1975) are available only since 1975. By JTWC standards, using the Dvorak classification scheme, the number of tropical cyclones in the N.I.O. is about 4.4 per year. This is about 1.3 fewer storms per year than indicated by previous Indian estimates. This is, as has been discussed, a consequence of the Indian Meteorological Agency classifying quite a few monsoon depressions as cyclone systems during the summer period.

Table 5 shows the number of tropical cyclones that occurred in each month during this nine year period (1975-1983). The second line lists the yearly averaged number of tropical cyclones in each month. As expected the autumn transition season was the most active period for tropical cyclone formation.

TABLE 5

Comparison of the number of significant tropical cyclones during 1979 with the number of tropical cyclones during the 9-year period 1975-1983 as determined by the JTWC.

	JAN	FEB	MAR	APR	MAY	JUN	JUL	AUG	SEP	OCT	NOV	DEC	TOTAL
North Indian Ocean													
All Tropical Cyclones In 1979	-	-	-	-	1	1	-	-	2	1	2	-	7
1975-1983													
Cases	1	-	-	1	6	4	-	1	3	9	12	3	40
Average	.1	-	-	.1	0.7	0.4	-	0.1	0.3	1.0	1.3	0.3	4.4

Among these 40 systems of tropical cyclones, 27 or about two-thirds formed in the Bay of Bengal region and 13 (or one-third) in the Arabian Sea. Two systems formed in the Bay of Bengal but traveled into the Arabian Sea and maintained their tropical storm intensity (maximum sustained winds $\geq$ 35 kts) in both basins. Among the 27 tropical cyclones that formed in the Bay of Bengal, 6 (or 22%) were estimated to have attained typhoon intensity ($\geq$ 65 kts). The average maximum intensity of these 27 Bay of Bengal tropical cyclones was 56 kts. In the Arabian sea region, 4 of the 13 tropical cyclones (or 31%) attained typhoon intensity. Their average maximum wind speed was 60 kts. There was about a two to one difference in the number of tropical cyclones that formed in the Bay of Bengal in comparison with the Arabian Sea. This is in general agreement with previous estimates. A higher percentage of Arabian Sea tropical cyclones appear to form in the spring period as compared with the Bay of Bengal. And a slightly higher percentage of the cyclones that form in the Arabian Sea reach hurricane intensity.

2.2 Favorable Environmental Setting for Cyclone Formation

We will now discuss the climatology of the general environmental setting in which tropical cyclones can form in the N.I.O.

Sea-Surface Temperature and Ocean Energy Contents. Warm ocean temperatures and the depth to which this warm ocean water penetrates into the N.I.O. are quite substantial in all seasons. These warm ocean temperatures are a necessary ingredient to tropical cyclone formation. Provided that wind and other dynamic factors are satisfactory, tropical cyclone formation (at least from an ocean energy point-of-view) can occur in any month in the N.I.O.

Figures 3 and 4 show seasonal values of these parameters. Note how the 28°C sea-surface temperature and ocean temperature above 26°C extends down to below 60 meters depth in all seasons in the southern half of both the Bay of Bengal and in the Arabian Sea. Tropical cyclone formation requires that ocean temperatures be above 26°C and that warm temperatures extend to a depth of 50-100 meters or so.

The lack of tropical cyclones in the N.I.O. during the summer season is due to dynamical processes asscciated with the shift of the monsoon trough to northern India, not to any reduction in ocean energy content.

Seasonal Cyclone Frequency Related to Seasonal Climatology. As previously discussed by the second author (Gray, 1975, 1979) long-term seasonal tropical cyclone genesis frequency (in all the global basins) is closely related to a combination of six seasonal meteorological features which will henceforth be referred to as primary climatological genesis parameters. These seasonal parameters are:

(1) low-level relative vorticity (ζ_r),
(2) Coriolis parameter (f),
(3) the inverse of the tropospheric vertical wind shear (S_z) of the horizontal wind between the lower and upper troposphere or ($1/S_z$),
(4) 'ocean thermal energy' - integrated sea temperature excess above 26°C to a depth of 60 m (E),
(5) vertical gradient of θ_e between the surface and 500 mb ($\partial\theta_e/\partial p$),
(6) middle troposphere relative humidity (RH).

A tropical cyclone Seasonal Genesis Index (SGP) can be defined as:

SGP = [(vorticity) x (Coriolis) x (vertical shear) parameters] x
[(ocean energy) x (moist stability) x (humidity) parameters] (1)

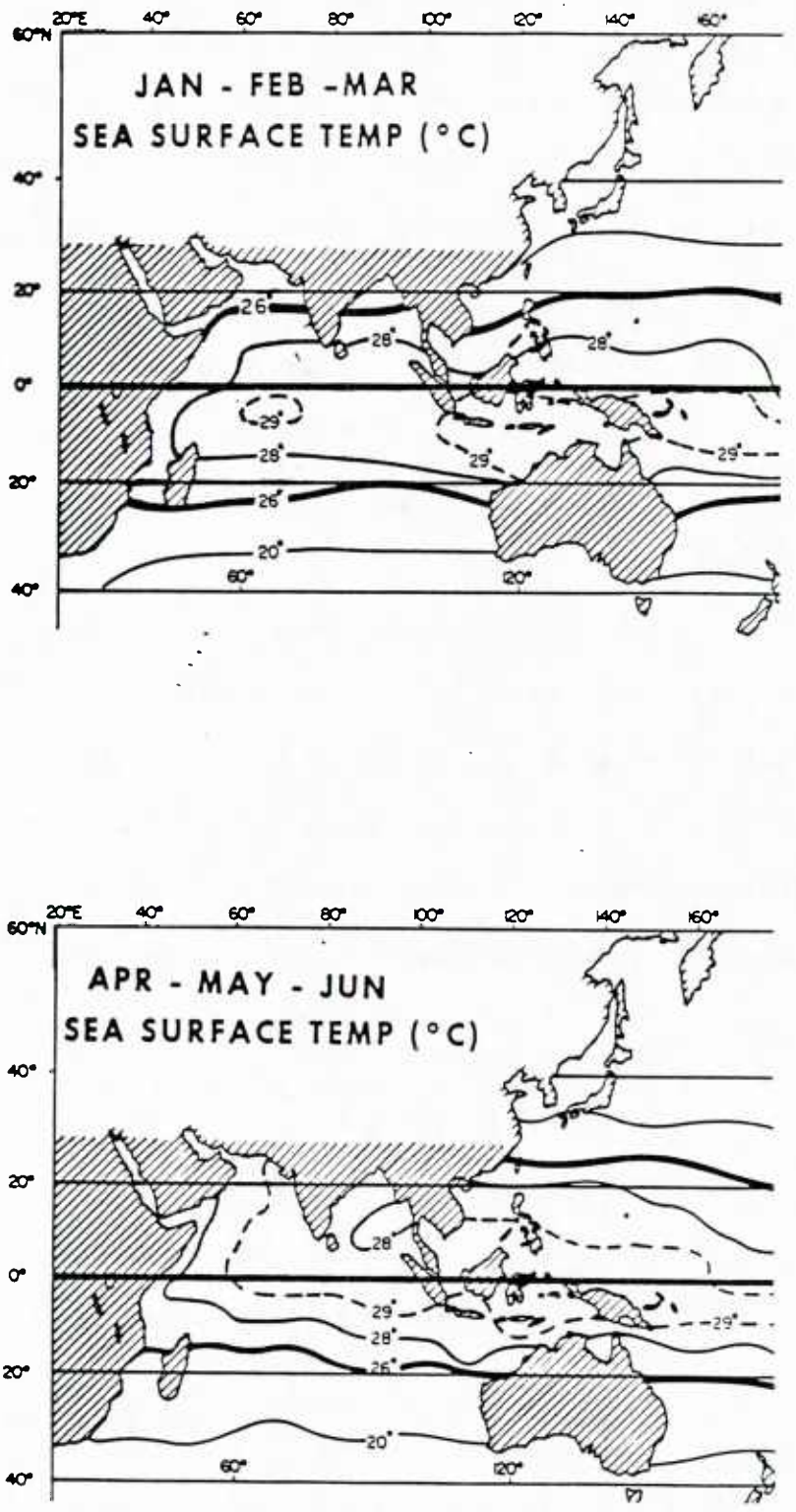

Fig. 3. Seasonal sea surface temperature over the Indian Ocean.

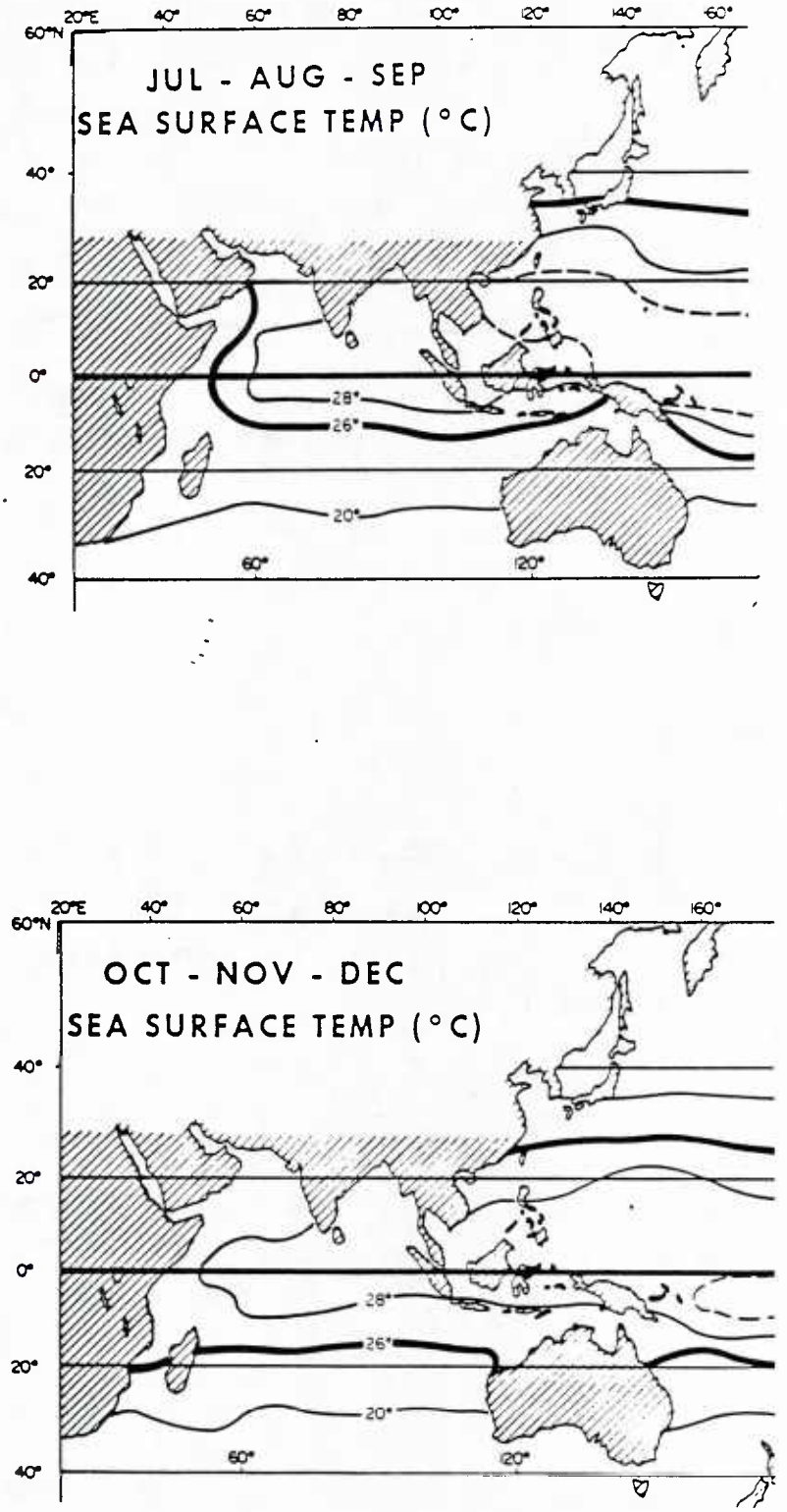

Fig. 3. Continued.

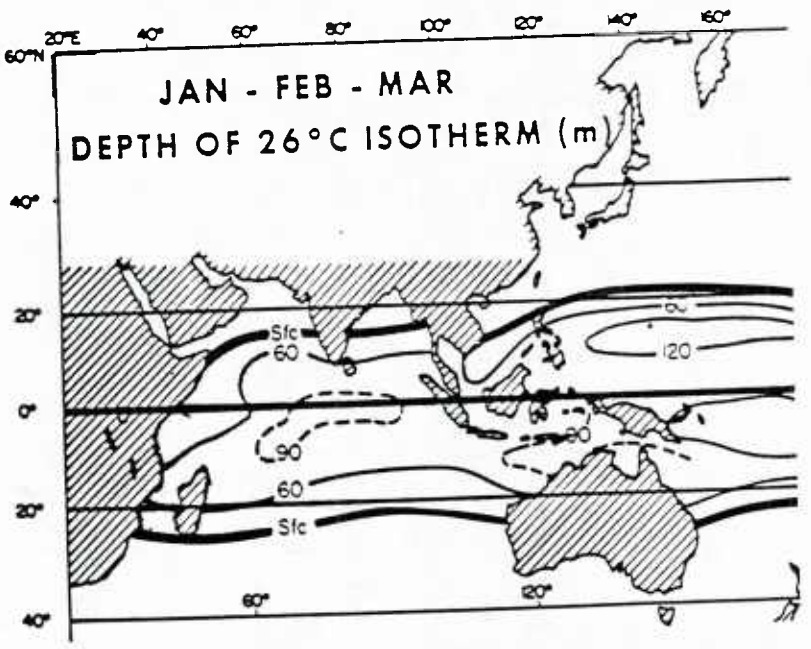

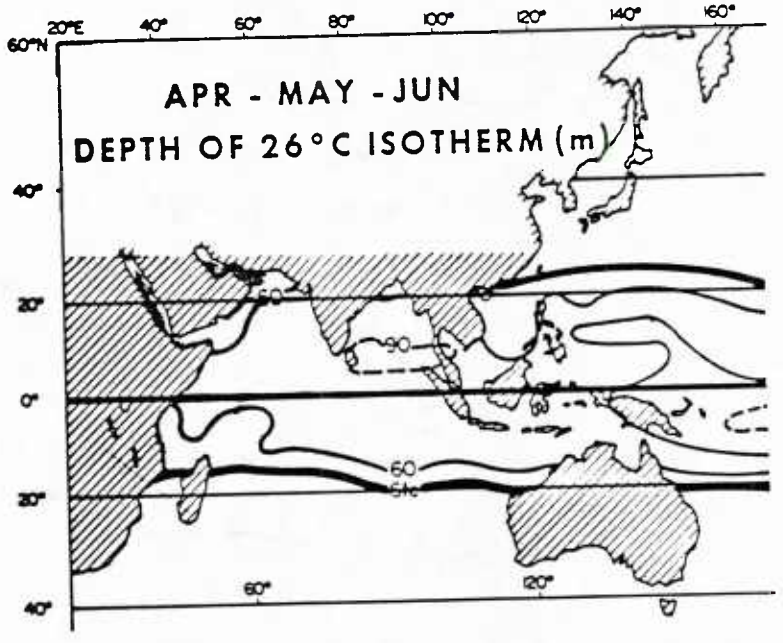

Fig. 4. Depth (in meters) of the 26° isotherm over the Indian Ocean by season.

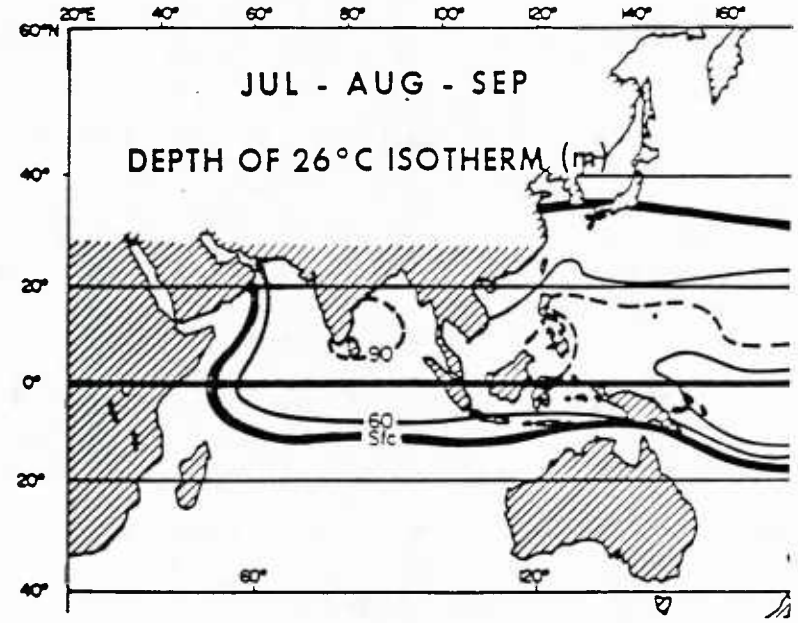

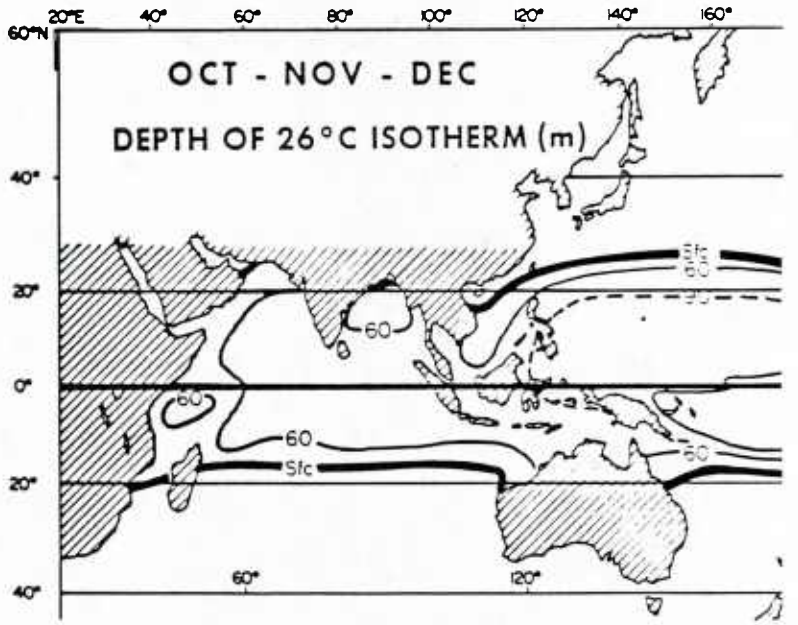

Fig. 4. Continued.

This seasonal tropical cyclone Genesis Index may also be thought of as in the form:

SGP = (dynamical potential) x (thermal potential).

where

dynamic potential = [(vorticity)x(Coriolis)x(vertical shear) parameters]

thermal potential = [(ocean energy)x(moist stability)x(humidity) parameters]

The product of dynamic potential and thermal potential is defined as the Seasonal Genesis Index. When expressed in this way with the proper units (see original papers) this SGP gives a very good estimate of the seasonal tropical cyclone genesis frequency in number per 5° latitude-longitude square per 20 years in all seasons and at all global locations.

The very close correspondence between predicted and observed seasonal cyclone frequency lends support to this argument concerning the relevant seasonal climatological factors which are necessary for cyclone genesis.

Figures 5 and 6 show these dynamic and seasonal potentials and their product (the Seasonal Genesis Parameter) for the spring and autumn periods of major cyclone formation. The bottom diagram in both of these figures shows the observed number of tropical cyclone formations per 5° latitude-longitude square per 20 years. This is to be compared with the third figure from the top.

It is seen how closely the seasonal climatology of these six parameters dictates the number of cyclones which form in the N.I.O. even though the days of cyclone genesis (1-15 per 5° square per 20 years)

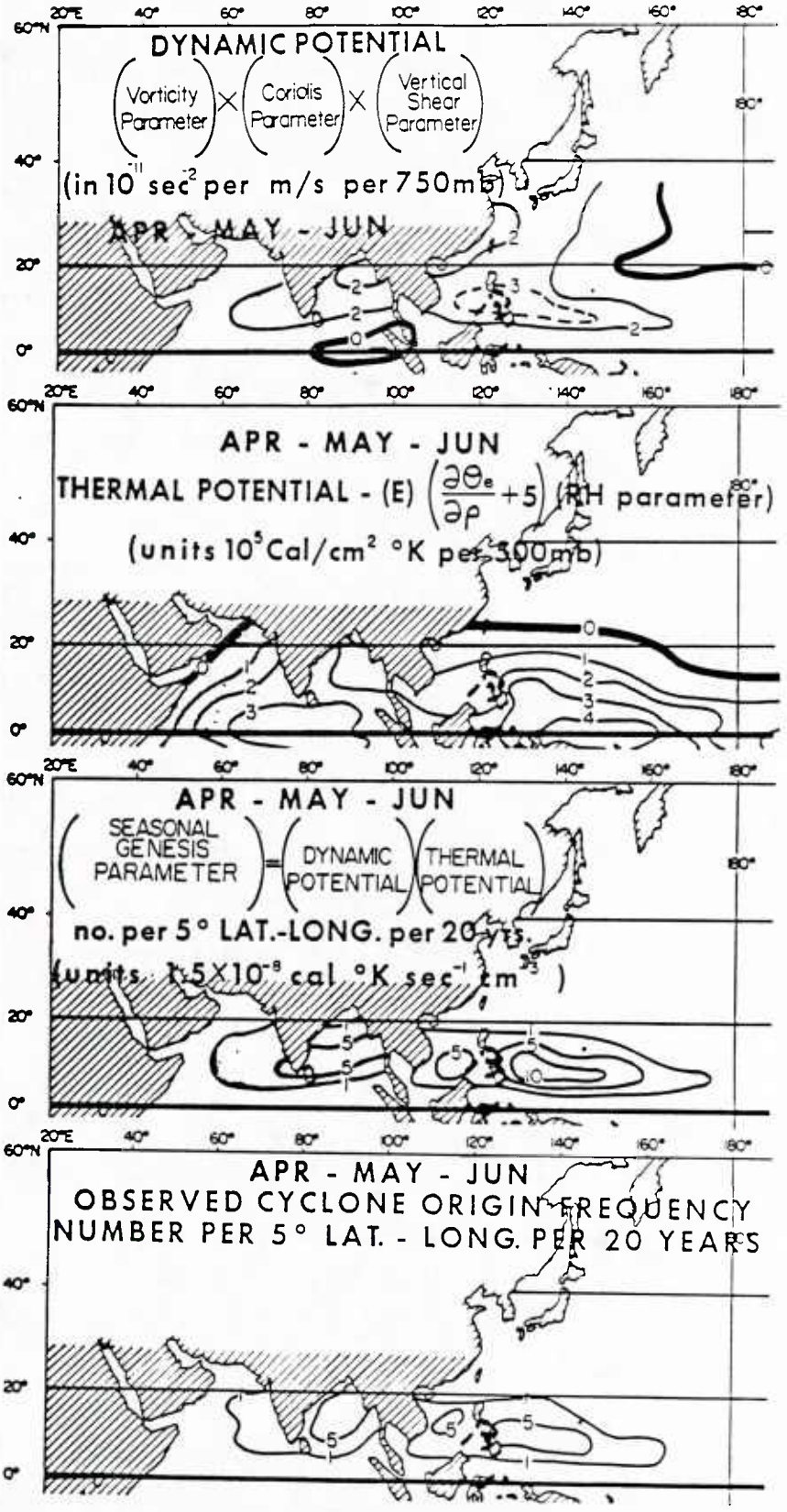

Fig. 5. North Indian Ocean April to June Dynamic and Thermal potentials. Seasonal Genesis Parameter and observed number of tropical cyclone formations per 5° latitude-longitude square per 20 years.

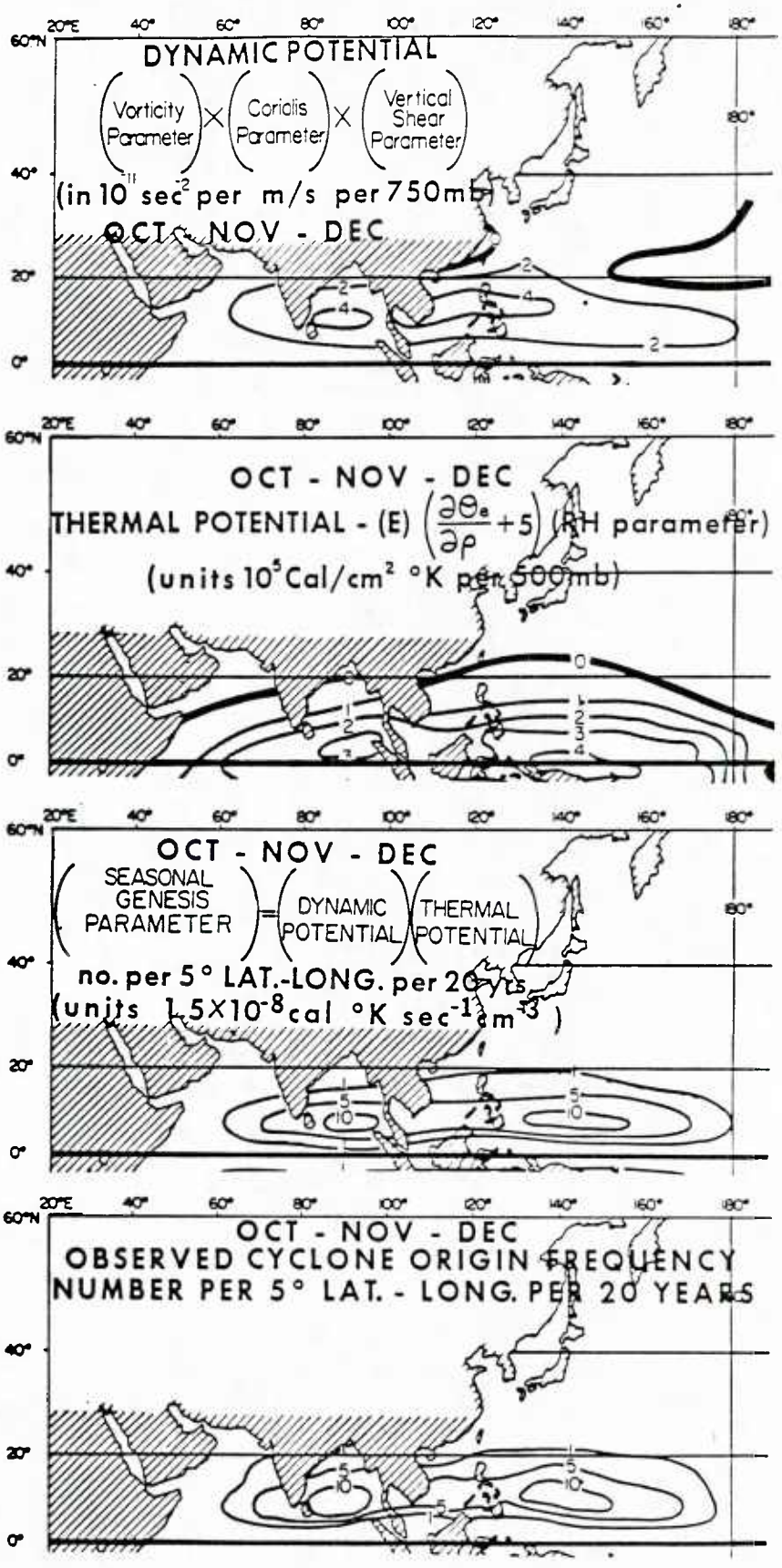

Fig. 6. Same as Fig. 5 but for October to December.

make up but a very small percentage of the season. It was not expected that the agreement between predicted and observed genesis frequencies would be this close. Not only is the correlation of the six seasonal parameters with genesis frequency noteworthy, but the physical rationale concerning the effects of these parameters which also is important. There is thus some rational quantitative explanation as to why the long-term frequency of tropical cyclones in the N.I.O. is as observed.

The N.I.O. thermal potential changes little during the spring and autumn seasons. It is mainly the day-to-day variations in the dynamic potential that must be watched for in predicting the day-to-day potential for cyclone formation. This is mostly determined by the strength and location of the monsoon trough. The presence of the monsoon trough between 5-15^{o}N latitude assures that upper tropospheric winds will be such that easterly zonal winds will prevail equatorwards of the monsoon trough and westerly zonal winds on the poleward side of the trough.

3. SYNOPTIC ENVIRONMENT IN WHICH NORTH INDIAN OCEAN TROPICAL CYCLONES FORM

Tropical storms form in the monsoon transitional seasons of spring and autumn in the N.I.O. because it is only during these periods that the monsoon trough is located sufficiently south (~ 5-15°N) that a broad oceanic area is available for cyclone development. During the summer periods of late June through early September, the monsoon trough is typically located over the Ganges Valley and at the head of the Bay of Bengal. Vertical wind shear over the Bay of Bengal and Arabian Sea are too strong to permit tropical cyclones in these seasons. As discussed by the second author (Gray, 1968, 1975), tropical storms form only when the tropospheric vertical wind shear over the incipient disturbance is very weak. Such small wind shear conditions typically occur only during the monsoon transitional periods of late April through June, and late September through early December. It is at these times that the tropospheric vertical shear of zonal wind (U) or $(U_{200mb}-U_{850mb})$ 10° to the poleward side of the monsoon trough is strongly positive while 10° to the equatorwards side this shear is strongly negative. The change of sign of this tropospheric zonal wind shear from south to north assures that a region of zero or minimum shear exist near the monsoon trough axis.

Figure 7 shows the type of tropospheric vertical wind shear conditions required for tropical cyclone formation in the N.I.O. $U_{200mb}-U_{850mb}$ must change sign as one proceeds northward from the equatorward to the poleward side of the monsoon trough. The greater the

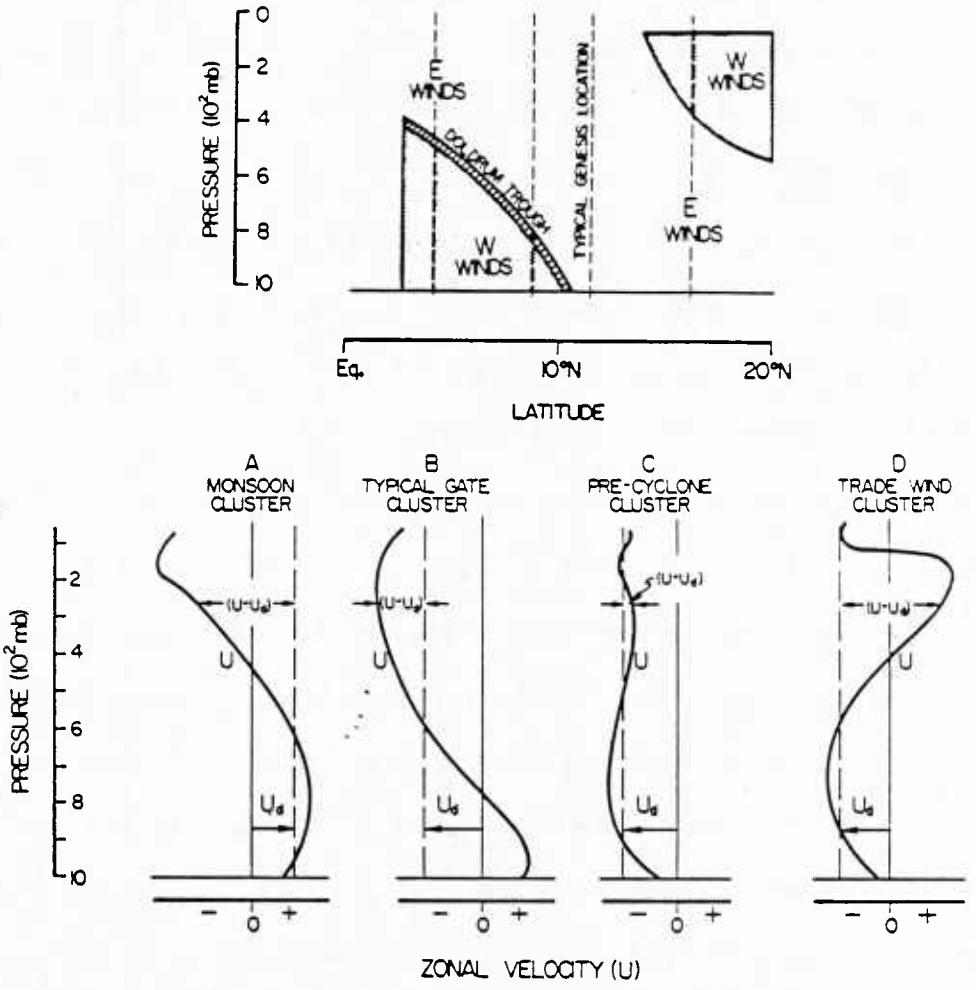

Fig. 7. North-south cross sections of the typical locations of various classes of tropical cloud clusters relative to the monsoon trough, and the usual zonal winds present with these systems (top diagram). The bottom diagram portrays the vertical distribution of typical zonal wind velocity, U, occurring with different, A to D, types of cloud clusters whose general location is specified in the top diagram. The usual zonal distribution or cluster velocity is designated U_d and the difference in cloud cluster and environmental wind velocity at any level is given by $U-U_d$.

magnitudes of 200 to 850 mb zonal wind shear at points B and D (as indicated in both figures) the greater is the strength of the monsoon trough and the greater is the potential for cyclone formation. Tropical cyclones, in general, do not form in weak monsoon trough conditions or when wind shear conditions at points B and D are weaker than normal.

As will be discussed in Chapter 6, all seven tropical systems that developed in the N.I.O during the 1979 FGGE year exhibited this type of vertical wind shear about the monsoon trough. In general, the potential for tropical cyclone formation increases the larger the tropospheric vertical wind shear is about 6^{o} north and about 6^{o} south of the incipient disturbance. See previous CSU research by McBride, 1981; McBride and Zehr, 1981 for more discussion of this genesis criterion. This criterion implies that the vertical gradient of vorticity between 850 mb and 200 mb around the incipient pre-cyclone disturbance at 6^{o} radius be as negative as possible. The more negative this value is, the higher the potential for cyclone development. The most important ingredient for tropical cyclone development is not just the amount and intensity of Cb convection associated with the tropical disturbance, but rather the existence of the tropical disturbance in a favorable strong monsoon trough environment. If the surrounding environmental wind conditions through the troposphere are not favorable then tropical cyclone formation will almost never take place irrespective of the amount and intensity of deep convection currently occurring.

Figures 8 and 9 show a composite of the 850 mb and 200 mb zonal wind patterns surrounding the initial location positions of 54 N.I.O. tropical disturbances which later developed into tropical cyclones. Note that the 850 mb westerly winds south of these disturbances are typically stronger than the trade winds to the north. Also note that 200 mb easterly winds are blowing over the disturbance center. Figure 10 shows the composite of 850 mb to 200 mb zonal wind shear patterns surrounding these pre-tropical storm cases. Note the westerly tropospheric wind shear to the north and the easterly tropospheric wind

shear to the south of these early stage developing systems. Also the near zero zonal wind shear near the center of these early stage developing systems.

These are very typical of the lower and upper tropospheric wind patterns which are associated with tropical cyclones which develop within the monsoon trough in this and at other global locations (Gray, 1968; Holland, 1984a,b,c).

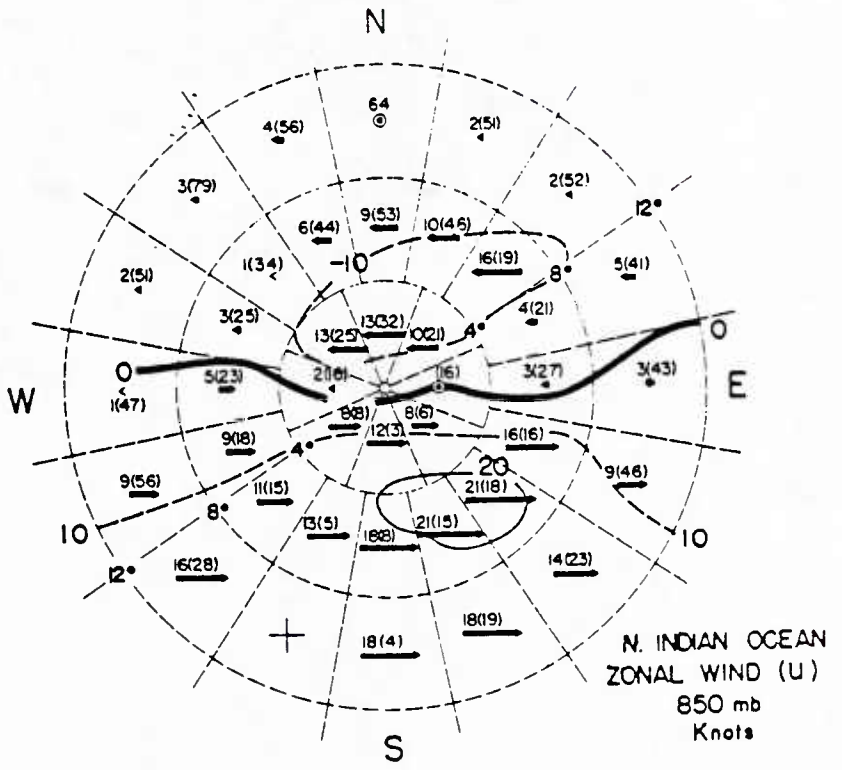

Fig. 8. Composite of average rawinsonde information in each area relative to the initial center positions of 54 tropical disturbances which later developed into tropical storms between 1955 and 1966. Length of arrows is proportional to wind speed in knots (at left). Values in parentheses are number of wind reports in each area average. Distance from the center is given by the lightly dashed circular lines at 4^{o} latitude increments (from Gray, 1968).

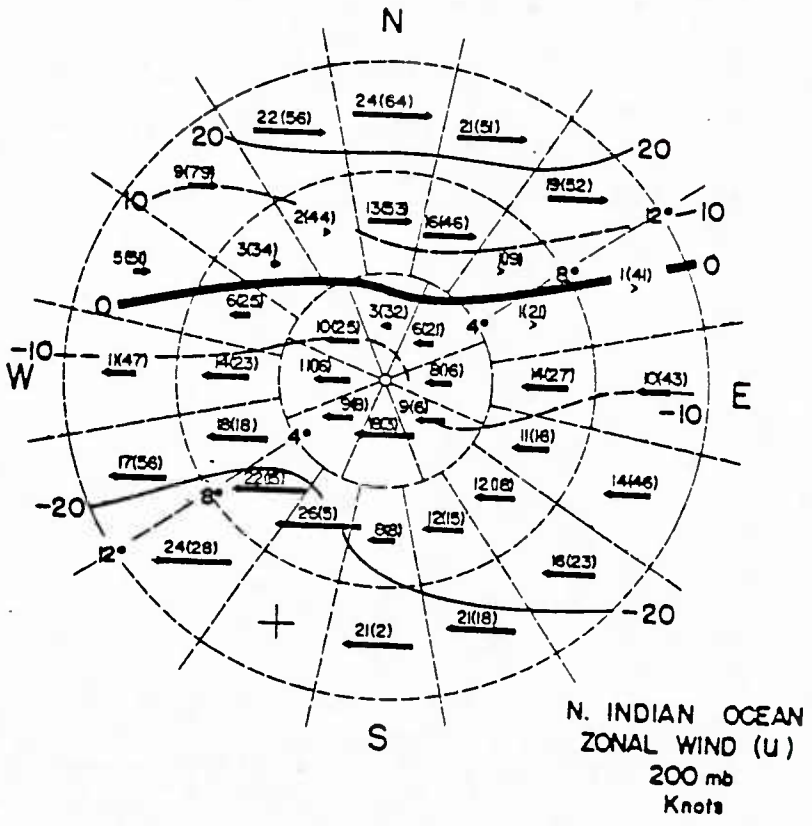

Fig. 9. Same as Fig. 8 but for the 200 mb level.

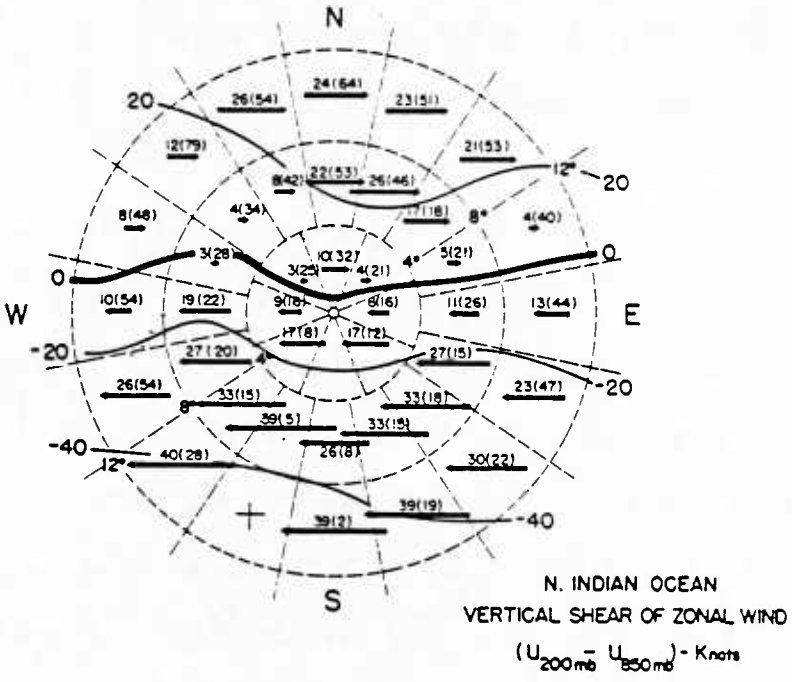

Fig. 10. Same as Fig. 8 but for the 200 mb minus 850 mb shear of zonal wind.

4. DATA SOURCES FOR CASE STUDY ANALYSIS AND CYCLONE STRUCTURAL DEFINITIONS

The data sources used in this study's analysis of individual N.I.O. tropical cyclones are the FGGE III-b data of the European Center for Medium-Range Weather Forecasts (ECMWF) and the National Oceanic and Atmospheric Administration (NOAA) polar-orbiting satellite (TIROS) picture. These satellite imageries are available on mosaics twice a day in both IR and visible images for most of the days during the period that tropical cyclones were present. The Annual Typhoon Report (ATR) published by the Joint Typhoon Warning Center (JTWC), Guam was used to determine the position and the intensity of our tropical cyclone cases. A supplementary data source was the flow features and satellite pictures during the summer MONEX (Quick look ''Summer MONEX Atlas'', Part I Saudi Arabia phase) edited by Florida State University (Krishnamurti, et al., 1980). These data are used for TC 17-79 (the most intense of the North Indian Ocean systems) because of the missing TIROS data during this time period.

The FGGE III-b data are available on plotted and analyzed charts in book form published by ECMWF in 1981 and on larger maps which were specially duplicated and purchased from the ECMWF facility. The original FGGE III-b data are also available on 1.875 degree latitude/longitude cartesian grids at 15 pressure levels. These data, including zonal and meridional wind (U,V), height, temperature, vertical motion, and specific humidity, are packed and contained in 82 Terabit

Memory volumes at the National Center for Atmospheric Research (NCAR). Full utilization was made of these archived data sources.

The FGGE level III-b data used in this study are the raw initial values of the horizontal zonal and meridional components. These data were extracted directly from the initial analysis of the pressure levels. They have not been subjected to any vertical interpolation. The analysis procedure used a primitive equation forecast for the first guess, but after the initial analysis step, no model initialization took place. For a complete description of the ECMWF analyzed FGGE III-b data, please refer to the FGGE data management manuals or the FGGE newsletter No. 1 (May, 1983).

For tropical cyclone studies, a cylindrical coordinate system is preferable. The FGGE data, which were initially on cartesian grids, have been linearly interpolated onto cylindrical grids. There are 13 radial and 16 azimuthal grid segments. The grid spacing is 1° latitude radius (starting from 2° out from the cyclone center) and 22.5° azimuth. The cylindrical grid point data of zonal and meridional wind components (U, V) are converted to radial and tangential wind components (V_r, V_t) with respect to the cyclone center. The radial wind is then mass balanced vertically from 100 mb to 1000 mb at every radius. The pressure levels used in this study are 100, 150, 200, 250, 300, 400, 500, 700, 850, and 1000 mb. However, due to their better quality, the low-level and upper-level data are more extensively used. (There are many more surface observations than there are rawinsonde data. Many satellite winds are used in the analysis).

By comparing the FGGE analysis with our independent rawinsonde data, Lee (1984) has previously shown that the FGGE data can reasonably

well represent the tropical cyclone circulation, especially beyond the 4-5° radius.

Layer Considerations. We have made much use of the ECMWF analysis of the outflow layers of those cyclone systems. This analysis was based on the combined satellite, rawinsonde and aircraft jet wind vectors taken during the FGGE year. Due to the uncertainty of the height of the satellite cloud vector wind, we considered it to be more appropriate to average the 150 mb, 200 mb (weighted by a factor of 2) and 250 mb wind vectors together to represent the upper level flow. This is an important thing to do because of different heights of the maximum outflow. Equatorial outflow layers are typically 25-50 mb higher than poleward outflow layers. By averaging the 150, 200 and 250 mb layers together we obtain a measure of the outflow which can be compared at all azimuths.

On the other hand, we considered the low-level circulation to be represented by the layer between 700 mb and 1000 mb. Low-level data are considerably better due to the larger number of surface observations.

Definitions of Cyclone Structure. In discussing the characteristics of tropical cyclones and comparing one cyclone with another it is important to have methods of structural classifying besides those of just maximum wind and central pressure. We have recently established a new method of defining the structure of tropical cyclones. It is based on the strength of the tangential wind at different radii. We defined the cyclone structure by the low-level tangential wind characteristics in four radial bands:

(1) Intensity - highest sustained low-level wind speed between 0-1° radius. (Intensity of the North Indian Ocean tropical cyclone listed in JTWC ATR is estimated by Dvorak scheme, 1975).

(2) Strength - mean low-level tangential wind between 1-3° radius.

(3) Outer Circulation - mean low-level tangential wind between 3-7° radius as measured from ECMWF and other analysis.

(4) Environment - mean low-level tangential wind between 7-15° radius as measured from ECMWF and other analysis.

One of the major points made by our studies of tropical cyclones in the northwest Pacific and Atlantic is that changes in one cyclone structural component (such as strength) do not necessarily imply changes in another structural component such as intensity. Figure 11 shows this relationship schematically. An increase in intensity does not require that the cyclone strength (or outer circulation) increase proportionately. In fact, the strength (outer circulation) may increase, decrease, or stay the same for a given change in intensity. In terms of a tropical cyclone's net rainfall and its inland destruction potential, it is likely that cyclone strength and, to some extent, outer circulation are as important or more important than cyclone intensity.

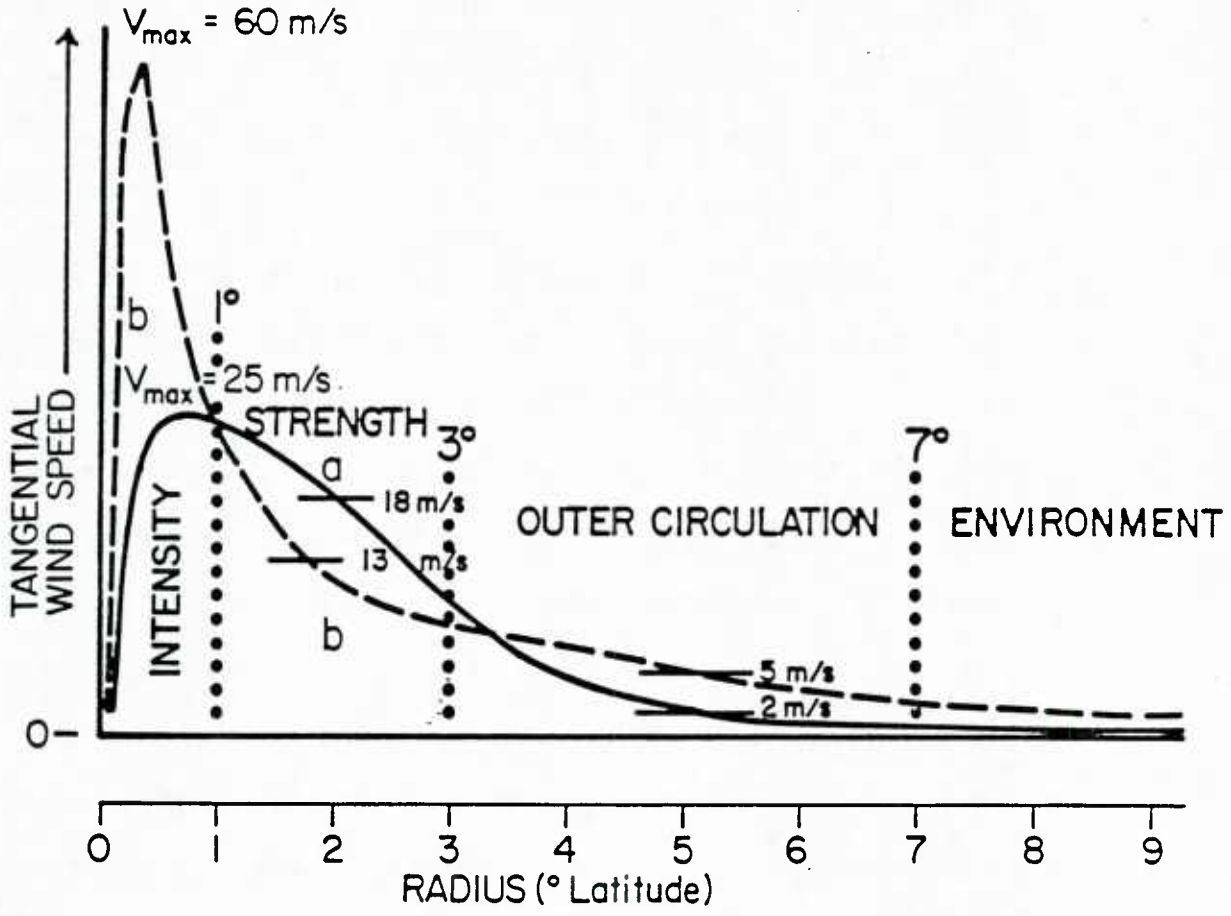

Fig. 11. Definition of tropical cyclone intensity, strength and outer circulation and their changes on a radial profile of azimuthally averaged tangential wind.

5. SUMMARY OF N.I.O. TROPICAL CYCLONES DURING THE FGGE YEAR AND THEIR BASIC LARGE-SCALE CIRCULATION PATTERNS

During the 1979 First GARP Global Experiment (FGGE) year, the JTWC observed seven tropical cyclones forming in the North Indian Ocean. This is higher than the averaged number of four and one-half which JTWC observed during the period of 1975-1983. Only one 1979 cyclone system attained typhoon intensity. This is slightly lower than the yearly average of 1.3. Table 6 gives a summary of the 1979 N.I.O. tropical cyclone systems. Figure 12 shows a summary of the storm tracks. The monthly distribution of these cyclone systems has already been presented in Table 5. As in most other years the most active storm period was the autumn.

Among the seven tropical cyclones in 1979, three, that is TC 17-79, TC 18-79, and TC 23-79 attained an intensity level whereby their maximum sustained winds (or V_{max}) was greater than 50 kts. TC 25-79 reached an intensity of 40 kts. It persisted as a tropical cyclone for two days. TC 24-79 attained an intensity of 35 kts and maintained this intensity for 12 hours shortly before it reached land. TC 22-79 and TC 26-79 did not quite reach an intensity level of 34 kts.

Generally speaking, these weaker tropical cyclones are relatively short-lived compared to those in other ocean basins, especially in the northwest Pacific and northwest Atlantic. This is because tropical cyclone formation in the N.I.O. typically occurs close to land. The short life of some systems makes it a little more difficult to ascertain

TABLE 6

NORTH INDIAN OCEAN

1979 FGGE YEAR TROPICAL CYCLONES

CYCLONE DESIGNATION	PERIOD OF WARNING	CALENDAR DAYS OF WARNING	MAX SUS WIND kts	EST MIN SLP mb	NUMBER OF WARNINGS	DISTANCE TRAVELLED (n mi)
TC 17-79	06 MAY-12 MAY	7	85	967	26	1267
TC 18-79	18 JUN-20 JUN	3	50	985	12	581
TC 22-79	21 SEP-23 SEP	3	25	1000	10	694
TC 23-79	21 SEP-25 SEP	5	55	980	14	1108
TC 24-79	29 OCT-01 NOV	4	35	995	13	720
TC 25-79	16 NOV-17 NOV	2	40	994	8	547
TC 26-79	23 NOV-25 NOV	3	30	995	10	1071
	1979 TOTALS	24*			93	

*Overlapping days included only once in sum.

the physical processes that are important to their development. The following case studies will emphasize the three stronger systems, two of which occurred over the Arabian Sea region where there is new interest in Arabian Sea tropical cyclones because of political tensions in the Persian Gulf. There is also new interest in the association between springtime Arabian Sea tropical cyclones and the onset of the summer monsoon (Krishnamurti, et al., 1981).

Tropical cyclones in the N.I.O. generally originate from cloud cluster disturbances embedded in the monsoon trough. The low-level wind flow is from the west on the equatorward side and from the east on the poleward side of the developing system. A strengthening of the westerly winds on the equatorward side or of the easterly wind to the poleward side (or both) is a common feature occurring prior to the formation of

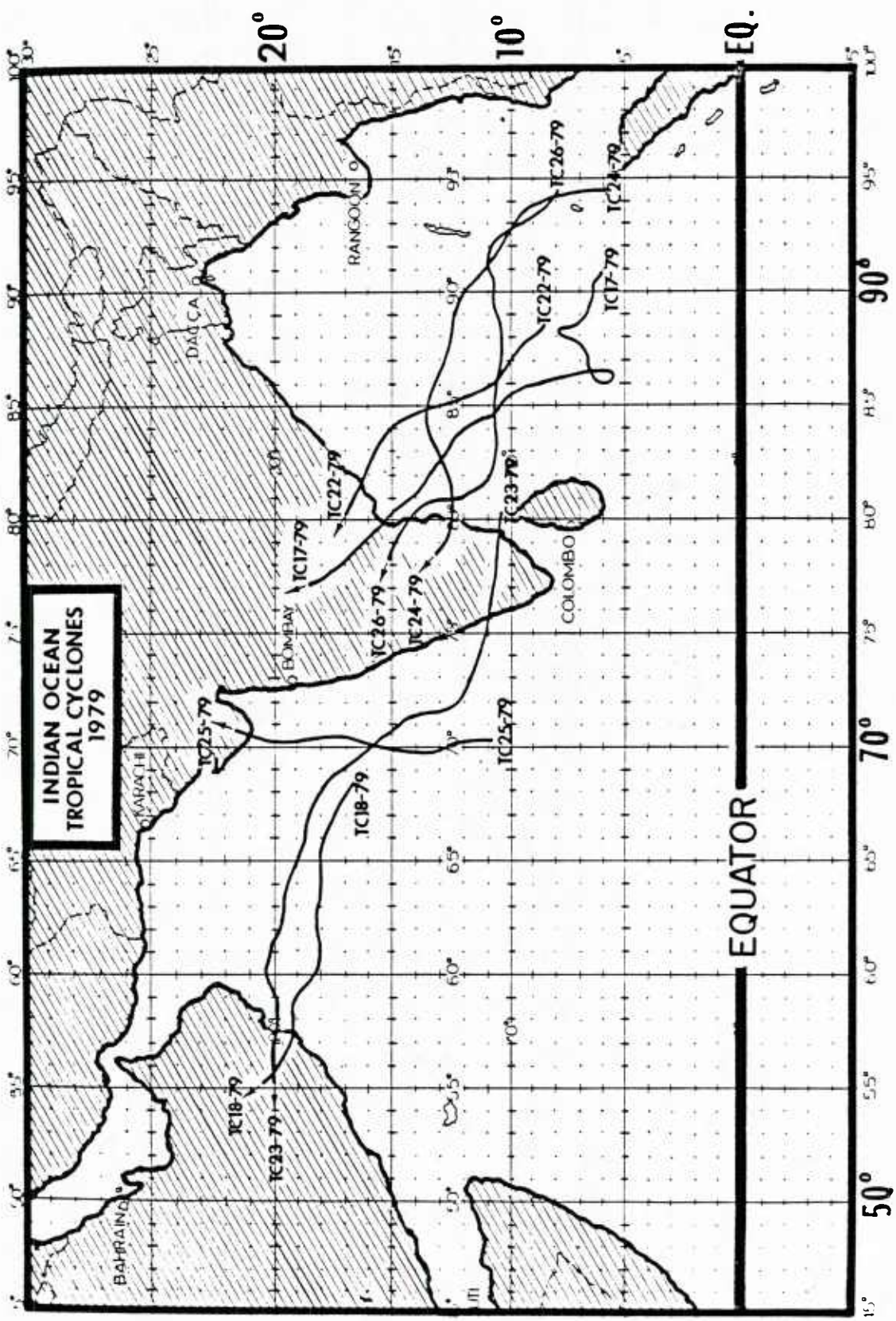

Fig. 12. The track of all 1979 North Indian Ocean tropical cyclones.

tropical cyclones in this and other monsoon trough regions where cyclone formation occurs (Love, 1982).

Figures 13 and 14 show the north-south and east-west vertical cross sections of zonal and meridional winds (U and V), averaged for all seven 1979 systems at their initial center position at their first reported 12Z time period. As expected, a surface to 400 mb deep layer north-south monsoon trough circulation exits at these initial periods. The strong upper level westerly flow to the north of the center is just the prevailing mid-latitude westerlies. Near the equator the winds are, as expected, strongly easterly at upper levels.

The combination of diagrams 13a and 14b represents the net rotational or vorticity part of the wind around the initial cyclone center. It is interesting to find that the vorticity inside 5° radius and through a deep layer around the initial cyclone is as large as it is. The most distinguishable feature of the N.I.O. cloud cluster systems that did not form cyclones was, in general, a lack of such a strong surrounding deep-layer cyclonic vorticity field. As the tropical cyclone spins up and gains inner-core strength this outer cyclonic circulation field undergoes little change, however.

The upper-level anticyclonic circulation is much shallower and much less defined. Figures 13b and 14a show the divergent part of the wind. To the south and west of the center this low-level convergence is very shallow and appears to have originated from the cross-equatorial monsoonal flow across the equator. Notice that the equatorial monsoon flow (and rotational part of the wind about the pre-cyclone disturbance) is present through a very deep layer but the convergence only through a shallow layer. In the upper level, divergence is found most in the

meridional direction with outflow channels towards the pole and the equator. The equatorial outflow branch corresponds to a cross-equatorial return flow.

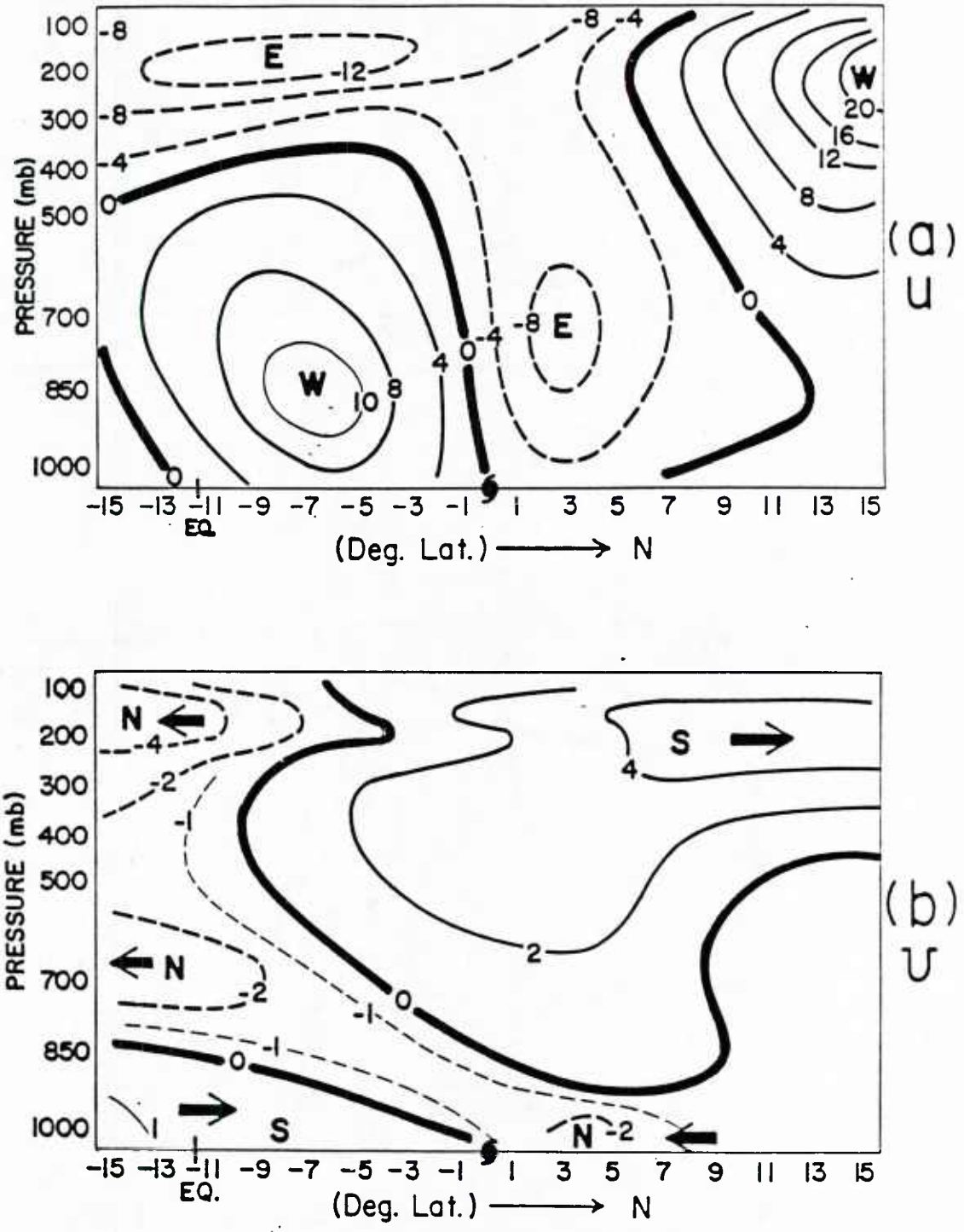

Fig. 13. North-south cross section of zonal (diagram a) and meridional (diagram b) winds in m/s, averaged with respect to the center of all seven North Indian Ocean tropical cyclones in 1979 at their first 12Z time period.

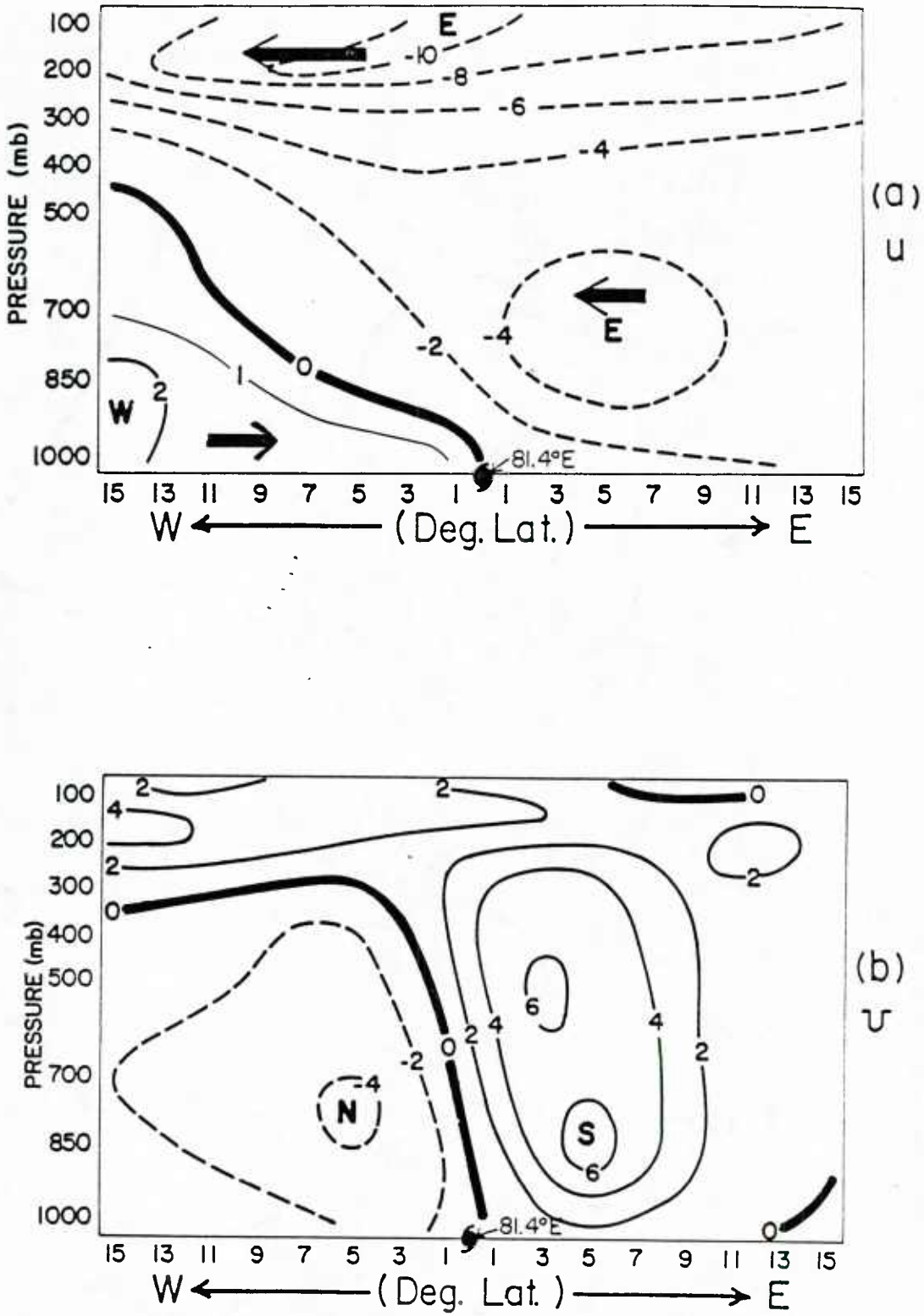

Fig. 14. East-west cross section of zonal (diagram a) and meridional (diagram b) winds in m/s, averaged with respect to the center of all seven North Indian Ocean tropical cyclones in 1979 at their first 12Z time period.

6. ANALYSIS OF INDIVIDUAL CASES OF NORTH INDIAN OCEAN TROPICAL CYCLONES DURING FGGE

We will now discuss the characteristics of each of the seven tropical cyclones that formed within the N.I.O. during the 1979 FGGE year. The observational information during this year was larger and its accuracy greater than in any period before or after 1979. This is because of the special network established during this period.

6.1 TC 17-79

TC 17-79 was the strongest tropical cyclone (V_{max} = 85 kts) in N.I.O. in 1979 (see Fig. 15.). It was the most destructive cyclone in India since TC 22-77 (Nov. 1977) which coincidentally followed a similar track and did great damage to the Madras area. TC 22-77 claimed 14,000 lives, while TC 17-79 caused about 700 deaths. The smaller death total with TC 17-79 is believed due to better preparation and to better heeding of the storm warnings as a consequence of the destruction of the previous cyclone. More than 300,000 people were evacuated in advance (DeAngelis, 1979) of TC 17-79. TC 17-79 was also responsible for sinking the United Vanguard ship before it could take evasion action.

At 1200Z on May 06, observations from ships participating in FGGE defined a cyclonic circulation near 7.0°N, 88.0°E with reported wind speeds of 20-25 kts. After an erratic and looping track, 2 1/2 days later at 00Z May 09, TC 17-79 attained typhoon intensity of $V_{max} \geq 65$ kts.

During this period another tropical cyclone was located in the South Indian Ocean about 750-800 n mi. to the southwest of TC 17-79.

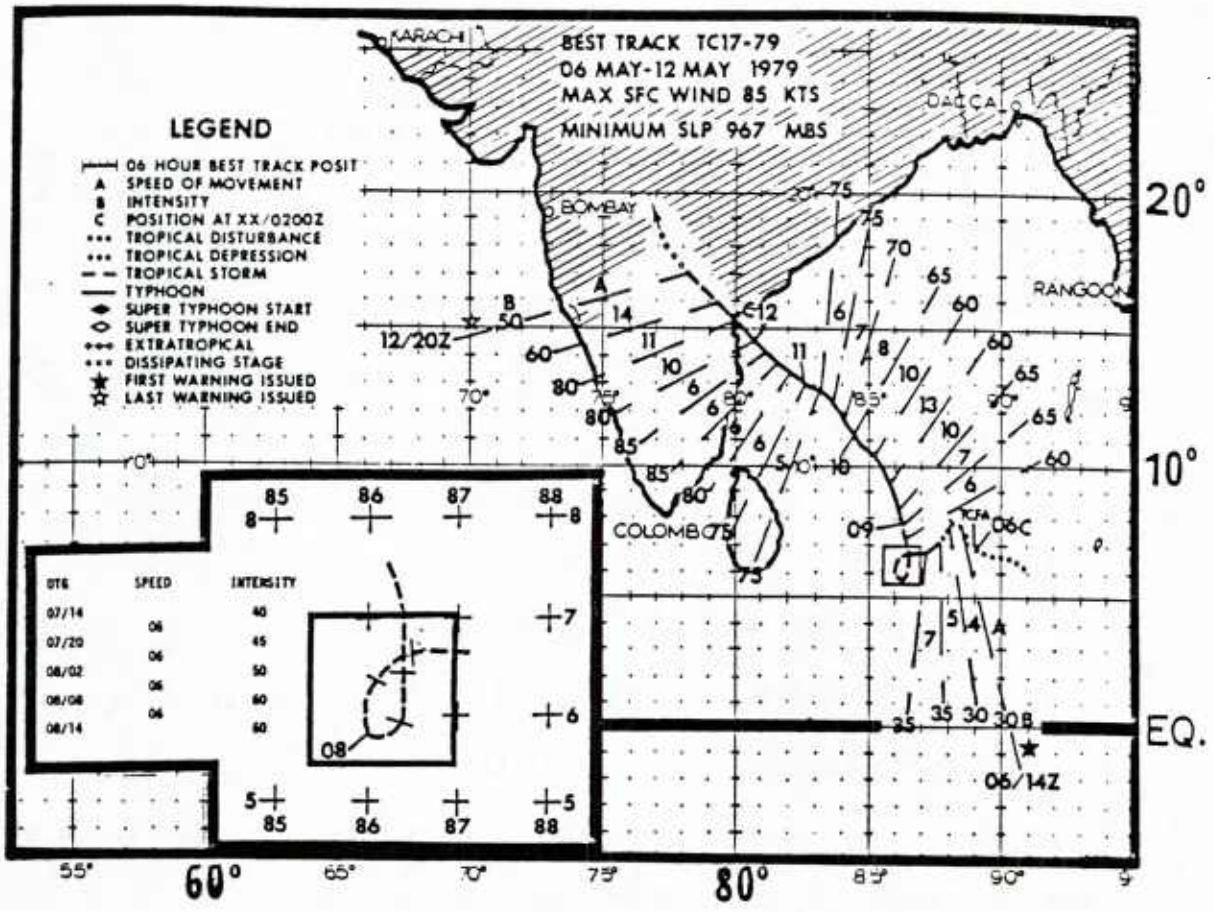

Fig. 15. Best track of TC 17-79 (JTWC ATR 1979).

The Southern Hemispheric tropical cyclone tracked slowly towards the southeast. Following a northwest track, TC 17-79 weakened a little in the next 24 hours and then reintensified to its maximum intensity on 12Z May 11 when maximum winds were estimated to be 85 knots and the center pressure 967 mb. TC 17-79 then rapidly lost its intensity and dissipated when it moved over the Indian subcontinent near Madras.

Time Series of Wind Parameters. The time series of estimated V_{max} (in knots) and the low-level outer circulation (700–1000 mb $\bar{V}_t$ at 6° radius in m/s) are shown in Fig. 16. It is interesting to note that the

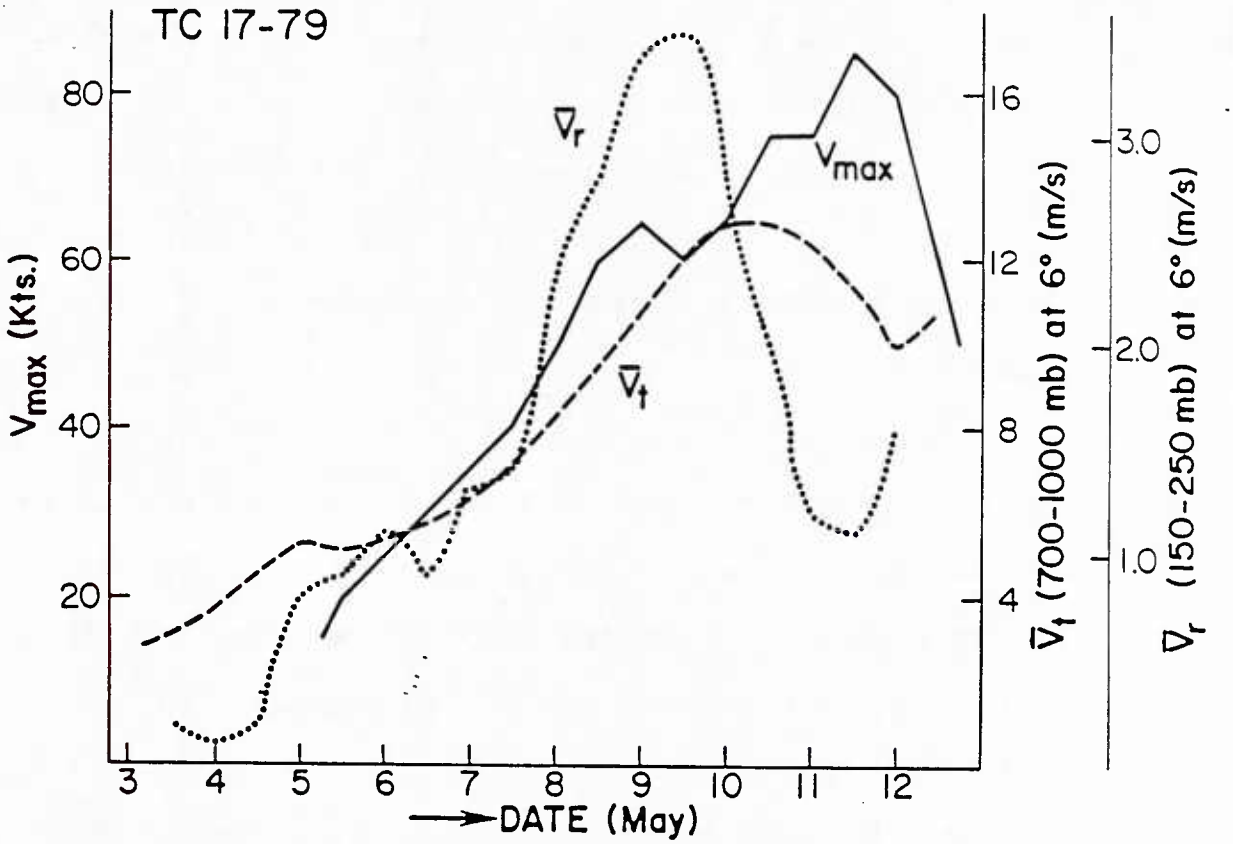

Fig. 16. Time series for TC 17-79 of its intensity (V_{max}) in knots, low-level (700-1000 mb) 6° radius outer circulation ($\bar{V}_t$) in m/s and upper-level (150-250 mb) outflow ($\bar{V}_r$) at 6° radius in m/s.

low-level outer 6° radius circulation ($\bar{V}_T$) was strengthening prior to JTWC's first report at 12Z May 05. From the 5th to the 7th of May, the V_{max} increased from 15 kts to 35 kts without a significant increase in the low-level outer circulation, however. The low-level outer circulation attained its peak magnitude at 00Z May 10, two days before TC 17-79 reached its maximum intensity.

The third curve in Fig. 16 shows the mean upper tropospheric outflow ($\bar{V}_r$) between 150 and 250 mb at 6° radius. This outflow ($\bar{V}_r$) was obtained by averaging the radial wind at the 150, 200, and 250 mb layers. A 3-point running mean (between 12-hour interval data) was taken to smooth out diurnal and other short time-scale variations.

(This 3-point running mean was applied to all time series with significant 00Z and 12Z variation.) The upper-level outflow of TC 17-79 increased significantly right before the system was officially reported by JTWC. Another major increase occurred between 12Z May 07 and 12Z May 08 when the system was undergoing its maximum intensification rate. There was a noticeable break in the increase of V_{max} between 00Z May 09 and 00Z May 10 associated with the decrease of the upper-level outflow.

Early Stage. Between 00Z May 03 and 00Z May 05, the ITCZ (Inter Tropical Convergence Zone) was located between the equator and 10°N from 60°E to 90°E with loosely organized cloud clusters spread over the entire region. The only significant change in the ITCZ strength during this stage was an increase of the low-level outer circulation of the pre-TC 17-79 disturbance. Figure 17 shows this low-level tangential wind out to the 14° radius about the position of 6.4°N, 90.6°E at 12Z May 03, 12Z May 04, and 12Z May 05. This is the location of TC 17-79 at 12Z May 05. The heavy curves are the 2 m/s tangential isotach.

At 12Z May 03, a maximum V_t of 12 m/s is located at 4-6° radius south and southwest from the center. North of the center, tangential winds are only 2-3 m/s. The 2 m/s isotach does not penetrate through the west side (V_t is negative here) to form a closed pattern around the center. By 12Z May 04, however, a closed pattern of 2 m/s isotach is found around the center, V_t to the north has increased to 5 m/s. The maximum V_t to the south and southwest of the center is maintained at 12 m/s. Negative V_t is still present at 12° radius to the south and 10° to the north and east of the center. However, positive V_t is spread over

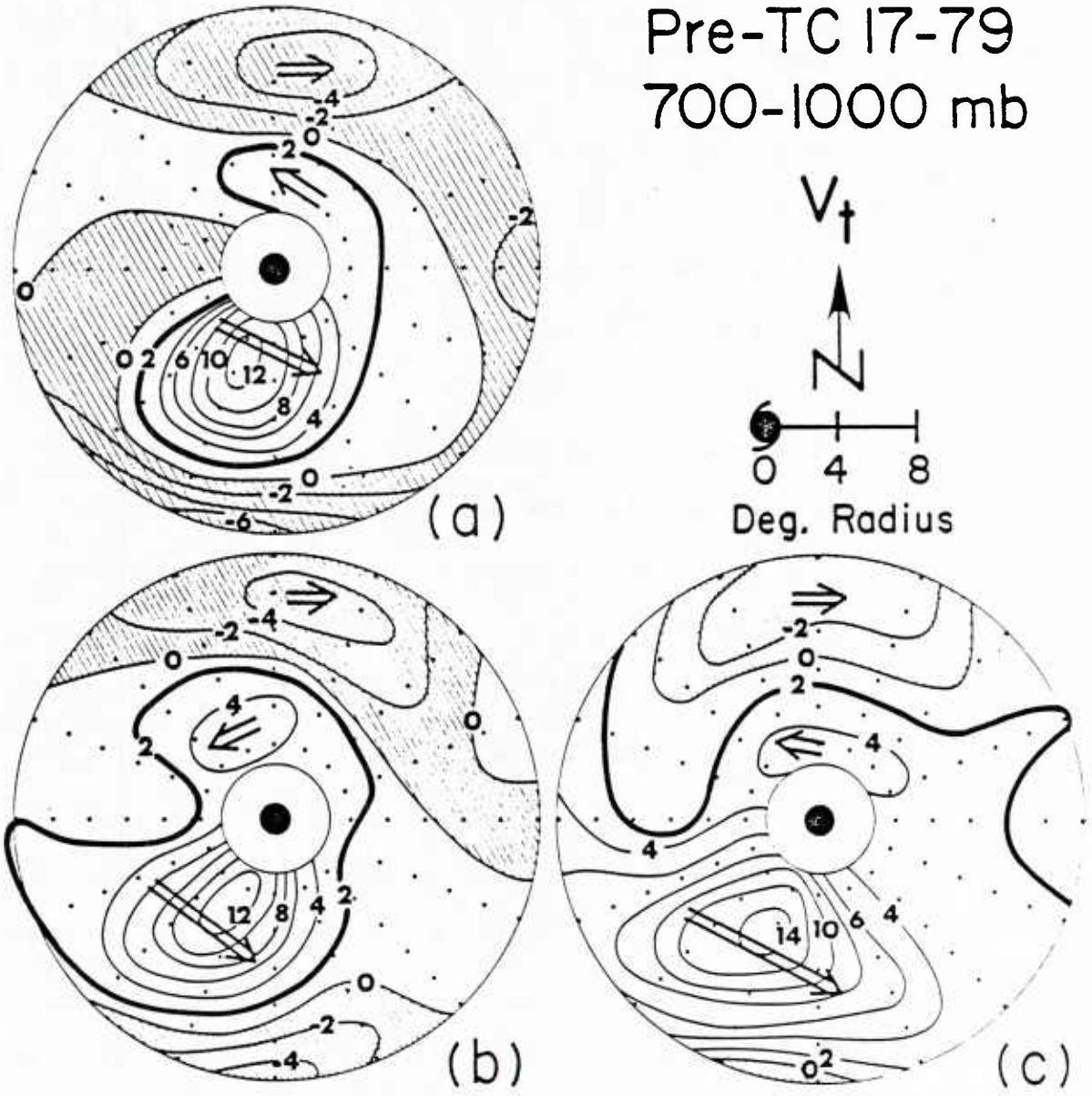

Fig. 17. Plan view of low-level circulation (700-1000 mb V_t) of TC 17-79 about 6.4°N, 90.6°E or the center of the pre-TC 17-79 disturbance at (a) 12Z May 03, (b) 12Z May 04, and (c) 12Z May 05. Values in m/s.

most of the region around the cyclone by 12Z May 05. The maximum mean $\bar{V}_t$ around the cyclone increased from 12 to 14 m/s during this period..

Figure 18 shows the low-level large-scale circulation pattern at 00Z May 05. A westerly wind maximum is located on the equator between 80°E and 90°E. The pre-TC 17-79 disturbance is located to the northeast or cyclonic side of this low-level wind maximum region. In the south Indian Ocean, TC 16-79 is located at around 7°S, 84°E. TC 16-79 attained tropical storm strength on May 04 and intensified to 50 kts and 60 kts on the 5th and 7th respectively (DeAngelis, 1979). The increase of TC 16-79's intensity appears to have helped produce these strong westerly winds near the equator. The cross-equatorial flow along the east Africa coast does not seem to play a significant role in producing this strong low-level coupling between TC 17-79 and TC 16-79.

At upper levels, an anticyclonic center is located around 15°N, 90°E, north of the pre-cyclone cloud cluster region where TC 17-79 will form. An upper-level trough is located 20° to the west - northwest of the anticyclone center. The flow is mostly northeasterly and easterly near the vicinity of the cluster region. No significant change in upper-level flow occurs during the three-day period of genesis except for an upper-level trough moving slowly eastward.

Developing Stage. At 12Z May 05, a well organized cloud pattern is found centered at 6°N, 91°E. Maximum wind at this time is estimated at 20 kts (JTWC ATR, 1979). A significant developmental feature appears to be the establishment of an upper tropospheric outflow channel to the north. This can be seen from the increase of the 150-250 mb radial wind from 12Z May 04 to 00Z May 05 in Fig. 16. The radial circulation

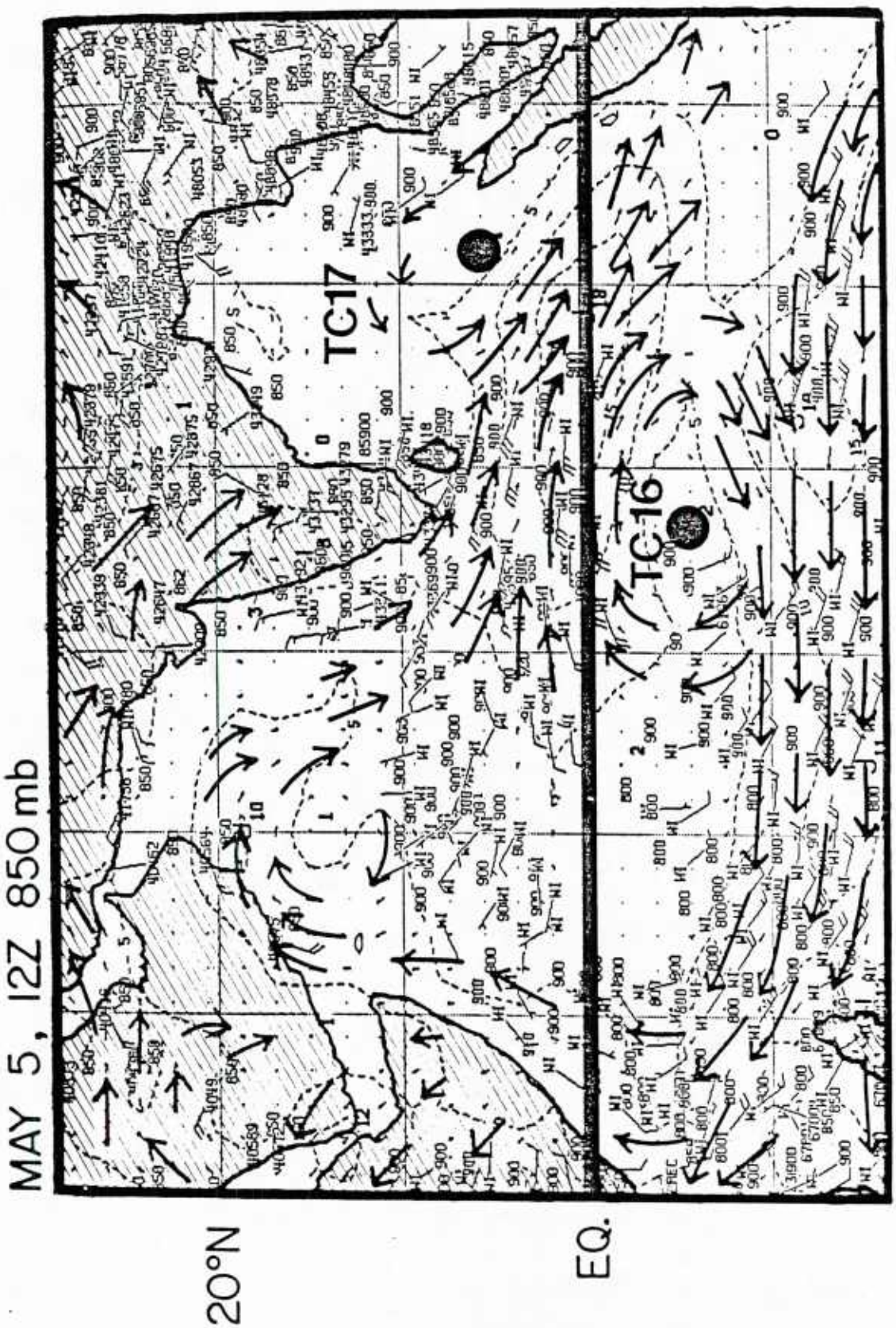

Fig. 18. 850 mb streamline field at 12Z May 05. Circles denote the center of TC 17-79 and TC 16-79.

increases slightly in the next 48 hours with the maximum wind going from 20 to 40 kts at 12Z May 07.

Radial-height cross sections of azimuthally averaged tangential wind ($\bar{V}_t$) at 12Z May 05, 12Z May 07, and 12Z May 09 are shown in diagrams a, b and c of Fig. 19. Cyclonic circulation extends up to 300-400 mb with maximum anticyclonic wind near 175 mb. This circulation pattern is very similar to those of developing tropical cyclone wind patterns in the northwest Pacific as discussed by McBride, 1981. Note how the outer cyclonic tangential circulation from the surface to 400 mb shows a steady increase while the upper-level anticyclone circulation shows little change until the maximum intensity is reached. Diagram a of Fig. 20 depicts the difference in the tangential wind between 12Z May 07 and 12Z May 05. The tangential wind increases over the whole depth of the troposphere between these two time periods.

A stronger intensification rate is noted between 12Z May 07 and 00Z May 09. The circulation pattern at 12Z May 09 is shown in diagram c of Fig. 19 and the tangential wind change from 12Z May 07 to 12Z May 09 is shown in diagram b of Fig. 20. A comparison with diagram a of Fig. 17 shows that the tangential wind increase is mostly at larger radii from 12Z May 05 to 12Z May 07, but at smaller radii from 12Z May 07 to 12Z May 09. In other words, the cyclonic circulation increases at all levels as the cyclone is in its early developmental phase from 20 to 40 knots but then has an increased inner tangential wind concentration in the later developmental stages from 40 to 60 knots maximum winds. The level of maximum tangential wind increase also shifts to a lower level in the later developing stages.

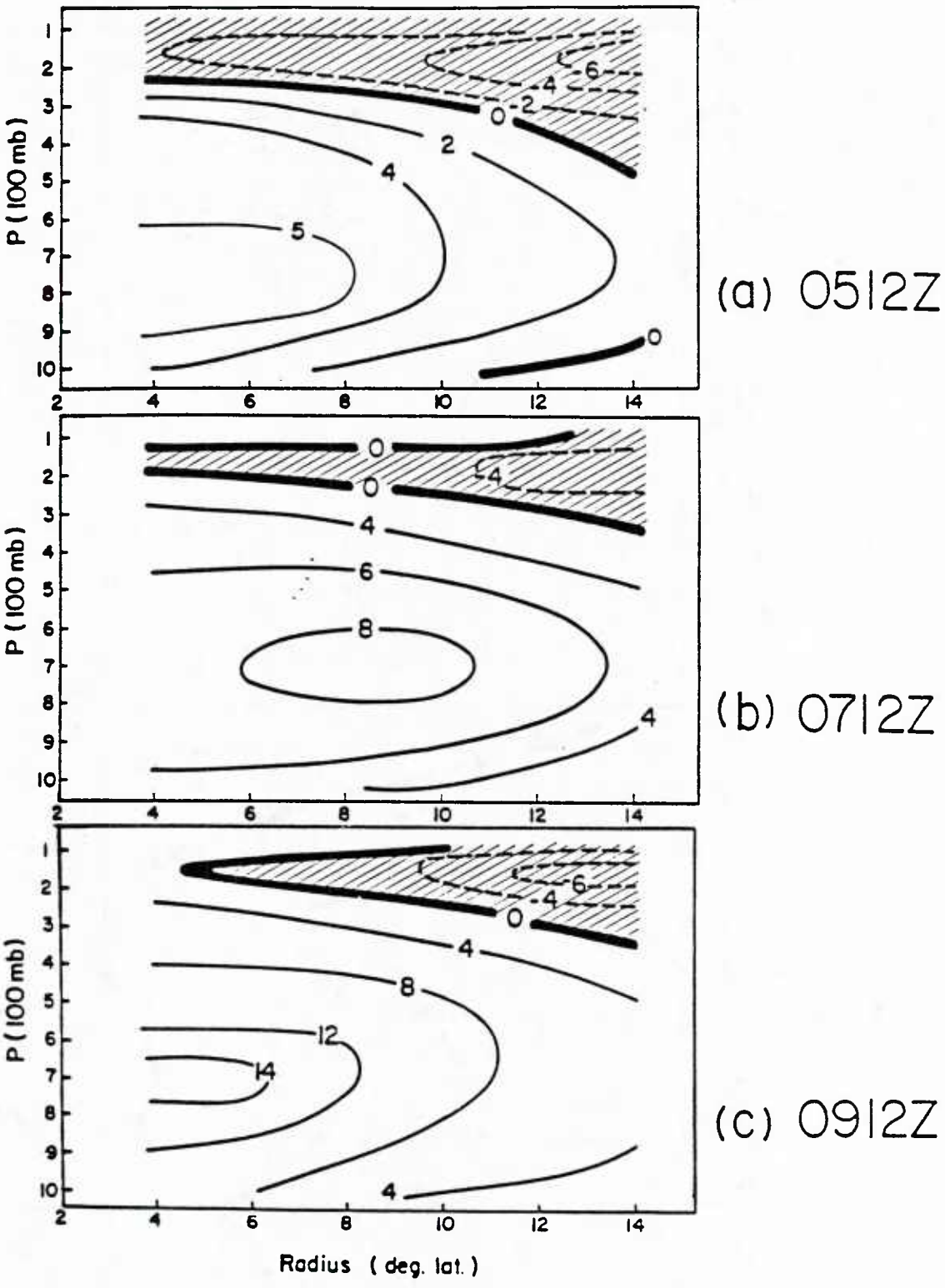

Fig. 19. Radius-height vertical cross sections of azimuthally averaged tangential wind (in m/s) for TC 17-79 at (a) 12Z May 05, V_{max} = 20 kts (b) 12Z May 07, V_{max} = 40 kts, and (c) 12Z May 09, V_{max} = 60 kts.

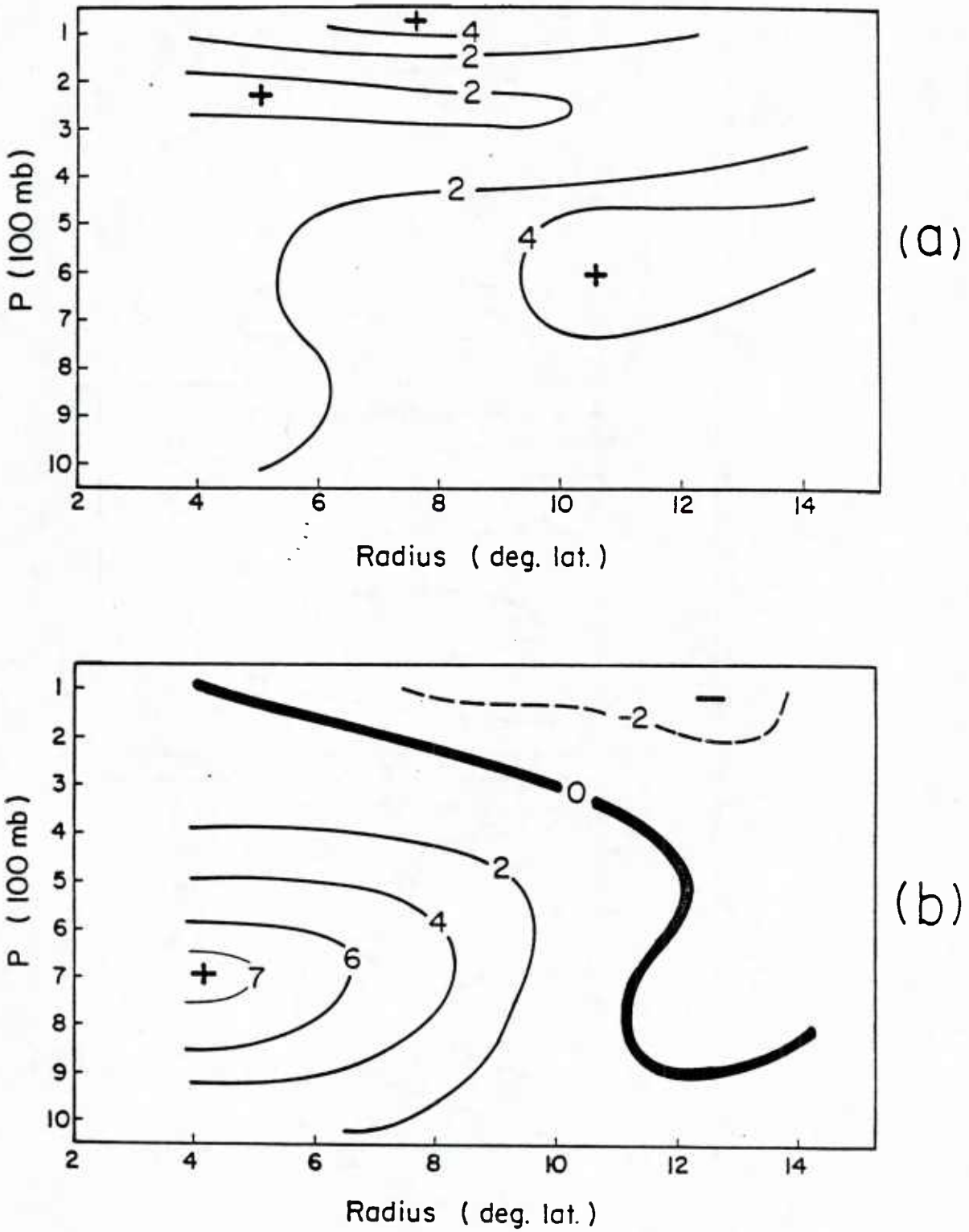

Fig. 20. Radial-height cross-section of 2-day tangential wind increases for TC 17-79 in m/s: (a) 12Z May 05 to 12Z May 07; (b) 07 12Z to 09 12Z. Plus sign means an increase in cyclonic circulation or a decrease in anticyclonic circulation.

During this time period, the 200 mb upper-level trough moves closer to the longitude of the cyclone center (Fig. 21). An upper-level outflow channel is established to the north of the cyclone center. Figure 22 shows the plan view of the 150-250 mb radial winds in a moving coordinate relative to the center of TC 17-79 at 12Z May 07. A major outflow channel is found to the north of the center. A broader outflow region is also located to the southeast of the cyclone center. The looping track of TC 17-79 starts around this time period. This looping is likely due to changes of the steering flow current resulting from fluctuations in the north vs. south strength of the surrounding monsoon trough as has been discussed by Xu and Gray, 1982.

Although the upper-level outflow started to weaken after 12Z May 09 the V_{max} still continued to show a general increase from 12Z May 09 to 12Z May 11. This appears to be related to the passage of the upper-level trough system. Convection gradually concentrated at inner radii especially on the east and southeast sides of the center. Figure 23 shows the satellite portrayal of this cyclone at 12Z May 09 and 12Z May 11. An upper tropospheric outflow has been established to the west and southwest of the center. Figure 24 shows the upper-level large-scale circulation pattern at 00Z May 10 and 00Z May 11. The upper-level radial wind (in the moving coordinate system relative to the cyclone center) is shown in Fig. 25. A pronounced outflow channel is located to the west of the cyclone center.

Decaying Stage. TC 17-79 makes its landfall at 06Z May 12 and maintains its intensity of 80 kts for another 6 hours or so. Its circulation patterns are well-maintained until 12Z May 12. It then rapidly dissipates as it moves inland.

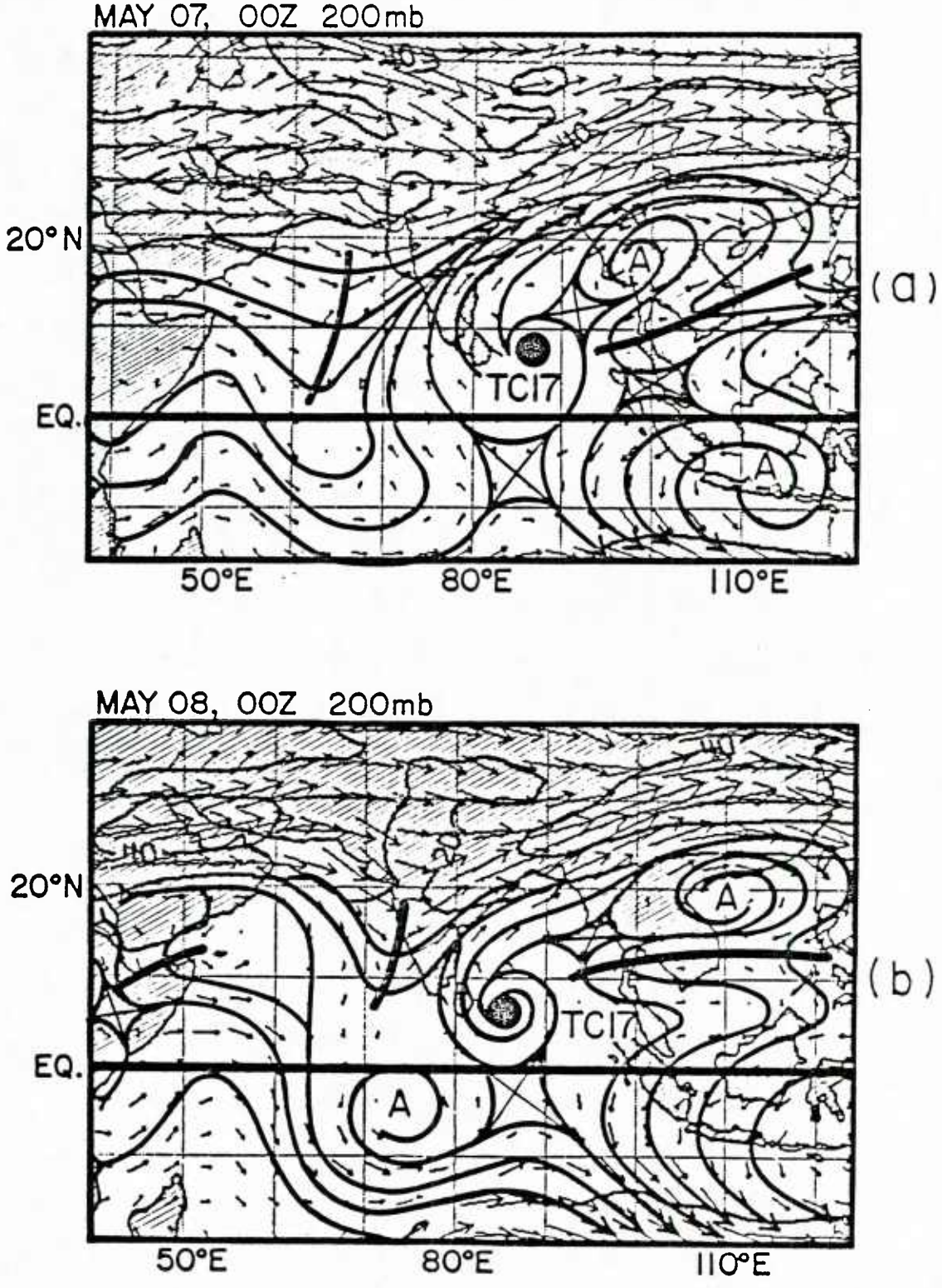

Fig. 21. ECMWF analyzed 200 mb wind field associated with TC 17-79 for (a) 00Z May 07, and (b) 00Z May 08. The large solid circle denotes the center of TC 17-79. Length of arrows is proportional to wind speed.

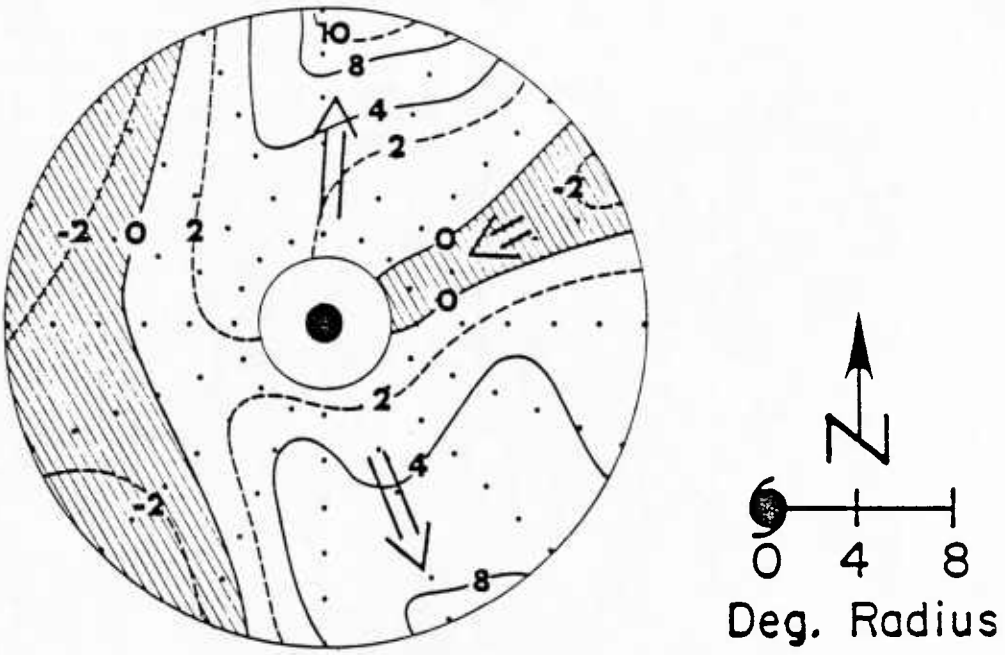

Fig. 22. Plan view of upper-level radial wind for TC 17-79 (150 - 250 mb, $\overline{V}_r$) at 12Z May 07, V_{max} = 40 kts, in a moving coordinate relative to the cyclone center. TC 17-79 is moving toward 275° at a speed of 3.1 m/s. Shaded area is negative or inflow region.

6.2 TC 18-79

TC 18-79 began as a monsoon depression in the Arabian sea at 14Z June 17. Maximum wind speed at that time was estimated to be 25 kts. TC 18-79 followed a westward track throughout its life. It dissipated over the Oman coast (Fig. 26). Its sustained wind increased to a maximum value of 50 kts in 36 hours. It maintained this magnitude for 24 hours until shortly before it hit the coast. Figure 27 shows the time series of V_{max}, the low-level outer circulation, and the upper-level outflows at 6° radius.

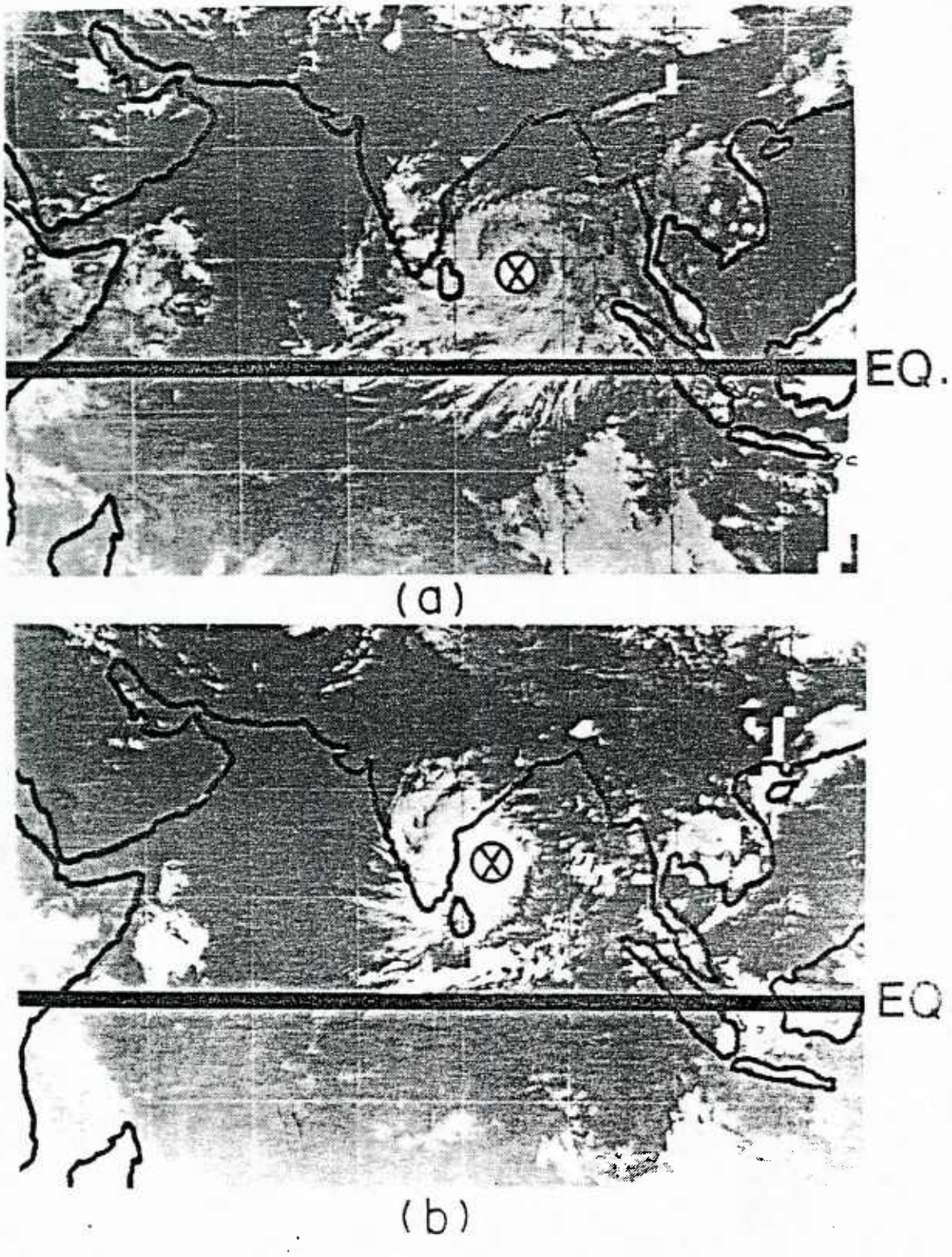

Fig. 23. Satellite picture of TC 17-79, center is circled, at 12Z on (a) May 09, (b) May 11.

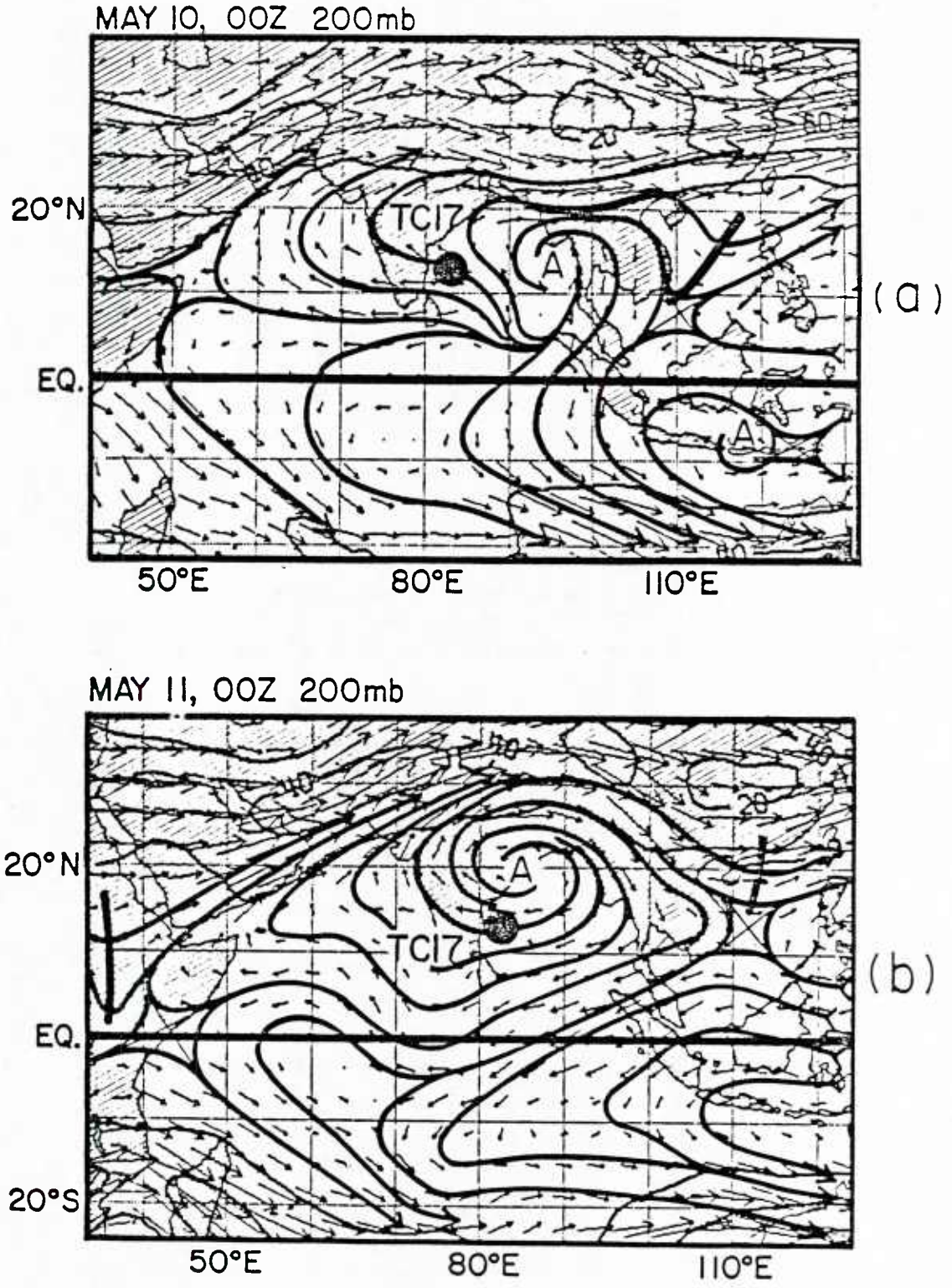

Fig. 24. 200 mb flow field relative to TC 17-79 (circled) for 00Z May 10 (diagram a) and 00Z May 11 (diagram b). Length of arrows is proportional to wind speed.

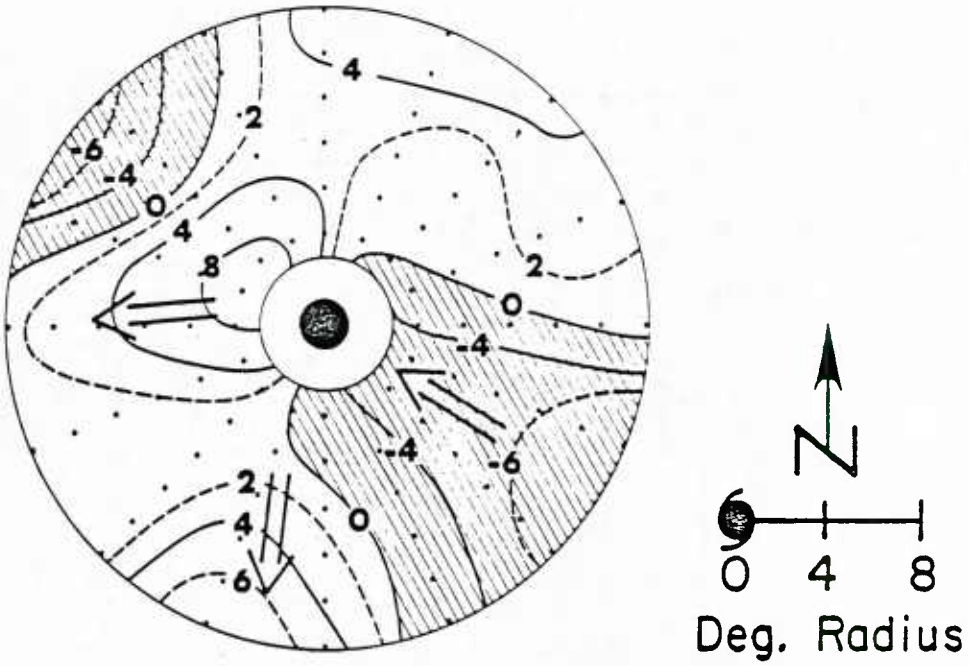

Fig. 25. Plan view of upper level radial wind (150 - 250 mb average V_r) for TC 17-79 at 12Z May 11. (V_{max} = 85 kts) in a moving coordinate system. The storm is moving toward 295° at 3.4 m/s).

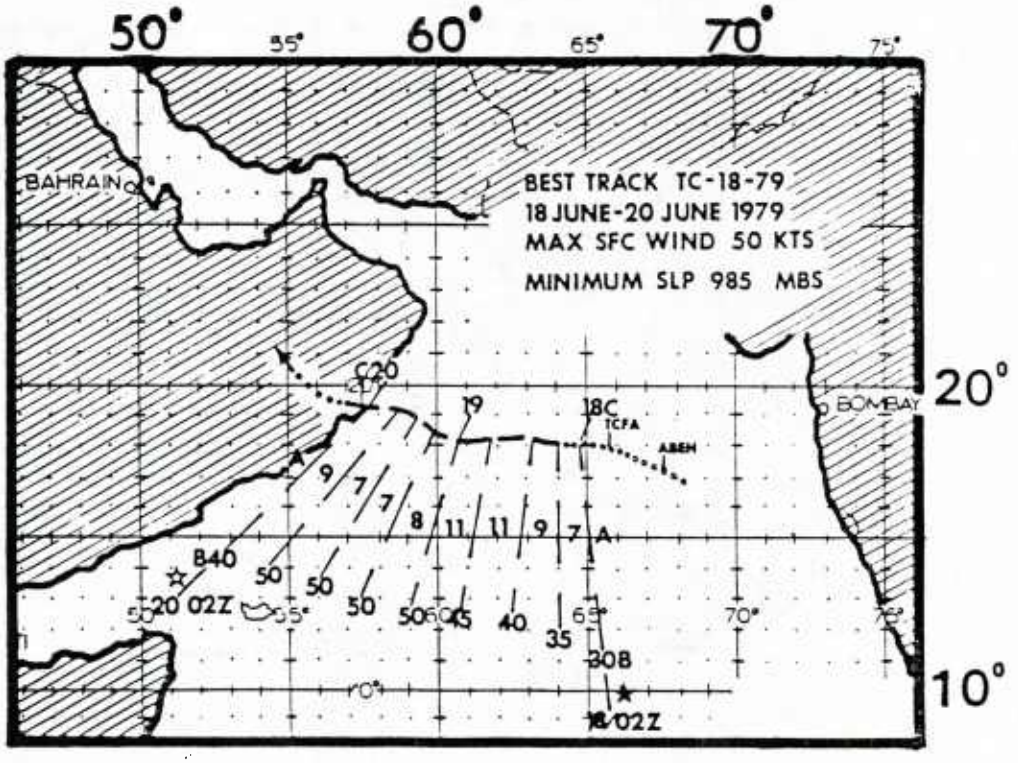

Fig. 26. Best Track of TC 18-79. (From JTWC ATR, 1979.)

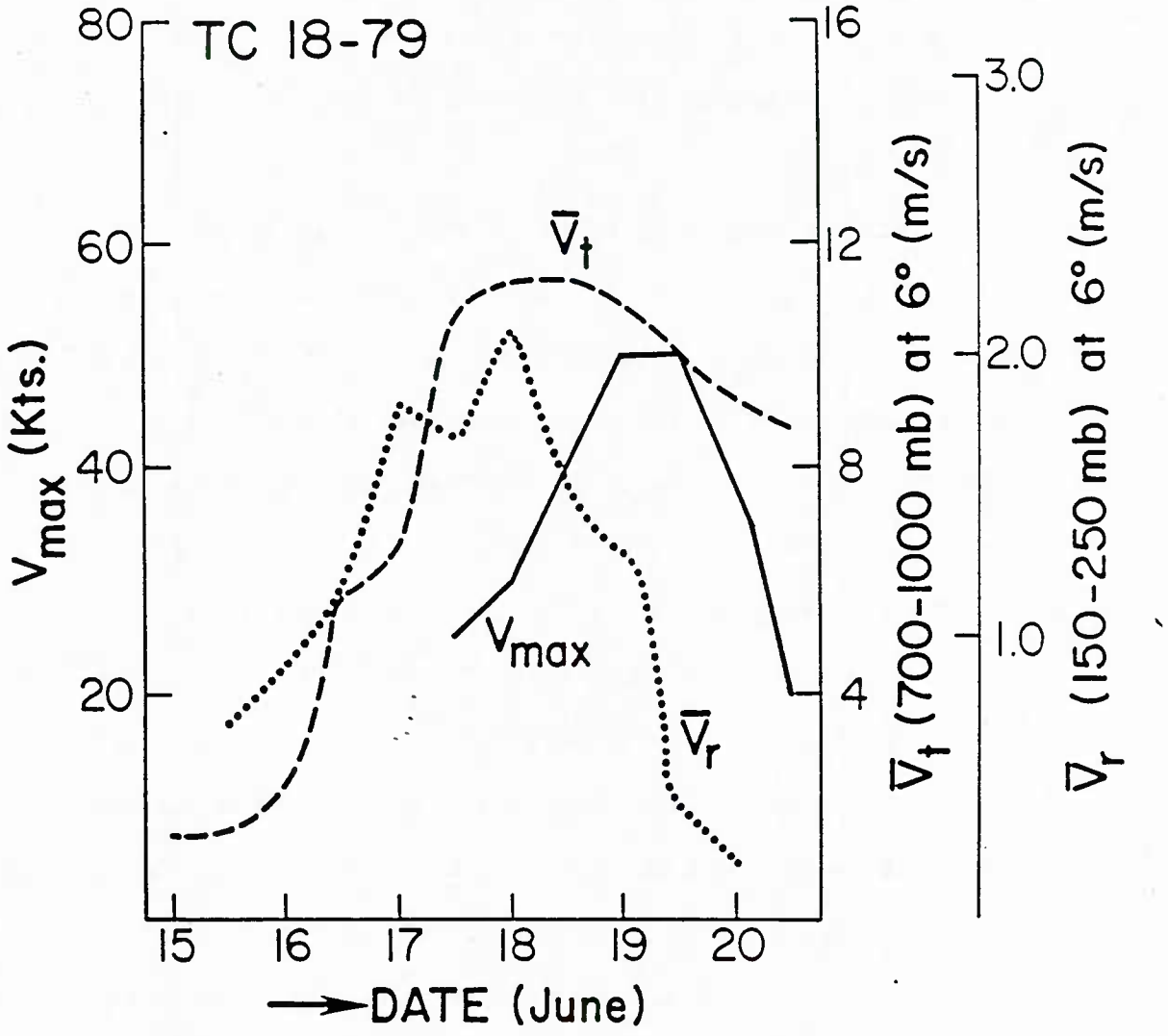

Fig. 27. Time series of TC 18-79 of its intensity (V_{max}) in knots, low-level (700-1000 mb) 6° radius outer circulation ($\bar{V}_t$) in m/s and upper-level (150-250 mb) outflow ($\bar{V}_r$) at 6° radius.

Prior to TC 18-79's formation, a frontal system moved eastward in the South Indian Ocean. A surge type flow propagated equatorward behind this front. This brought about a strengthening of the low-level wind maximum along the Somali coast. This low-level band of strong winds extended eastward across the entire Arabian Sea. Although this low level wind maximum is climatologically always along the Somali coast during this season, its strength was greater than normal strength during the period of TC 18-79's formation. This appeared to aid in the

formation of TC 18-79 by increasing the westerly winds on the southern side of the pre-cyclone disturbance and generally enhancing its low-level circulation.

This strengthening of the low-level jet can be seen from the plan view of the low level (700-1000 mb) tangential wind field around the center of TC 18-79 at 12Z June 17 when the center was located at 17°N, 68°E. Figure 28 shows these plan views at 12Z June 15, 12Z June 16, and 12Z June 17. At 12Z June 15 (48 hours before the beginning of TC 18-79), a low-level wind speed maximum of 16-17 m/s was located 10° south of the pre-cyclone center. Cyclonic circulation is found only on the south side of the center. This is part of the prevailing southwesterly flow from the low-level Somalia jet. The pre-cyclone disturbance center is located just on the poleward (or cyclonic shearing side) of this low-level wind speed maximum. To the north side of the pre-cyclone center only a weak anticyclonic circulation is present.

By 12Z June 16, 24 hours later, the maximum wind to the south increases slightly. The most distinctive new alteration of the low-level flow is the spreading of the cyclonic circulation to the east and north sides of the developing system. Note how the 2 m/s isotach has now formed a closed pattern around the center. The low-level anticyclonic region has greatly decreased. The maximum wind increased to 23 m/s by 12Z June 17 and moved closer to the system center. The cyclonic wind spreads over almost the whole region. This gradual building-up of the low-level circulation is similar to that of TC 17-79.

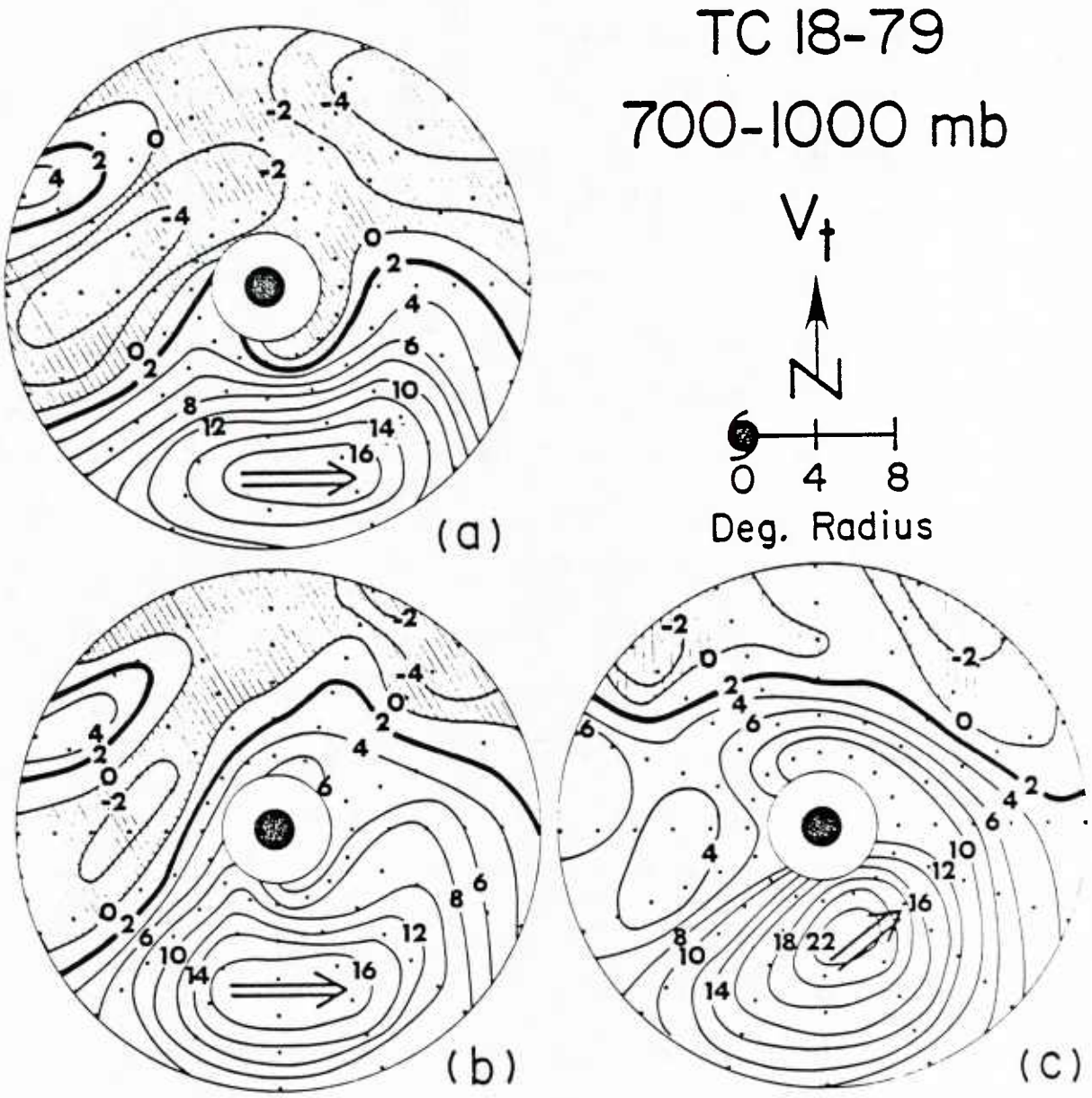

Fig. 28. Plan view of low-level circulation (700–1000 mb V_t) in m/s relative to the center of TC 18-7 at 12Z June 15 (diagram a), 12Z June 16 (diagram b) and 12Z June 17 (diagram c).

The gradual strengthening of the average low-level 6° radius cyclonic circulation around the entire cyclone system in the early stages can also be observed in Fig. 27. At 12Z June 15, the azimuthal average of tangential wind at 6° radius was only 1.7 m/s. However, by 12Z June 17 (two days later), the wind speed at this same radius has increased to 10.7 m/s. Compared to that of TC 17-79, this magnitude is much greater (at the formation stage) even though TC 18-79 never reached the same intensity level that TC 17-79 did. The cyclonic circulation of TC 18-79 was not only strong, but it also extended over a very broad region. Diagrams a and b of Fig. 29 show vertical cross sections of azimuthally averaged $\bar{V}_t$ at 12Z June 17 and 12Z June 19 when V_{max} are estimated to be 25 kts and 50 kts, respectively. Again, the cyclone circulation patterns are quite similar to those found in northwest Pacific tropical cyclones. However, the outer and environmental circulation of TC 18-79 is much stronger at this early stage, compared to the average of the other cases. A lower tropospheric azimuthally averaged wind speed of 7-8 m/s at 10° radius as is present at 12Z June 17 is quite large. It is interesting to note that the upper- and lower-level circulation beyond 4° radius does not change much during this 48-hour period, but the maximum inner core cyclone intensity doubles its magnitude during this time interval.

It should be noted that the 6° radial outflow increases greatly prior to the beginning of TC 18-79's formation but does not increase during the period when the maximum winds increase the most between 12Z June 17 and 00Z June 19. However, the 200 mb outflow concentrates in channels to the west and southwest of the center as shown in Fig. 30

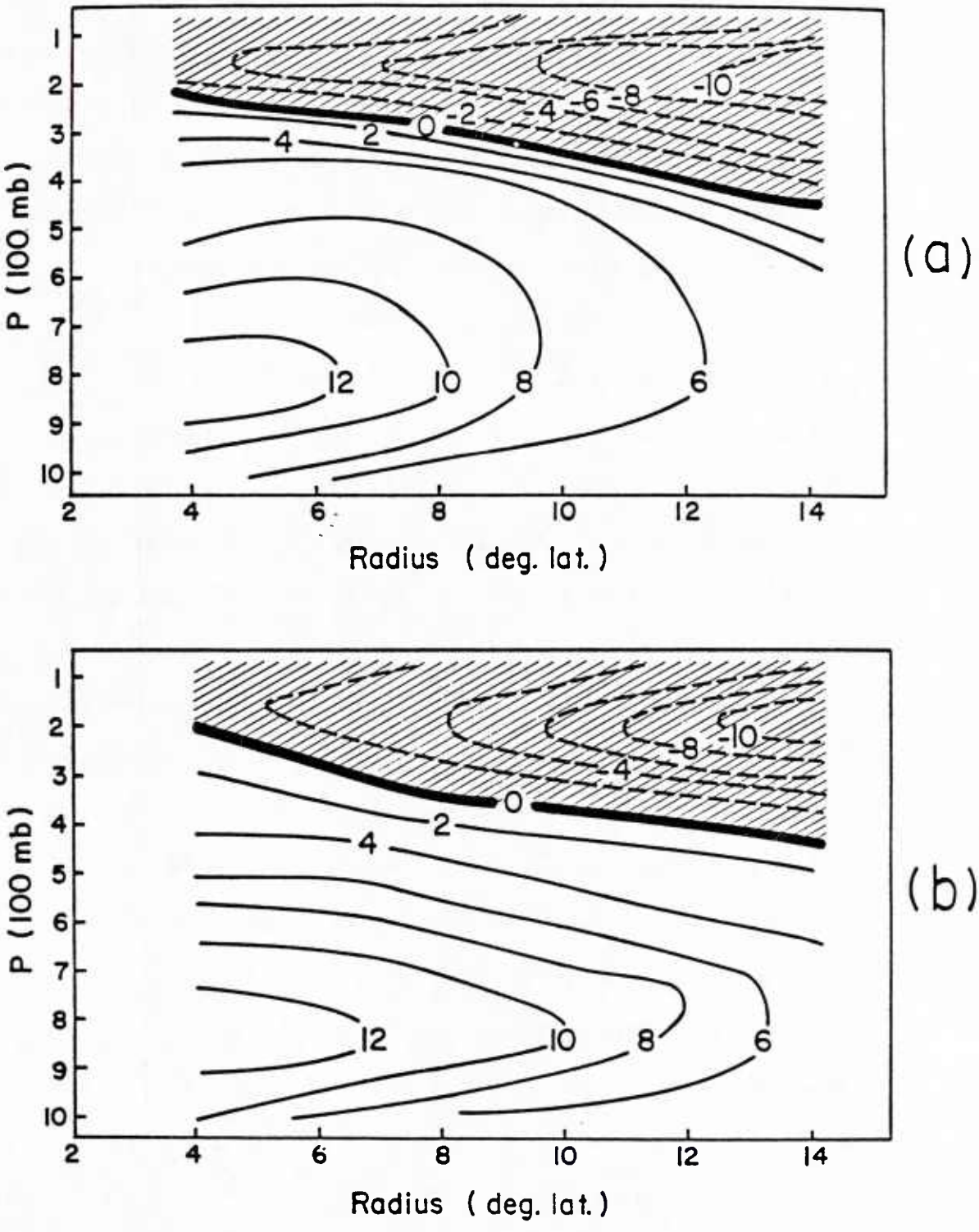

Fig. 29. Radial cross sections of the azimuthally averaged tangential wind (V_t) in m/s for TC 18-79 at 12Z June 17 (diagram a) and 12Z June 19 (diagram b).

for the period of 00Z June 17 and 00Z June 18. An examination of the upper-level circulation pattern shows that the center of TC 18-79 is located south of an upper-level anticyclone center. This results in a strong prevailing easterly wind over the vicinity of TC 18-79. This prevailing easterly wind and westward stretching of the Southern Hemisphere anticyclone have eliminated the outflow to the east and enhanced the outflow channel to the west and southwest. Figure 31 shows the plan view of the upper-level radial wind at 12Z June 17 in which a major outflow channel can be seen toward the southwest. It is this outflow channel that might have caused the intensification of TC 18-79. Documentation of outflow channel increase and cyclone intensification has been previously discussed by Chen and Gray (1984). A physical hypothesis for this process has been advanced by Holland and Merrill (1984) of our project.

Although TC 18-79 was still increasing in inner-core intensity from 00Z June 18 to 00Z June 19, the upper-level outflow began to weaken at this time (a feature similar to that of TC 17-79). This was due (we believe) to the increase of the upper-level inflow on the eastern side produced by the strong westward directed flow at this level. Besides causing outflow decreases, this strong upper-level easterly flow appears also to have acted to bring about a shearing off of convection. This brought about a rapid weakening of TC 18-79 before it reached the Oman coast. Figure 32 shows the satellite IR picture of TC 18-79 at 18Z June 19, when TC 18-79 starts to weaken. The clear region and sharp edge of the cloud pattern on the east side indicate an inflow to the storm system from the east. Another reason for TC 18-79's rapid weakening is

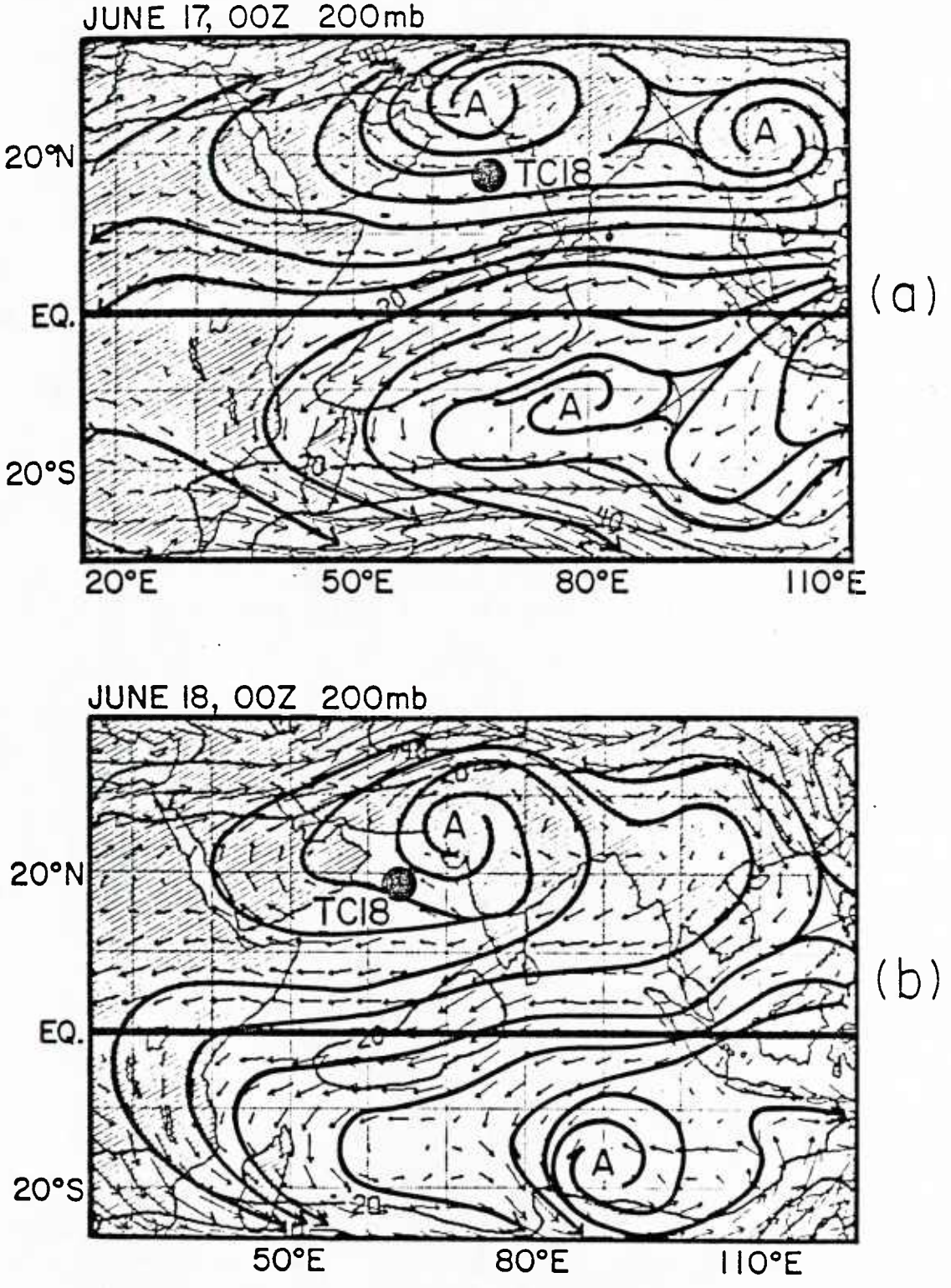

Fig. 30. 200 mb flow field for TC 18-79 at 00Z June 17 (diagram a) and 00Z June 18 (diagram b). The large dot shows the center of TC 18-79. The length of the arrows is proportional to wind speed.

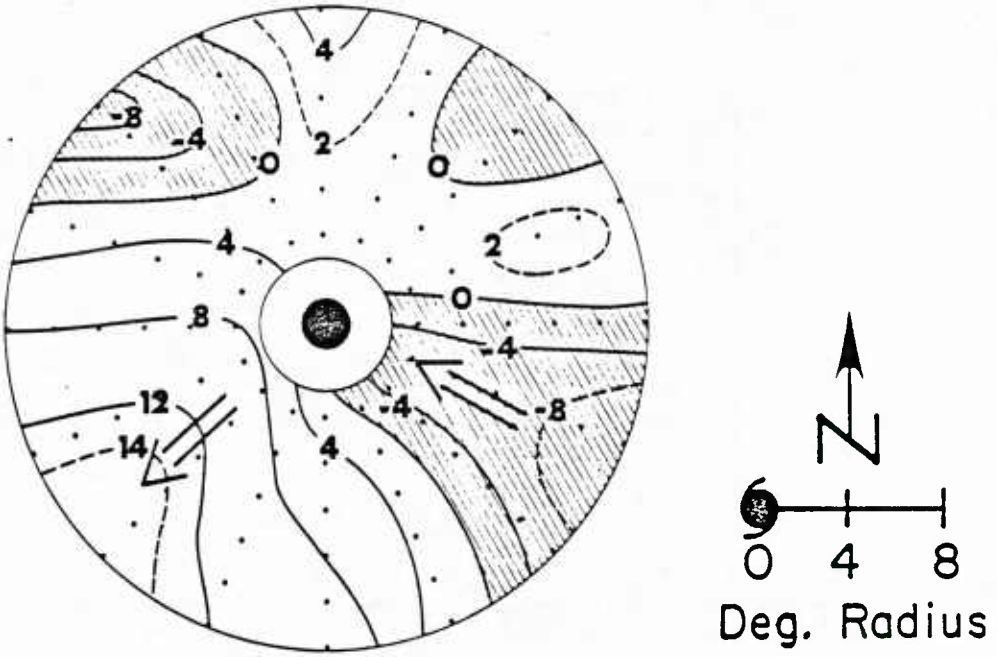

Fig. 31. Plan view of upper-level radial wind (150-250 mb V_r) for TC 18-79 at 12Z, June 17, in a moving coordinate (277° and 4.0 m/s).

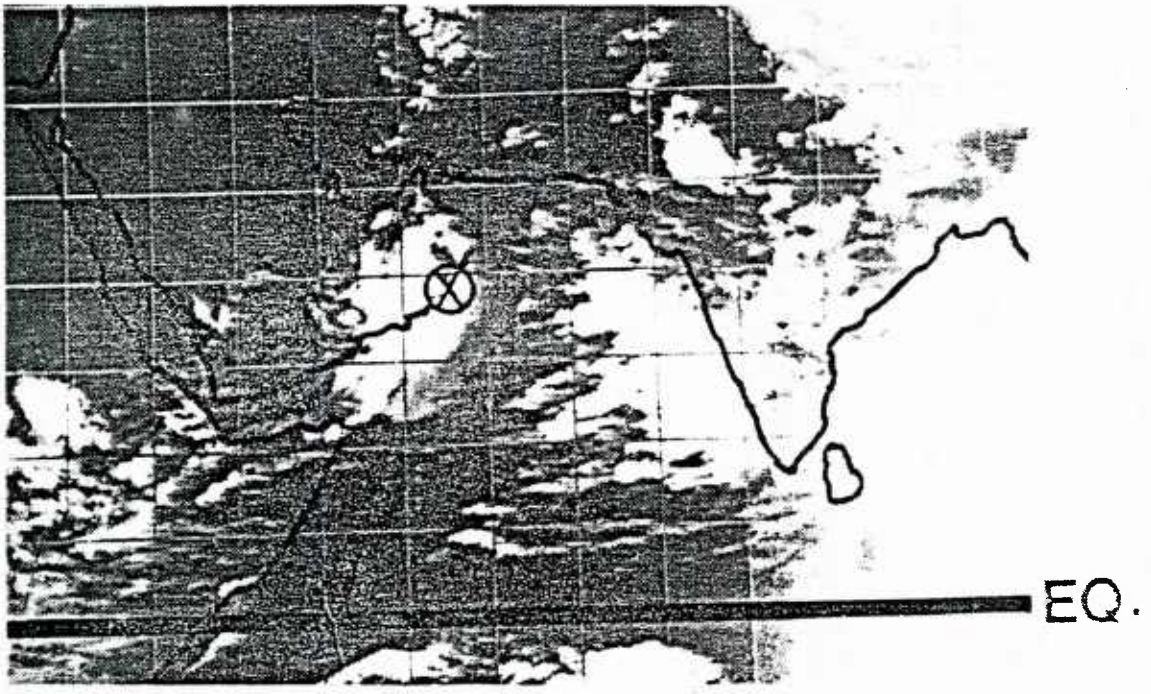

Fig. 32. Satellite pictures of TC 18-79 at 18Z, June 19. Center is circled.

its moving close to the dry Arabian Peninsula. Similar weakening of tropical cyclones can occur off the northwest Australian Coast if dry desert air should be advected into the storm system.

Although TC 18-79 weakens rapidly after 18Z June 19, both the low-level and upper-level outer circulation patterns are well maintained until 12Z June 20 (V_{max} = 20 kts) as seen in diagram a of Fig. 33. Despite the zero line of this figure moving to a lower altitude, the low-level cyclonic circulation still has a magnitude of 5-7 m/s at 10° radius. Diagram b of Fig. 33 indicates that a closed cyclonic circulation is still present over a broad region at this time even though the inner maximum wind strength has greatly decreased. Maximum winds have also shifted to the south and southeast of the center. This is due to a westward movement of TC 18-79 away from the strong low-level ITCZ westerly flow which held its position at the same location. DeAngelis (1980c) has speculated that TC 18-79 helped bring about the advance of the southwest monsoon over the western portions of the Indian subcontinent. Krishnamurti, et al. (1981) have presented evidence that a low-level tropical cyclone vortex often forms in the Arabian Sea just prior to the advancement of the summer monsoon over India in June.

6.3 TC 23-79

TC 23-79 was first reported as a monsoon depression at 02Z Sept. 18. Prior to this time, JTWC had traced the pre-TC 23-79 tropical disturbance for more than two days. It tracked westward across the southern end of the Indian subcontinent (Fig. 34) and into the Arabian Sea. Loosely organized convection was associated with this disturbance. The upper-level prevailing wind was from the east. The plan view of the

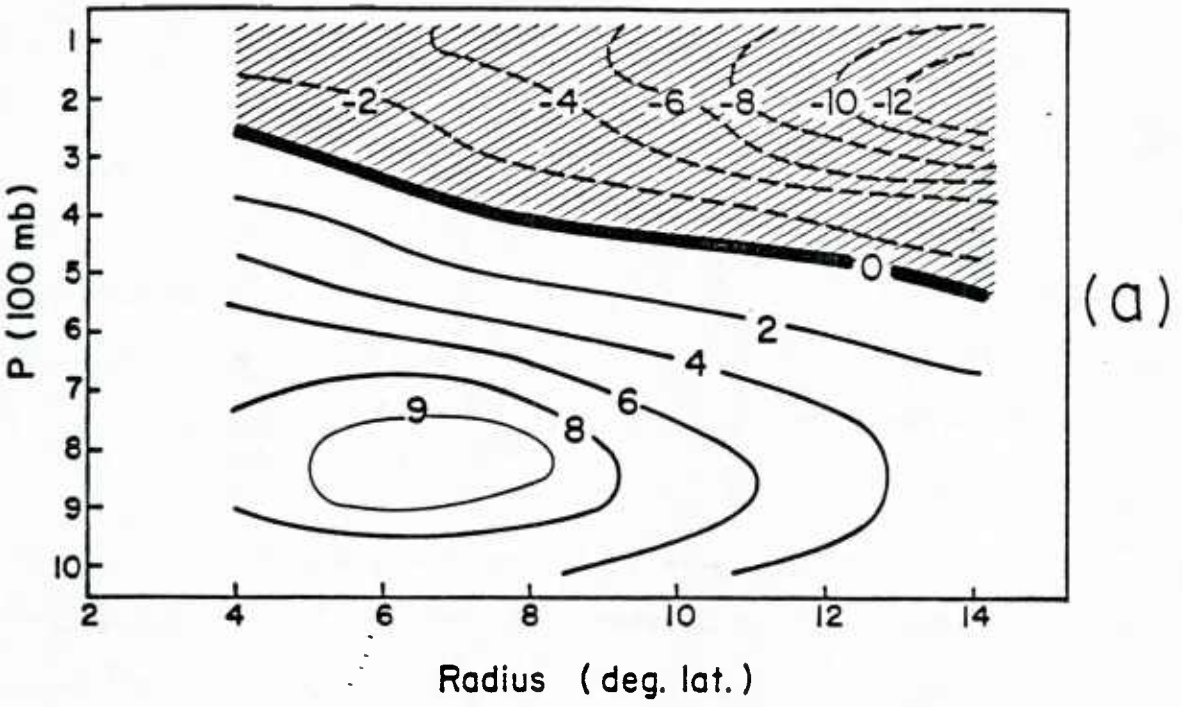

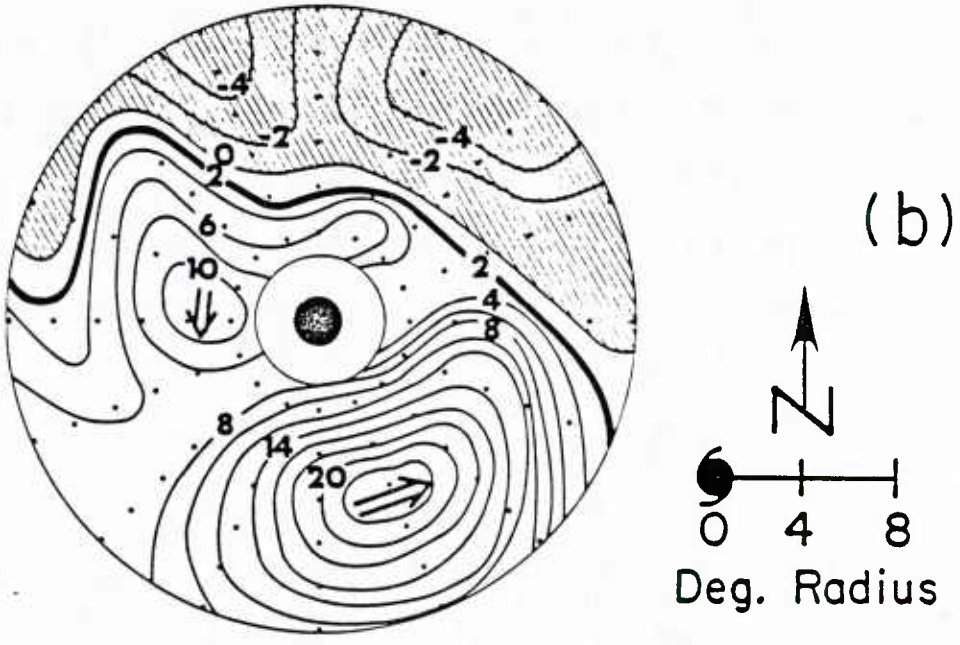

Fig. 33. The cross section of average tangential wind (V_t) of TC 18-79 at 12Z June 20 (diagram a) and the plan view low-level 1000 to 700 mb average tangential wind (V_t) at 12Z June 20 (diagram b). Wind speeds in m/s.

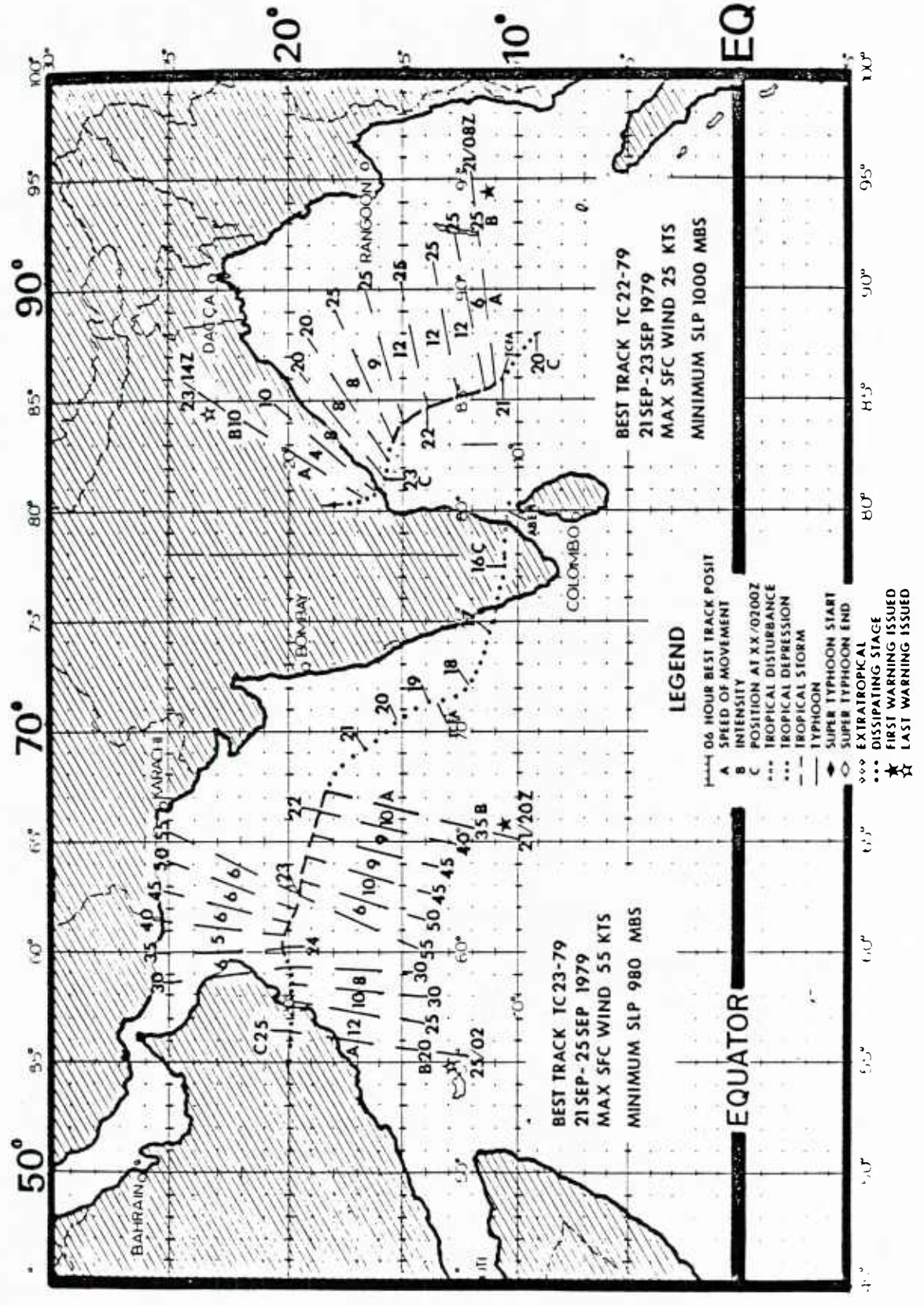

Fig. 34. Best track of TC 23-79 and TC 22-79 (JTWC ATR 1979).

upper-level radial wind at 12Z September 17 showed an inflow on the eastern side and an outflow to the western side of the center (diagram a of Fig. 35) or a westward blow-through at upper levels. This outflow shifted with time (diagram b - September 18th) and, on the 20th (diagram c), there is a double outflow to the southwest and the northeast. Double outflows are, in general, more conducive to cyclone intensification.

The time series of the V_{max}, the low-level outer circulation, and the upper-level outflow are shown in Fig. 36. Like those of TC 17-79 and TC 18-79, the low-level outer circulation increases (from 3.2 m/s to 6.4 m/s) prior to the formation of TC 23-79. Diagrams a and b of Fig. 37 show the plan view of the low-level circulation at 12Z September 16, 12Z September 17, and 00Z September 18 in a moving coordinate relative to TC 23-79's center. As with the two previously discussed cyclone systems, the initial cyclonic circulation is concentrated in the southern part of the region; while in the northern part, the flow is hardly cyclonic at all. The maximum tangential wind is located 8-10^{o} south of the center with a magnitude of 16-17 m/s. On the synoptic chart, the pre-TC 23-79 disturbance is located north-northeast to a low-level westerly wind maximum which is likely driven by the cross-equatorial monsoonal flow from the east coast of Africa.

Note how the flow on the north side of the TC 23-79 system becomes more cyclonic and extends out to 6-8^{o} radius. This results in an increase of the low-level outer circulation despite the decrease of the maximum cyclonic circulation to the south. At 00Z September 18, the

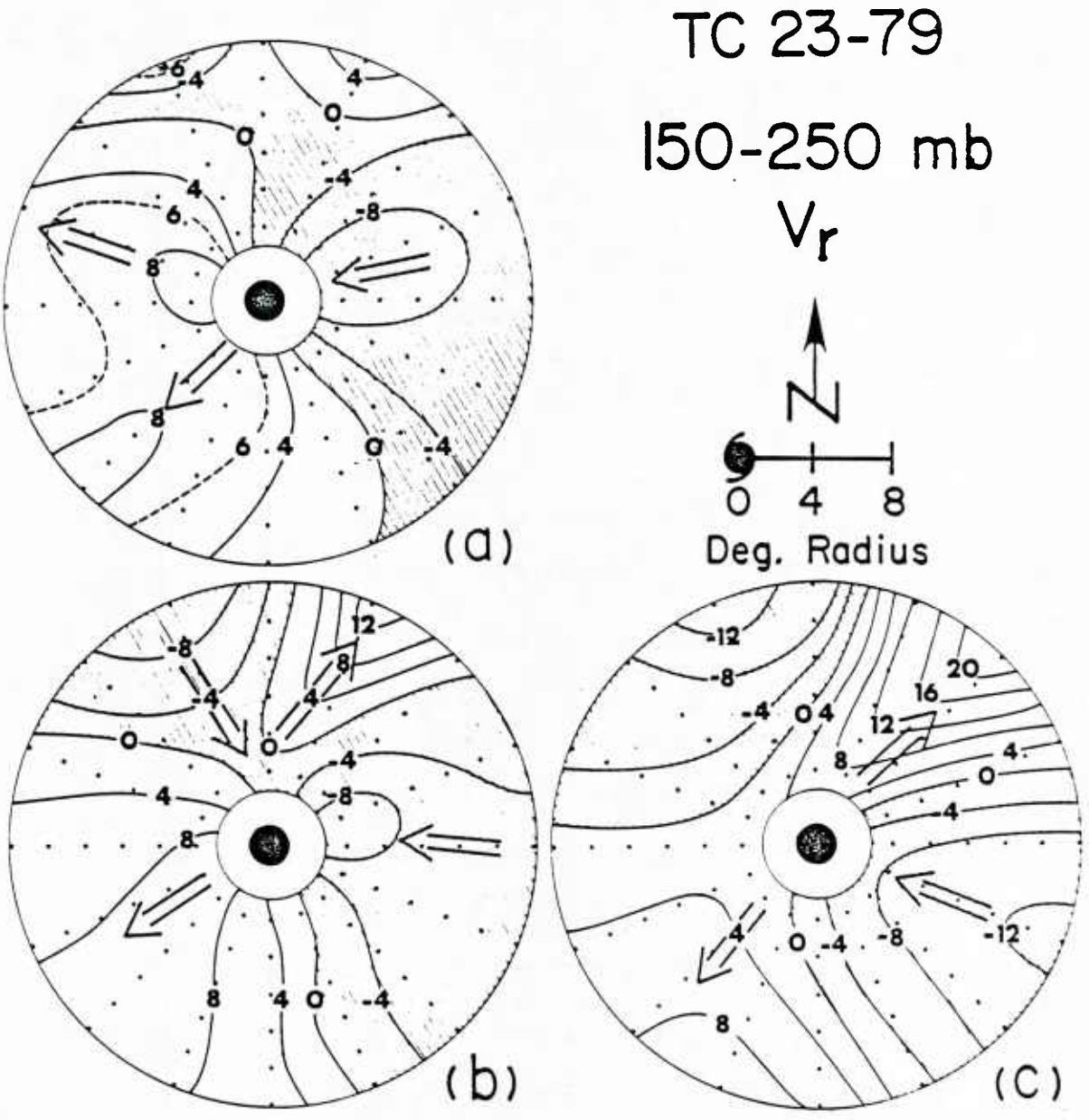

Fig. 35. Plan view of upper-level mean radial wind (V_r) in m/s between (150-250 mb levels relative to the moving center of TC 23-79 at 12Z September 17 (diagram a), 12Z September 18 (diagram b), and 12Z September 20 (diagram c) moving coordinate.

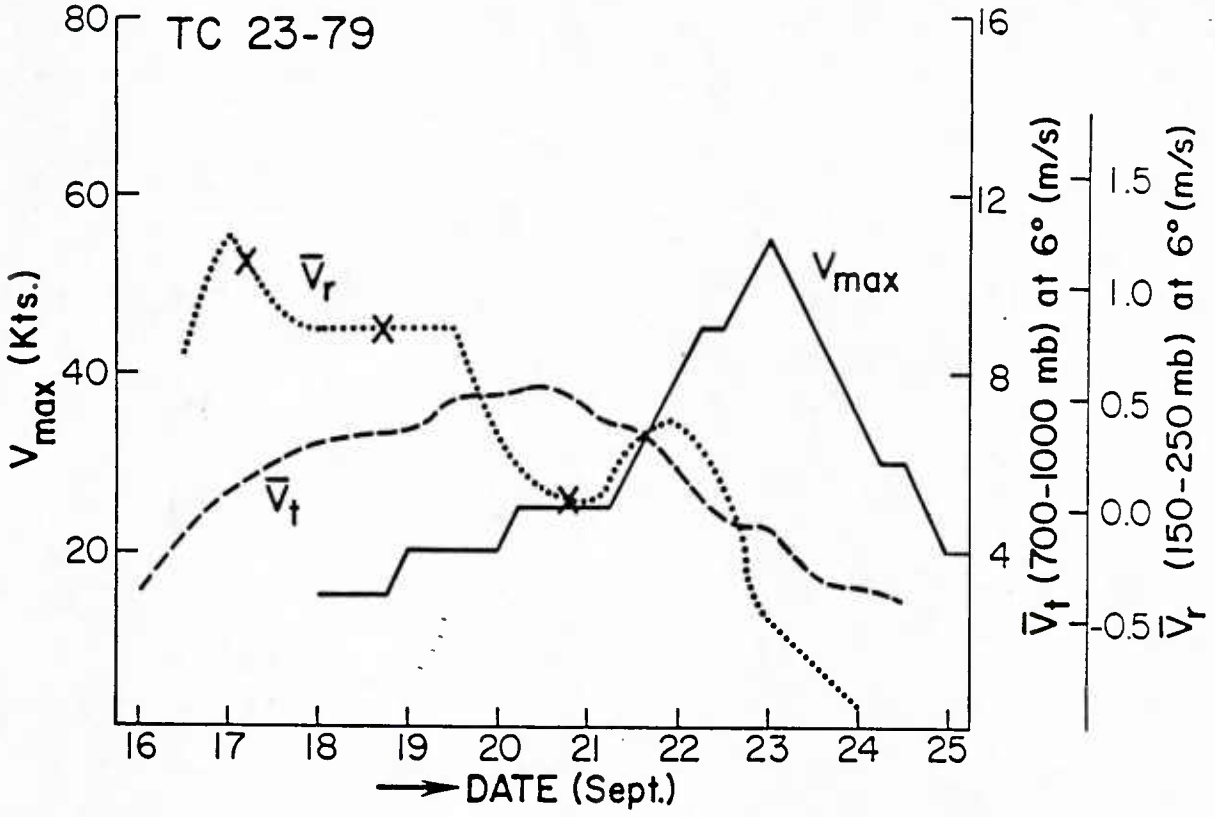

Fig. 36. Time series of cyclone intensity (V_{max}) and low-level outer circulation ($\bar{V}_t$) and upper-level outflow ($\bar{V}_r$) at 6° radius for TC 23-79.

maximum cyclonic circulation increases to 16 m/s and moves in closer to the center. The cyclonic circulation to the north and northeast of the center also shows a gradual increase of the circulation about TC 23-79.

Unlike TC 17-79 and TC 18-79, the development of TC 23-79 is rather slow after the initial organizing of the system on 00Z September 18. Intensity increases only from 15 kts to 25 kts in three days. The low level outer circulation increases only slightly from the 18th to the 20th and then decreases. The most peculiar feature in the time series is the early peaking of the 6° radius upper-level outflow at 00Z September 17 and then the decrease of the outflow between 00Z September 17 and 00Z September 18. A much greater decrease occurs between

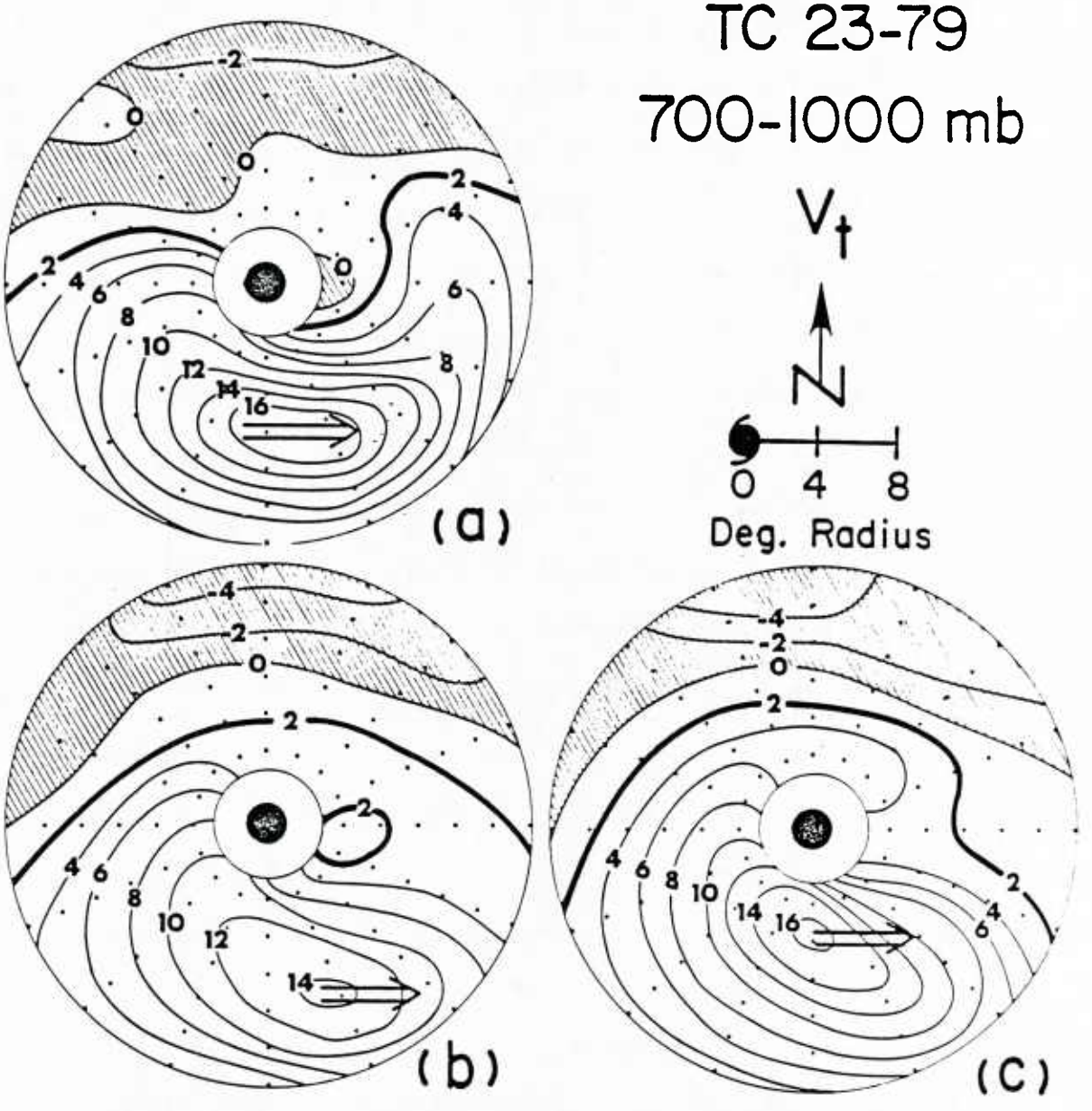

Fig. 37. Plan view of low-level circulation (700-1000 mb V_t) of TC 23-79 at (a) 16 12Z, (b) 17 12Z, and (c) 18 00Z of September for pre-TC 23-79 disturbance in a moving coordinate.

12Z September 19 and 00Z September 21. This is likely a result of the inward concentration of the convection at the expense of the outer convection and a change in the surrounding flow patterns.

The IR satellite pictures of TC 23-79 at 06Z September 17, 18Z September 18, and 18Z September 20 are shown in Fig. 38. The corresponding radial outflows at these three time periods are shown as "X" marks in Fig. 36. Cloudiness at 06Z September 17 is spread over a much larger domain than on the 18th or the 20th. The prevailing easterly flow causes a major outflow to the western side of the convection as is seen in diagram a of Fig. 35. A northeast outflow jet is established on the 18th. This is due to the approaching of the upper-level trough to the northwest of the system.

At 18Z September 20, the cirrus coverage becomes greatly reduced. The outflow to the northeast side increases while the outflow to the west, southwest and south sides reduces and becomes confined to a much narrower region. These features can be seen from both the satellite IR image (diagram c of Fig. 38) and the upper-level radial winds (diagram c of Fig. 35). The prevailing upper-level flow has undergone a change to be more from a southerly as opposed to an easterly direction as TC 23-79 moves from the south side to the west side of the upper-level anticyclone center. The ECMWF upper-level 200 mb flow fields at 00Z September 21 and 00Z September 22 are shown in Fig. 39. TC 23-79 is now located to the west side of the anticyclone. This 200 mb anticyclone does not change its location through the life cycle of TC 23-79. TC 23-79 moves from the south to the west side of the anticyclone.

TC 23-79 experiences a much stronger intensification rate after 06Z September 21. The upper-level outflow also increases slightly at this

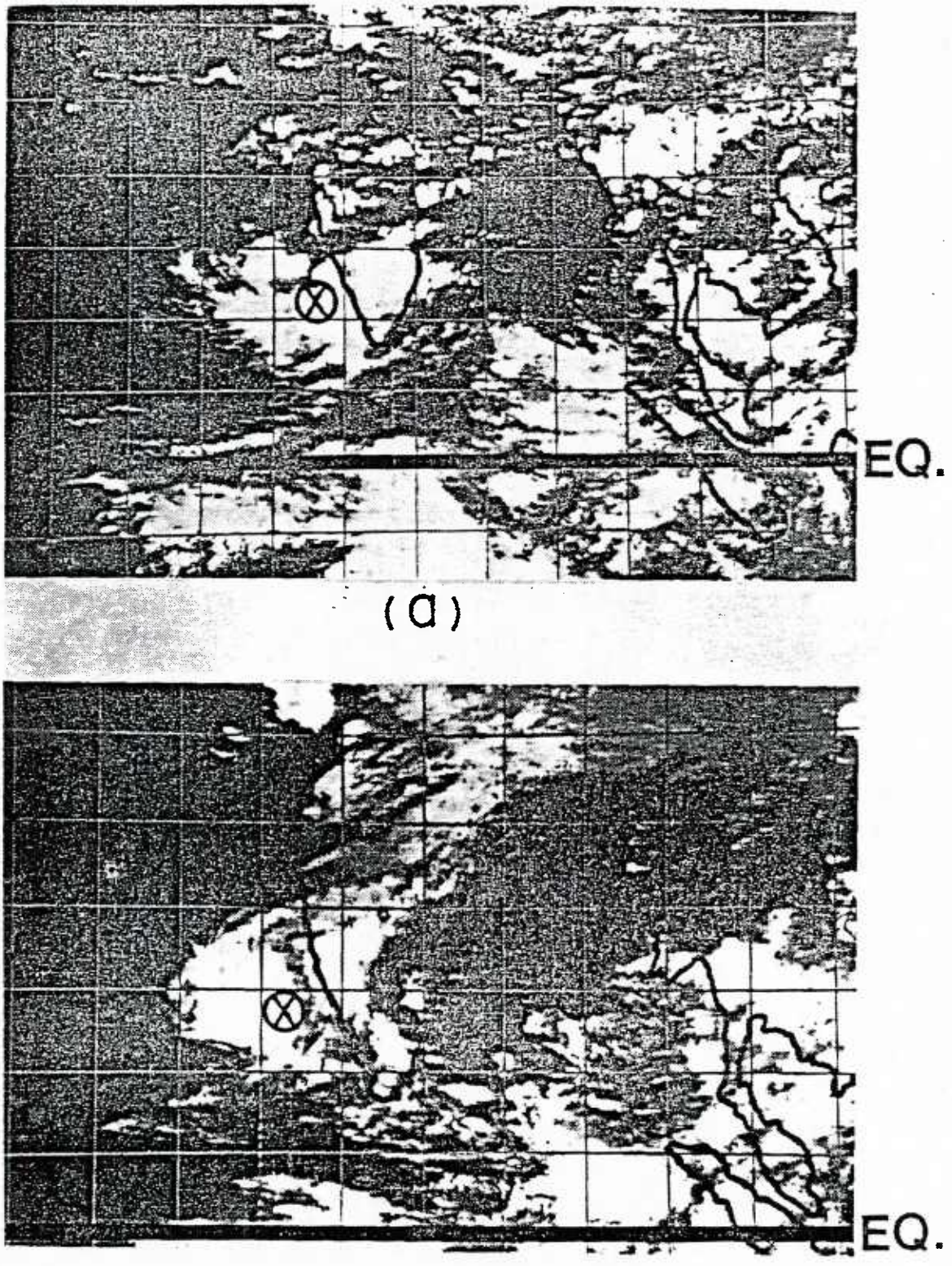

((Figure 38 -- caption on following page))

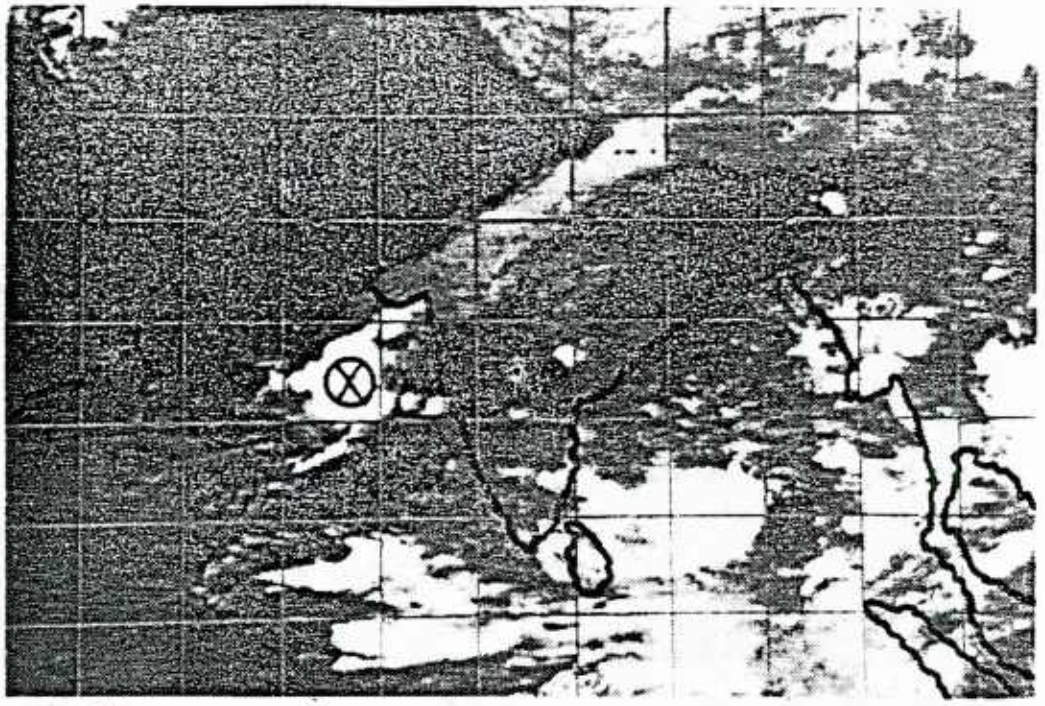

(C)

Fig. 38. Satellite picture of TC 23-79, center is circled, at 06Z September 17 (diagram a), at 18Z September 18 (diagram b), and at 18Z September 20 (diagram c).

time but decreases greatly after 00Z September 22. This outflow was much stronger 2-3 days before this major intensification period, however. This stronger intensification rate on the 22nd and 23rd is believed due to the approach of the upper-level trough from the northwest. This creates a poleward outflow jet as seen in diagram c of Fig. 35. The upper-level circulation patterns at 00Z September 21 and 00Z September 22 (Fig. 39) show this interaction between upper-level trough and the cyclone. As discussed by Chen and Gray (1984) and Sadler (1976), such an increase in outflow jets is usually favorable for tropical cyclone intensification.

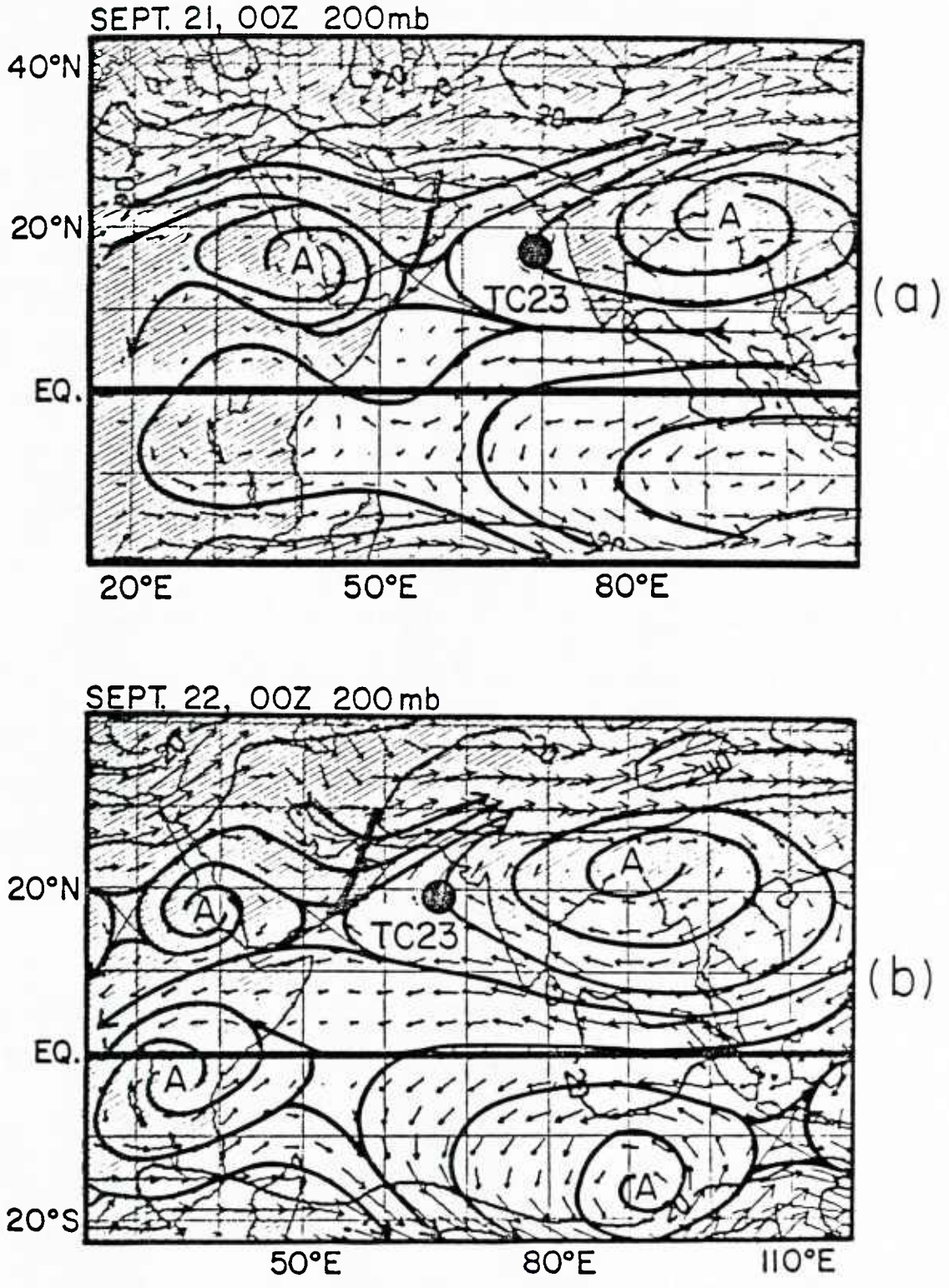

Fig. 39. 200 mb flow field at 00Z of (a) September 21 and (b) September 22. Circle is the center of TC 23-79. Length of arrows is proportional to wind speed.

6.4 TC 22-79

Although named before TC 23-79, TC 22-79 formed in the Bay of Bengal after TC 23-79. It was officially named as a tropical cyclone at 02Z Sept. 20 with estimated maximum sustained winds of 20 kts. The best track for TC 22-79 is shown in Fig. 34. Since TC 22-79 formed very close to the Indian subcontinent, it did not last long (only three days) before it hit the land. No significant intensification was observed.

TC 22-79 formed east of the region where TC 23-79's initial cloud cluster had originated. Both systems were much affected by the westerly winds of the summer monsoon. Besides the equatorial flow off the east coast of Africa, another cross-equatorial flow also existed between 75-80°E or southwest to the center. (See Fig. 40). This cross-equatorial flow is likely a result of the strengthening of the circulation around Southern Hemisphere Tropical Cyclone TC 21-79 centered at 6°S, 82°E. DeAngelis (1980a) indicates that TC 21-79 formed on the 15th of September and attained its maximum intensity of 45 kts on the 22nd. This was the same period during which TC 22-79 was developing. The increase of the low-level outer circulation of TC 22-79 is also portrayed in Fig. 41. The plan view of the low-level tangential wind (figures not shown) indicated that this increase (as with the three previous systems) occurred mostly in the southwest quadrant at radii of 6-10° where the influences of the Southern Hemisphere tropical cyclone and the westerly monsoon flows merged.

At the upper level, an anticyclonic center is located near 20°N, 100°E causing a prevailing easterly wind over the vicinity of the pre-TC 22-79 cloud cluster. The increase of the upper-level outflow is a result of the increase of convection on the western side of the system.

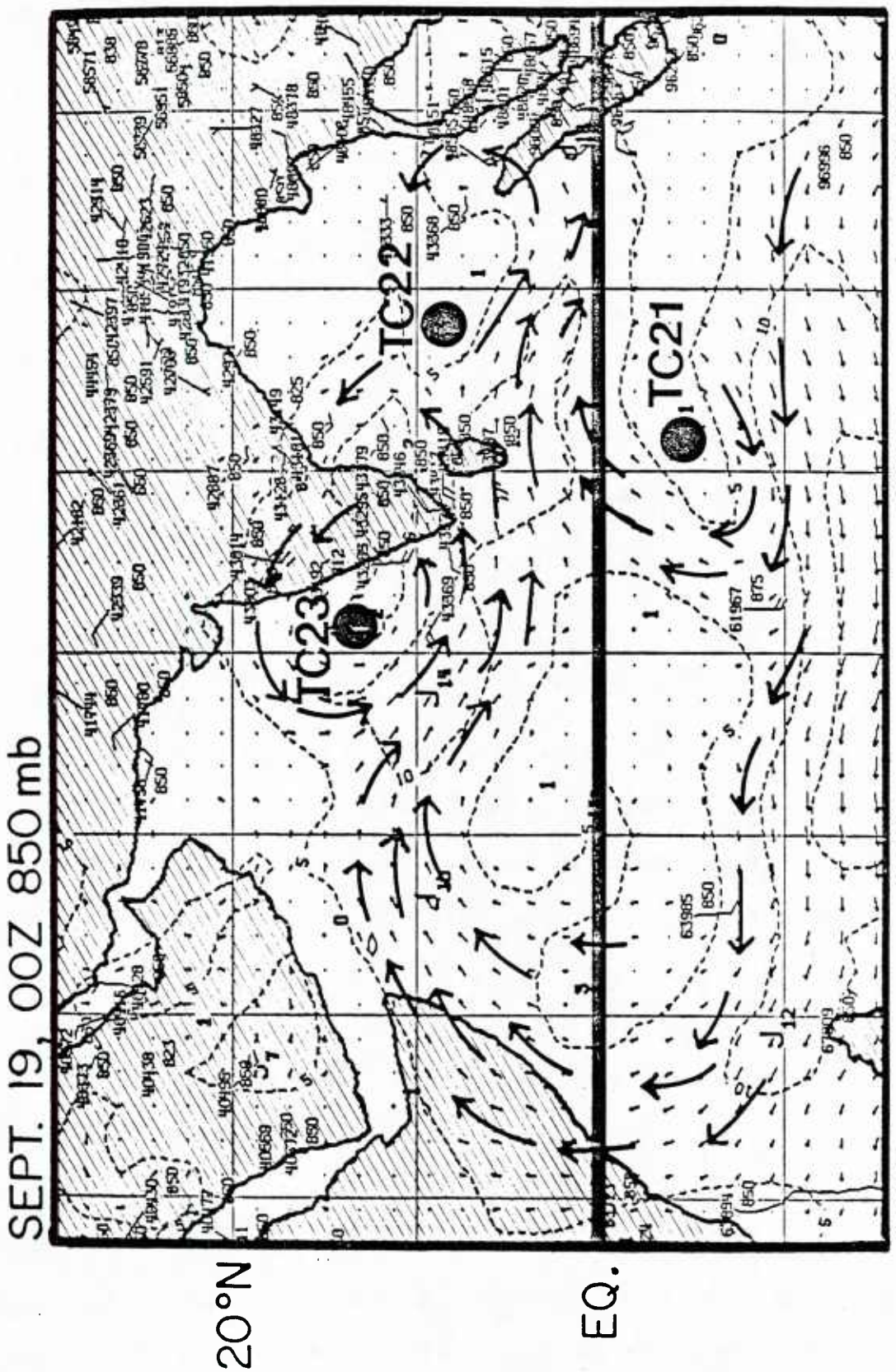

Fig. 40. 850 mb flow field at 00Z, September 19. Circles are the centers of TC 22-79 and TC 23-79.

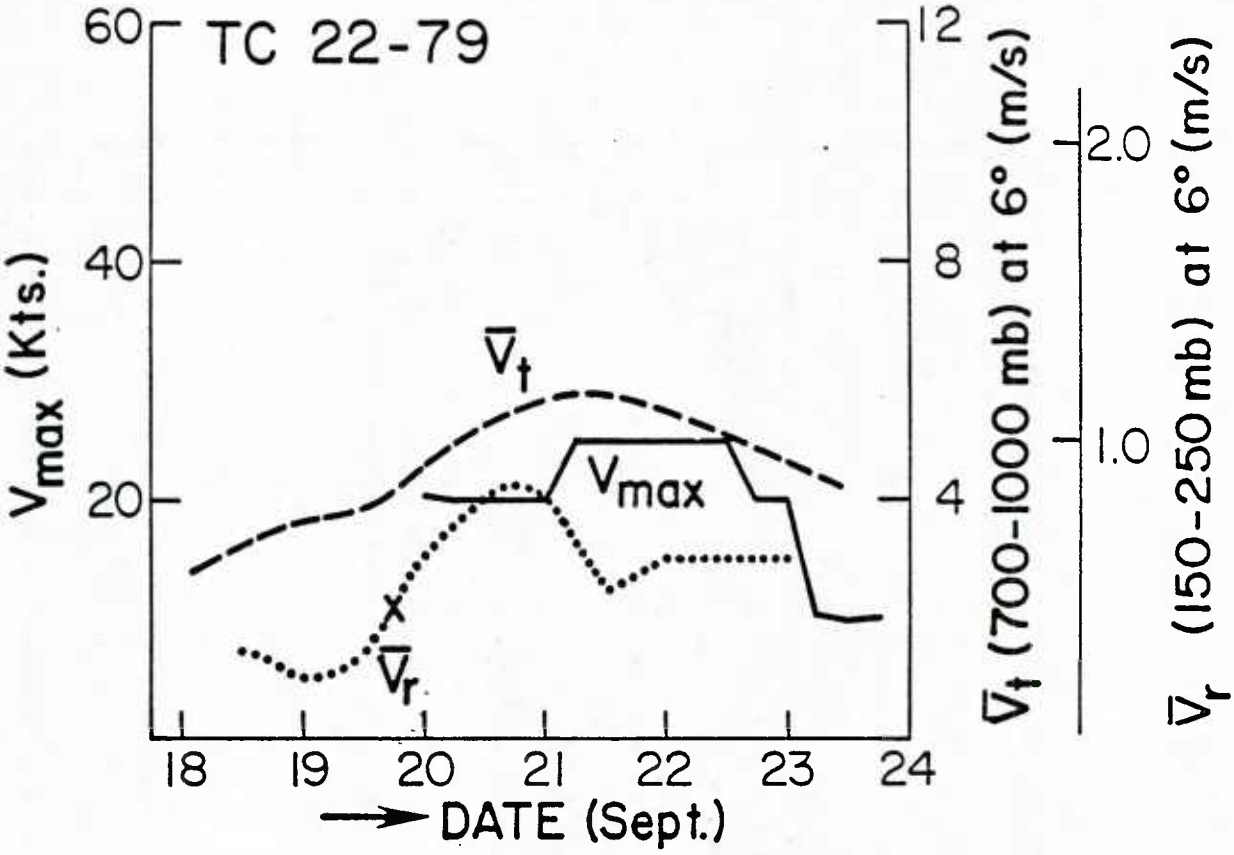

Fig. 41. Time series of cyclone intensity (V_{max}) and low-level outer circulation (V_t) and upper-level outflow (V_r) at 6° radius for TC 22-79.

Figure 42 shows the satellite picture at 18Z September 19 (this time marked by an X in Fig. 41), which indicates that the deep Cb convection and outflow is located mainly at the western side of the system. The plan view of the upper-level radial wind (not shown) also indicates an increase of outflow in this region. This further demonstrates that upper-level divergence which is associated with Cb convection around a tropical cyclone does not necessarily result in a significant intensification of the system. Our project's research in recent years has clearly shown (Arnold, 1977) that the amount of deep convection in a tropical system is not well related to the intensity or the intensity change of that system. It is the concentrated nature of the outflow into narrow channels that is the important ingredient of

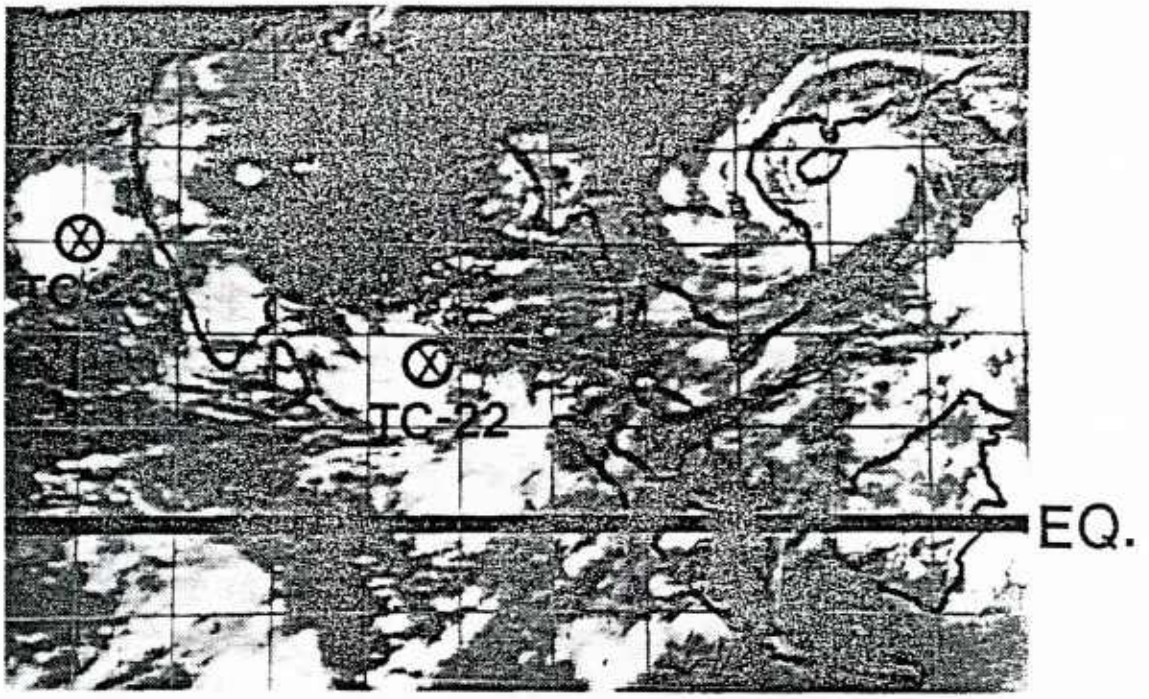

Fig. 42. Satellite picture of TC 22-79 at 18Z, September 19. Centers of TC 22-79 and TC 23-79 are circled.

intensification. This is not to say that the amount of deep convection is not better related to the strength of the cyclone as defined in section 4.

On the 22nd of September, the upper-level trough, which caused a major intensification of TC 23-79, moves eastward to the north of TC 22-79. However, no intensification is observed with TC 22-79 during this time period. One possible reason for this lack of TC 22-79's intensification is its close proximity to land at this time. Another reason, which is likely more important, is that the trough was too far away from the cyclone center. As can be seen from Fig. 43, the outflow associated with the trough to the north of TC 22-79 is not very strong and does not penetrate close to the storm center. This is more evident when a comparison is made with Fig. 35(c) which shows the upper-level

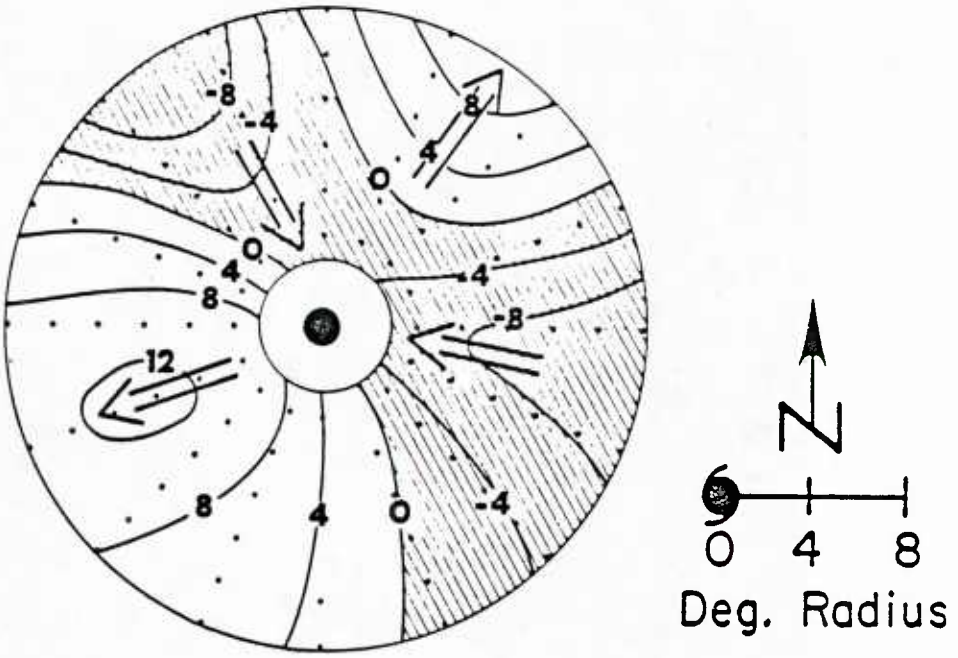

Fig. 43. Plan view of upper-level radial wind (150-250 mb $\bar{V}_r$) for TC 22-79 at 12Z September 22 in a moving coordinate.

outflow pattern of TC 23-79 associated with the passage of the upper-level trough. The outflow is not only much stronger with TC 23-79 but it extends inward very much closer to the cyclone center.

6.5 TC 24-79

Prior to the formation of TC 24-79 in the Bay of Bengal, loosely organized cloud clusters were spread all over the North Indian Ocean between the equator and 15° north. JTWC post-analysis identify the pre-TC 24-79 cloud cluster at 00Z October 27. This cloud cluster tracked north-northwestward on the first day (see Fig. 44). At 00Z September 28, the pre-TC 24-79 disturbance moved to the southwest side (cyclonic shear side) of the low-level southeasterly trade winds. It

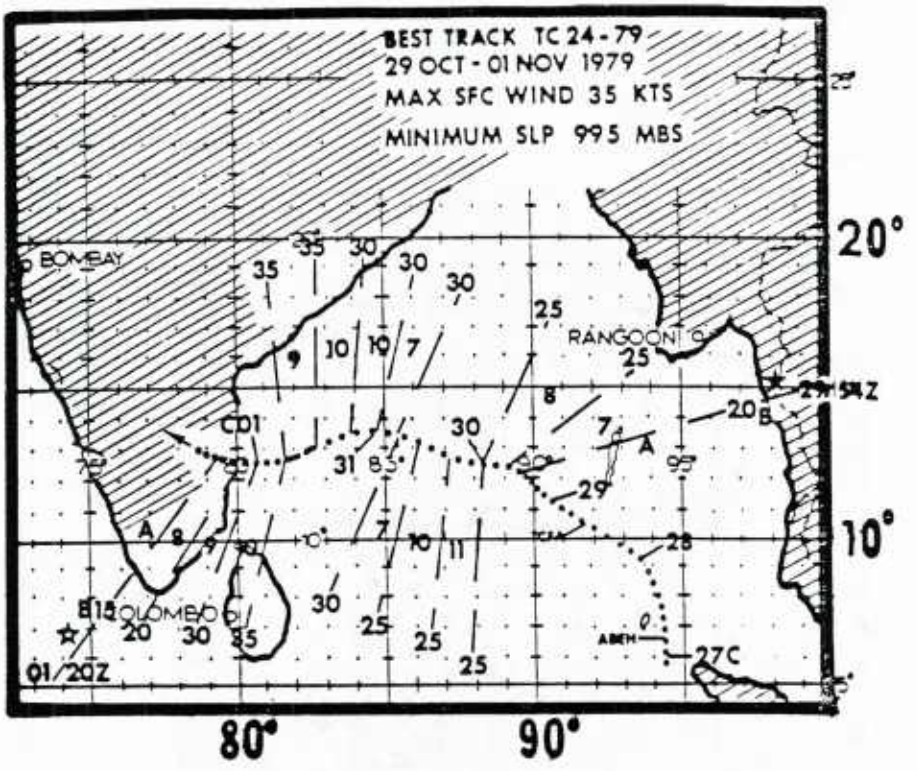

Fig. 44. Best track of TC 24-79 (JTWC ATR, 1979).

then turned on a northwest track and started to organize its convection. At 00Z September 29, it was named TC 24-79 with estimated maximum wind speed of 20 kts. The 850 mb flow at this time is shown in Fig. 45. Note in Fig. 45, that the low-level wind speed maximum is likely a consequence of the beginning influence of the winter season northeasterly monsoon flow. The organization of this tropical cyclone is thus distinctly different from that of the four previous systems where the initial cyclonic flow was initiated on the equatorward side from westerly winds. Following this low-level prevailing easterly flow, TC 24-79 tracked westward throughout most of its life and gradually increases its intensity before striking the Indian coast near Madras. The low-level cyclonic circulation of TC 24-79 is much

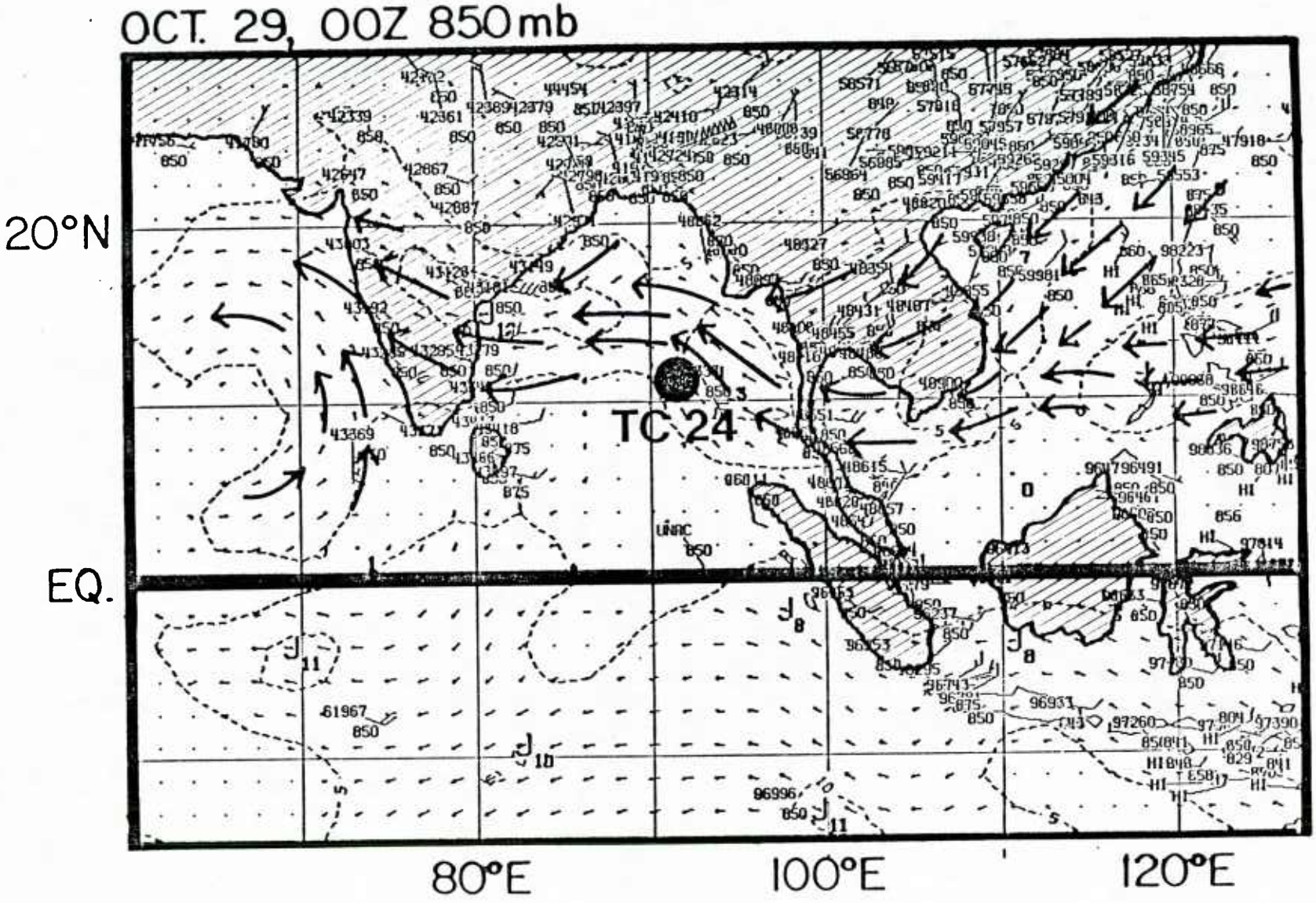

Fig. 45. 850 mb flow field at 00Z, October 29. Center of TC 24-79 is circled.

weaker than that of the other systems, even at its maximum intensity (Fig. 46). The low-level circulation was also much shallower in comparison with the other TC systems. In fact, TC 24-79 is a relatively small (in view of the radial domain) system especially in the coverage of its satellite cloudiness. The mechanism which maintains TC 24-79's slow developing appears to be the coupling between the low-level vorticity and the upper-level anticyclonic circulation. TC 24-79 had a strong upper level anticyclonic surrounding circulation throughout its life.

6.6 TC 25-79

TC 25-79 was a large tropical system. Gusts up to 35 kts were in evidence out to 300 miles from its center (DeAngelis, 1980b). This was, however, a very strange tropical cyclone for two reasons. First, it did not have a recognizable cloud pattern -- something almost always associated with any tropical cyclone that forms. Even at its maximum intensity (40 kts) at 06Z November 16, convection was still not well-organized near the center. Secondly, TC 25-79 followed a basically straight northward track as shown in Fig. 47. To understand why it moved straight northward, we have to look at both upper- and low-level flows. At upper levels, a trough was located over the Arabian Peninsula with strong south-southwesterly flow existing over the Arabian Sea region. At low levels a southeast monsoon flow was found over the Indian sub-continent. TC 25-79 was located on the southwest side (cyclonic shear side of a low-level southeast monsoonal wind speed maximum). The northward track of TC 25-79 is a result of the combination of the upper-level southwesterly and low-level southeasterly steering flows. The net zonal steering component was near zero.

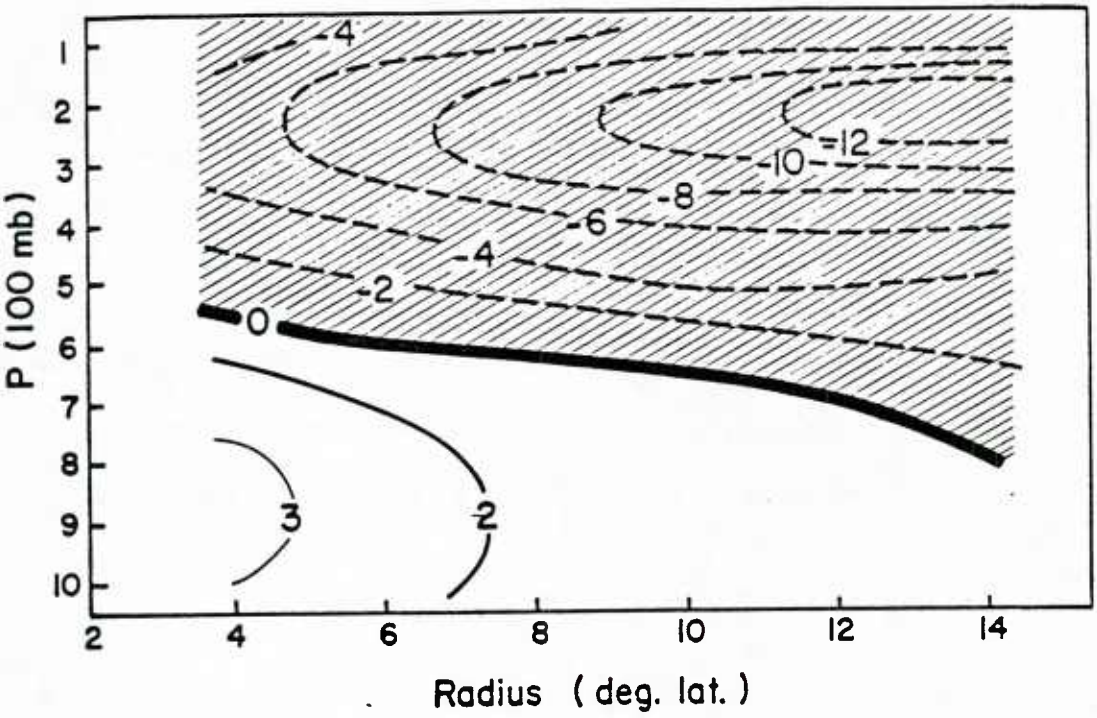

Fig. 46. Cross section of tangential wind for TC 24-79 at 12Z, October 31.

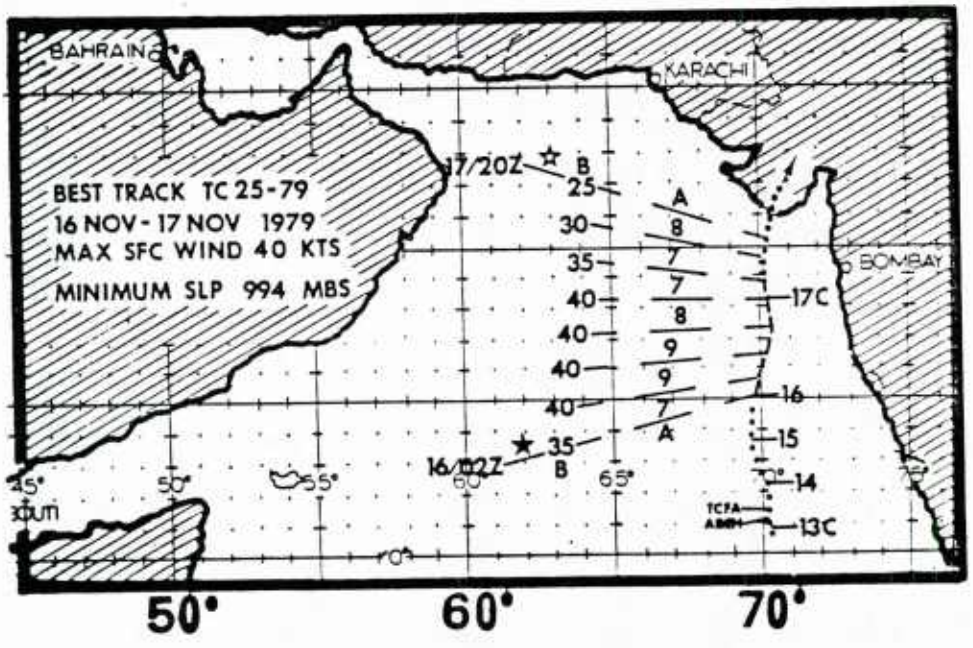

Fig. 47. Best track of TC 25-79 (JTWC ATR, 1979).

Since TC 25-79 does not have a well organized cloud pattern, the post-analysis by JTWC does not have it identified until 12Z November 14. However, its low-level circulation was well-established at 00Z November 13. Figure 48 shows the time progression of the maximum wind (V_{max}), the low-level outer circulation, and the upper-level outflow. Note that the low-level circulation increases greatly from 00Z November 12 to 00Z November 13. It is likely that JTWC post-analysis should have named TC 25-79 a little earlier. Also, note that, as with the previous system, the upper tropospheric outflow ($\overline{V}_r$) peaks before the maximum intensity of the cyclone is reached.

The upper-level outflow is very strong until 00Z November 16. Two significant increases of upper-level outflow occur between 12Z November 12 and 00Z November 14 and between 12Z November 15 and 00Z November 16. The former one is due to the enhanced convection to the west of the center of the pre-TC 25-79 cluster. (No significant intensification was associated with this increase of outflow.) The nighttime IR satellite images at 18Z November 13 is shown in Fig. 49. An upper-level trough is located to the northwest of this convective region. Note that this cloud pattern largely dissipates in 24 hours and leaves a less defined cloud pattern. The upper-level outflow to the north and northeast is also very pronounced, however.

The second increase of upper-level outflow is a result of the approaching of the upper-level trough that strengthens the northeast outflow jet. Figure 50 shows the 200 mb flow features at 00Z November 15. The northeast outflow jet is found mainly to the north and northeast of TC 25-79. It is this outflow jet that probably leads to the intensification of TC 25-79 between 12Z November 15 and 18Z November 16.

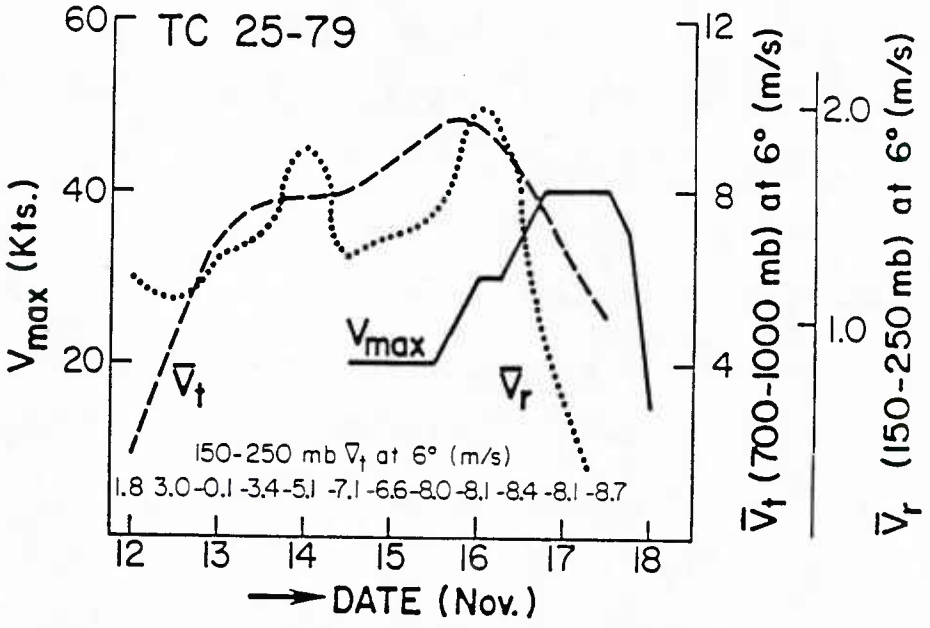

Fig. 48. Time series of cyclone intensity (V_{max}) and low-level outer circulation (V_t) and upper-level outflow (V_r) at 6° radius for TC 25-79. Also shown is 150 mb - 250 mb tangential wind at 6° radius.

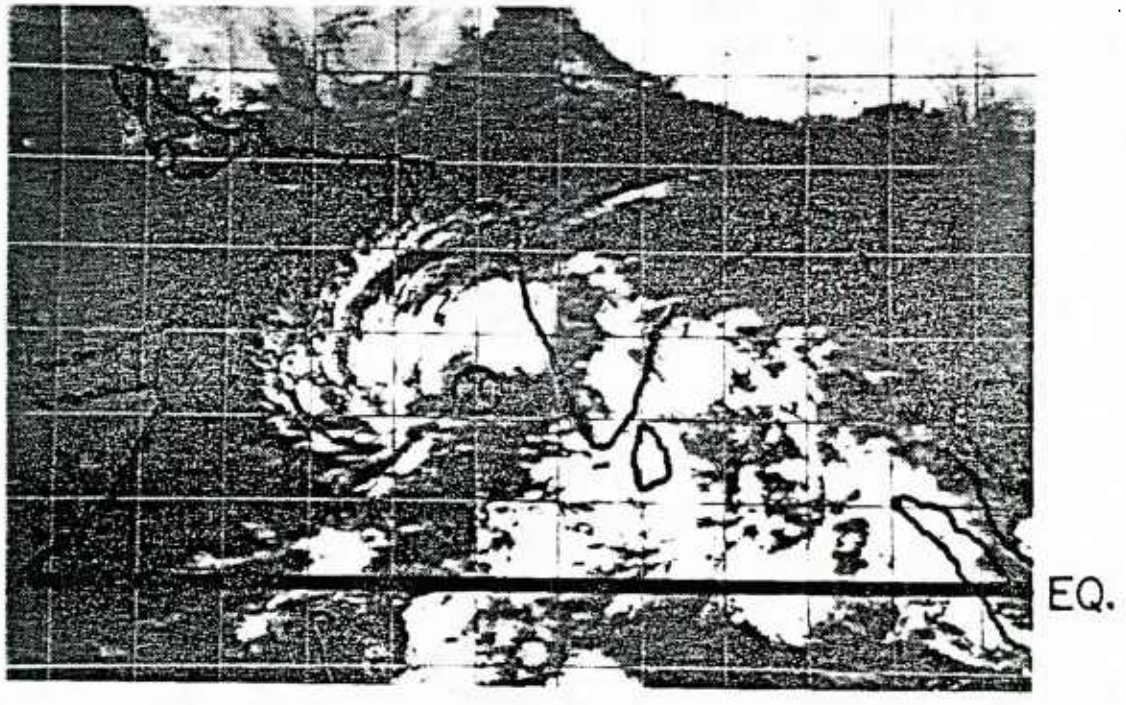

Fig. 49. Satellite picture of TC 25-79 at 18Z, November 13. Center is circled.

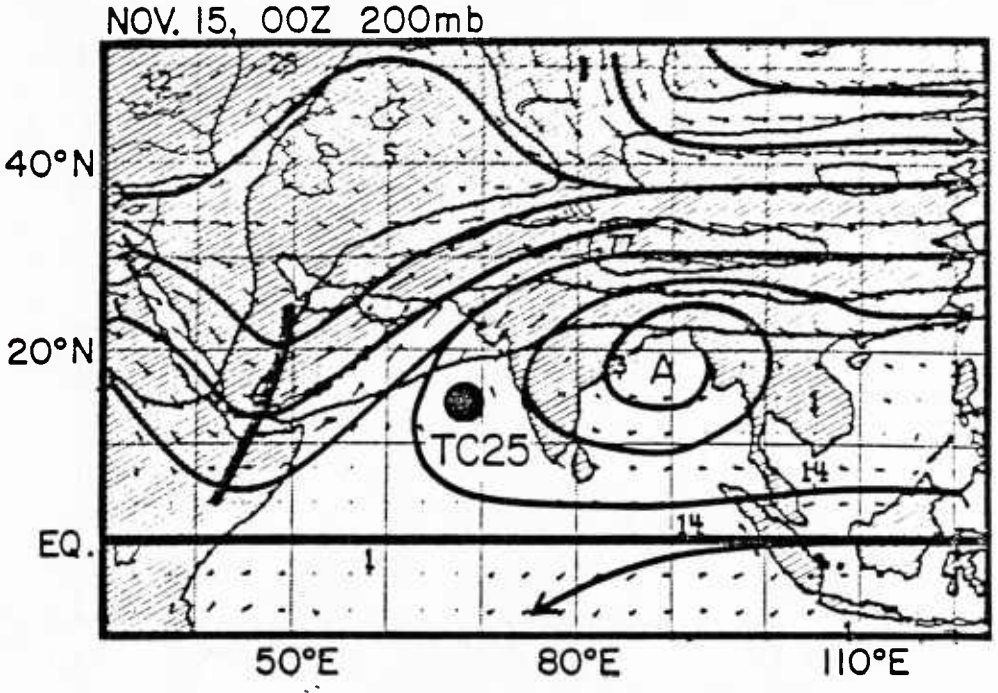

Fig. 50. 200 mb flow field at 00Z, November 15. Center of TC 25-79 is circled. Length of arrows is proportional to wind speed.

6.7 TC 26-79

TC 26-79 developed in the Bay of Bengal in late November with easterly trade wind flow on its north side (Fig. 51). It was very similar to TC 24-79 in both its track and the influence of the low-level trades on its poleward side. Figure 52 shows the 850 mb flow pattern at 00Z November 21 when TC 26-79 starts its organization. Note that TC 26-79 is located just to the southwest (cyclonic shear side) of the low-level wind speed maximum.

Although named at 12Z November 20, TC 26-79 does not have a clearly defined cloud pattern until 00Z November 23. Its low-level circulation pattern was also not well-established when it was named. However, the low-level vorticity was still large near the system during its early stages. At upper levels, an anticyclone center was located over the north border of the Bay of Bengal, with prevailing southeast wind over

the cyclone region. The upper-level anticyclonic circulation of TC 26-79 experienced a steady increase. No apparent strong outflow channels or significant intensification was observed with this system.

Using the results of the analysis of these seven individual cases, the next section will attempt to synthesize some of the important physical processes that seem to be occurring in N.I.O. tropical cyclones.

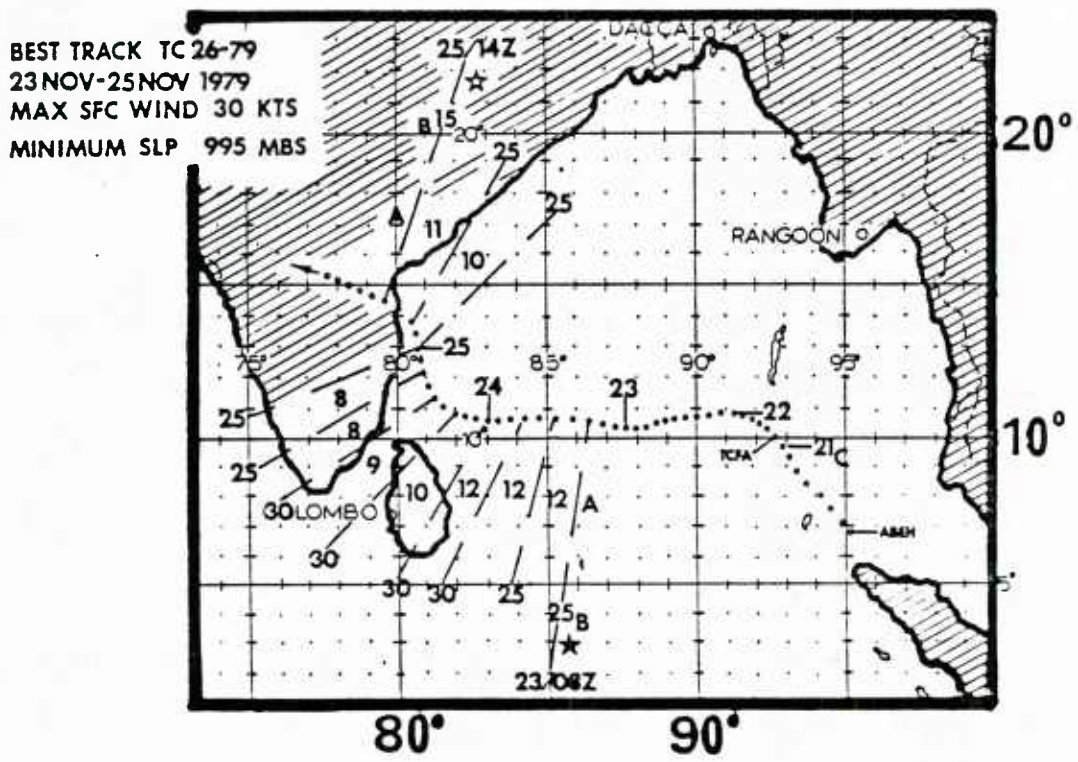

Fig. 51. Best track of TC 26-79 (JTWC ATR 1979).

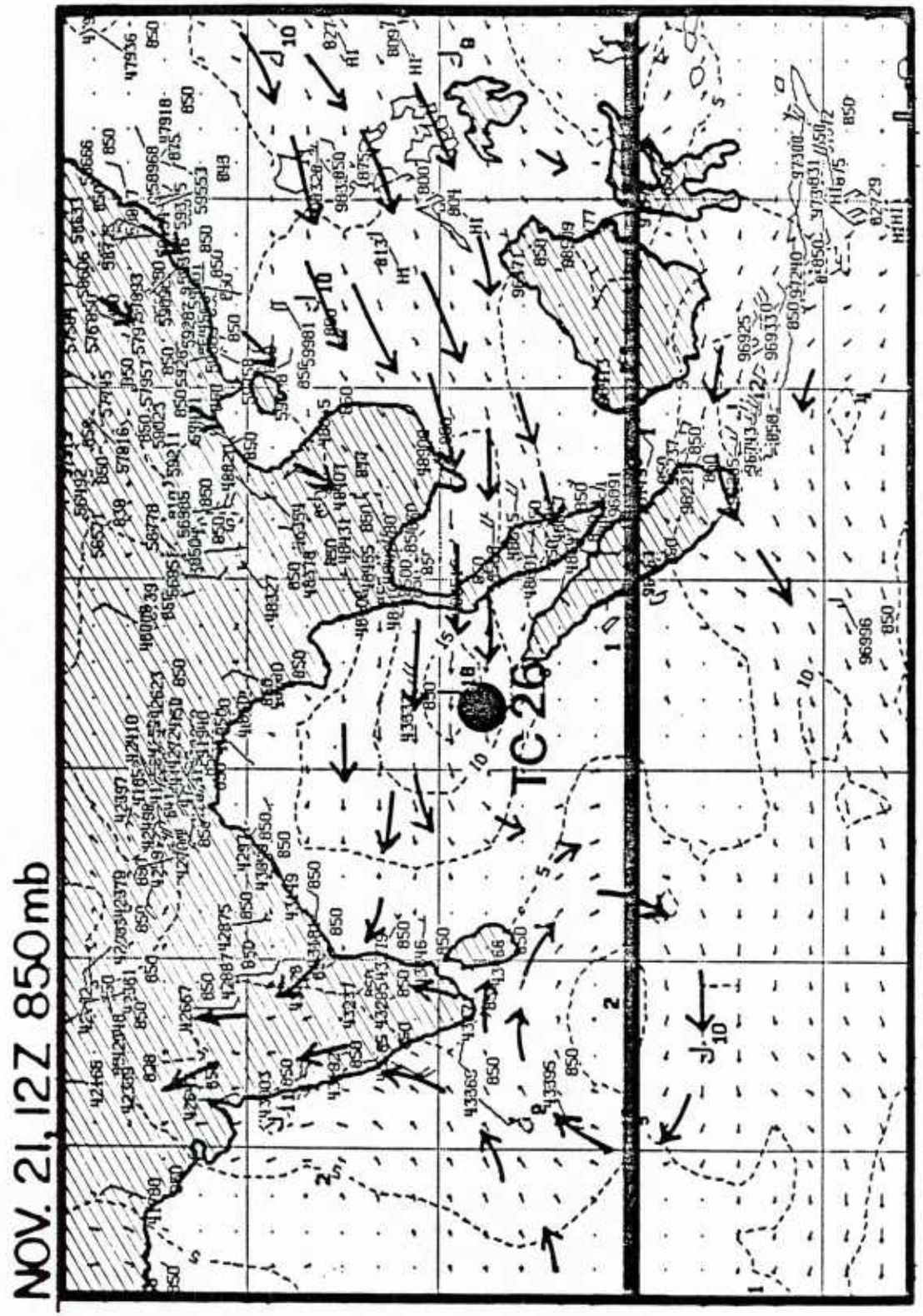

Fig. 52. 850 mb flow fields at 12Z, November 21. Center of TC 26-79 is circled.

7. DISCUSSION OF RELEVANT N.I.O. TROPICAL CYCLONE FEATURES

The previous section analyzed the large-scale circulation patterns for all seven tropical cyclones that formed in the North Indian Ocean during the 1979 FGGE-year period. Although there may be some inadequacies in the FGGE III-b data and analysis techniques, these data are still the best information available for any cyclone season. We believe the ECMWF analysis shows most of the important large-scale wind characteristics about these cyclone systems, particularly the rotational component of the wind field and the large-scale divergence patterns of the upper troposphere. We will now discuss the important general physical processes related to these tropical cyclones in terms of their influence on the genesis, intensification, structure and motion. It is recognized, however, that discussions based only on 1979 cyclone information may not always strictly apply to tropical cyclones occurring in this region for other years.

7.1 Characteristics of the Large-Scale Circulation Patterns During Tropical Cyclone Formation and Development

Like tropical cyclones in the northwest Pacific, N.I.O. tropical cyclones form within the monsoon trough region. To show this similarity to northwest Pacific cyclones, we have performed a similar north-south cross section averaging of zonal wind for the initial stages of all 39 systems that later became tropical cyclones in the northwest Pacific during the same FGGE year. Results are shown in diagram a of Fig. 53. Note the general similarity when comparison is made to the same average of the seven N.I.O. pre-tropical cyclones as seen in diagram b of Fig. 53.

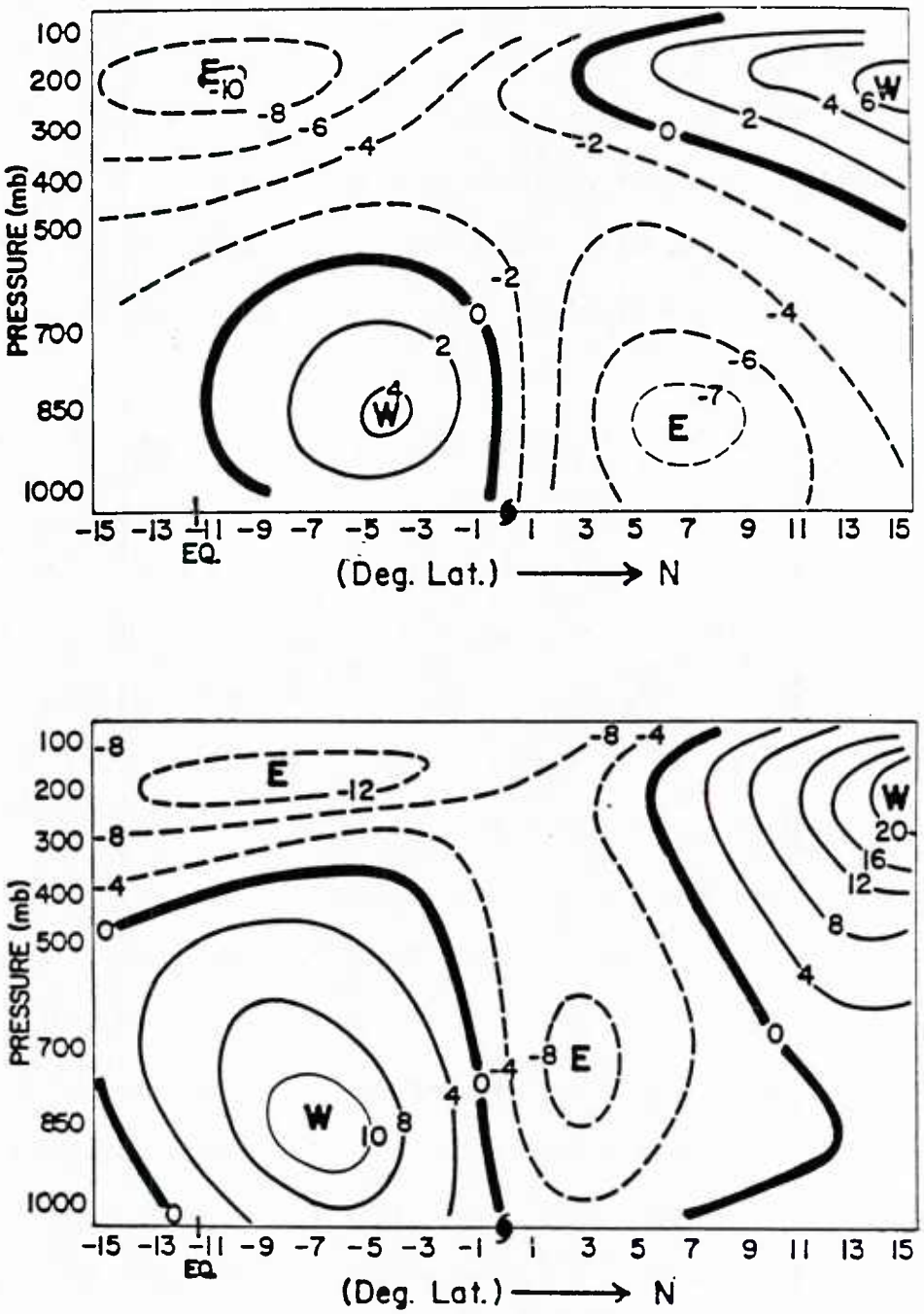

Fig. 53. North-South cross section of zonal winds (U), averaged for all 39 northwest Pacific tropical cyclones (a) and 7 North Indian Ocean tropical cyclones (b) in 1979, at their first 00Z time periods.

A few differences are to be noted, however. The easterly trade winds on the poleward side are much broader in the northwest Pacific; but the N.I.O. trade winds are of a comparable magnitude and are closer to the disturbance center.

The N.I.O. cases have a much stronger and broader monsoon-generated westerly wind component on their equatorward side in comparison to that of the northwest Pacific cases. Not only is this westerly monsoon flow stronger than in the Pacific, it is also much deeper. This implies that the equatorward westerly wind influences are more important to N.I.O. tropical cyclone formation than are equatorial westerly wind influences in the west Pacific.

The average wind fields for all the seven N.I.O. cases in 1979 reveal a very deep monsoon-generated cyclonic circulation around the center of the tropical cyclone formation region. An important feature from our previous case analysis is that there is always a build-up of the low-level cyclonic circulation prior to the formation of the tropical cyclone system. This feature is similar to the ITCZ type tropical cyclones of the northwest Pacific as has been observed by Lee (1984). Our analysis also shows that this low-level circulation build-up is mainly a result of the cross-equatorial monsoonal surges or other features that strengthen the westerly wind on the equatorward side of the pre-cyclone disturbances. Love (1982) has also observed similar equatorial side westerly wind increases about Pacific and Australian region tropical disturbances from opposite hemispheric middle-latitude cold surge penetrations into the tropics as illustrated in Fig. 54. The N.I.O. tropical cyclone forecaster should always be aware of such cold surge penetrations occurring in the Southern Hemisphere and their

potential for enhancement of the N.I.O. monsoon trough and TC formation.

In the latter part of the autumn season (mid-October to December), however, the needed low-level cyclonic circulation increase for TC formation may occur more on the poleward than the equatorward side of

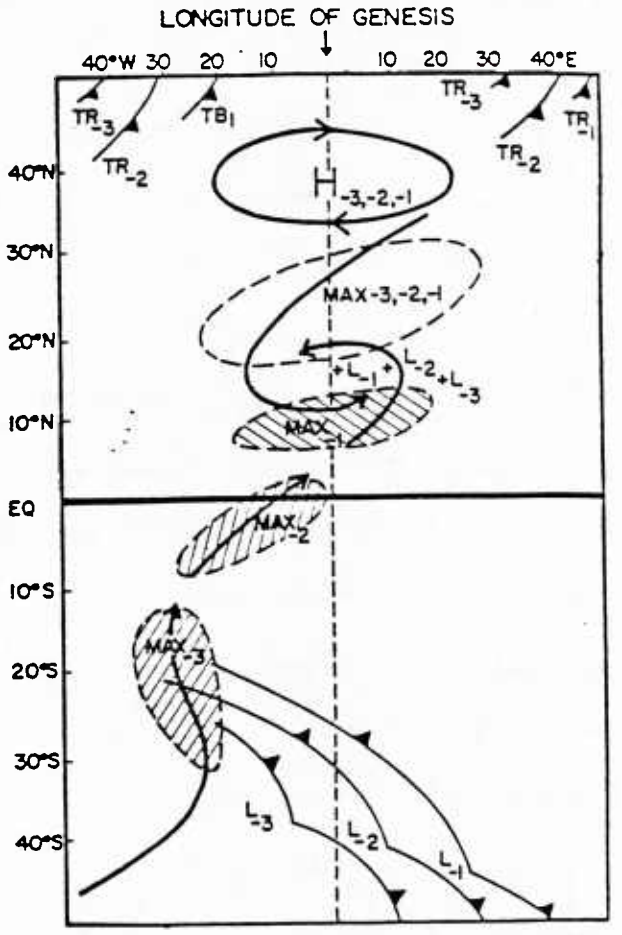

Fig. 54. Highly idealized gradient level streamline chart for the three days preceeding tropical storm genesis in the Southern Hemisphere. Subscripts -3, -2, -1 refer to the position of the system that number of days before genesis. The momentum burst has been shaded (from Love, 1982).

the pre-cyclone N.I.O. systems. It is thus possible for the main low-level cyclonic circulation build-up of N.I.O. systems to occur on either the equatorward or the poleward sides. The poleward trade wind circulation build-up may result from beginning East Asian winter season surges or other processes that act to enhance the trade winds.

Another special feature of the N.I.O. basin is the role of dual cyclones on either side of the equator. The strengthening of the equatorial circulation about a tropical cyclone in one hemisphere can cause a similar increase in the equatorial low-level circulation of the other hemisphere. Two of the seven 1979 cases were so affected. Keen (1982) and others have observed cross-equatorial tropical cyclone pairs to occur in both the Indian Ocean and in the Pacific.

A strong low-level positive vorticity field is thus very important to tropical cyclone formation in the N.I.O. as it is in most monsoon trough genesis regions as previously discussed by the second author Gray (1968, 1979). It is to be noted that the initial enhancement of low-level circulation about the pre-cyclone disturbance is typically on only one side of the disturbance (i.e., equatorward side or poleward side) and that the tip-off to early cyclone formation and later growth rests with the gradual wrapping around of the tangential wind field to the other sides of the cyclone.

It is to be noted by the time series of the individual storm profiles of V_{max}, $\bar{V}_T$ (700-1000 mb) and $\bar{V}_r$ (150-250 mb) at 6° radius - see Figs. 16, 27, 36, 41, 48 - how little related are these parameters. $\bar{V}_T$ can decrease or not decrease as V_{max} increases. These observations show how difficult it is to relate the maximum intensity of a N.I.O. tropical cyclone to the strength of the storm's outer circulation. These observations also show how little the magnitude of the cyclone's net upper tropospheric radial outflow (i.e. $\bar{V}_r$) is related to the cyclone's intensity. It is interesting, however, how the net upper-level radial outflow (and likely also the net deep cumulus convection) of most of these N.I.O. system peaked about 2 days before the date of

the observation of the maximum wind. A similar measurement has also been reported by E. Rogers (personal communication) in like-time series analysis of 20 Atlantic tropical cyclones. These observations would indicate that a blow-up or enhancement of deep cumulus convection (as might be measured by the satellite) in a tropical disturbance or weak tropical storm may be indicative of that system's future 1-3 day intensification.

Upper-level Flow Characteristics. McBride (1981), McBride and Zehr (1981) and others have emphasized the importance of the upper-level anticyclonic vorticity (besides the low-level positive vorticity) for tropical cyclone genesis in the northwest Pacific and Atlantic. We do not see the crucial role of the upper-level anticyclonic vorticity in the early stage genesis of our N.I.O. systems. Upper-level anticyclonic flow features might play an important role in the later intensification stages of N.I.O. cyclones, however.

We are finding that the increase of maximum winds (V_{max}) in a TC is not well related to the net upper-level outflow ($\bar{V}_r$) occurring around the tropical cyclone, but rather is more related to the concentration of this outward motion into narrow outflow channels (see Holland and Merrill (1984) and Chen and Gray (1984) for more discussion). Upper-level anticyclonic vorticity is required for the establishment of these narrow and strong outflow channels. The net radial outflow increase which is produced by an increase in the enhanced deep Cb convection within the tropical disturbance or tropical cyclone appears to be more related to the change in cyclone strength or the 1-3° mean tangential wind of the cyclone.

Chen and Gray have discussed the variety of upper-tropospheric

outflow patterns which can occur with tropical cyclones undergoing central-core intensification. An idealization of the variety of these outflow patterns is shown in Fig. 55. The type of outflow patterns associated with most N.I.O. tropical cyclones are those of pattern a, b, c, and d. A southwest outflow channel is sometimes established by the strengthening and westward movement or stretching of an upper-level anticyclone in the South Indian Ocean. Poleward outflow channels are typically produced by an eastward propagating upper-level trough to the poleward side of the cyclone. It is observed that a tropical cyclone can undergo an even more rapid intensification if double outflow channels are present to both the poleward and equatorward sides of the cyclone.

We have to emphasize that these outflow channels are the result of the interaction between the tropical cyclone and its surrounding environmental flow features which may, to a large extent, be independent of the particular internal processes of the cyclone.

7.2 Comparison of the Structural Characteristics of N.I.O. Tropical Cyclones with Western North Pacific Tropical Cyclones

Many cross sections of tangential winds for individual N.I.O. tropical cyclones have been shown. These tangential circulation patterns are in most respects quite similar to the tangential circulation patterns of the individual northwest Pacific cyclone systems. To verify this statement we have averaged the tangential wind field for three time periods for N.I.O. TC 17-79 just before it attained its maximum intensity of 85 kts. Result are shown in Fig. 56 - diagram a. Three weak typhoon systems in the northwest Pacific, Typhoon Ellis (85 kts), Typhoon Cecil (80 kts), and Typhoon Irving (90 kts) are selected for comparison with TC 17-79 (which was of an intensity close

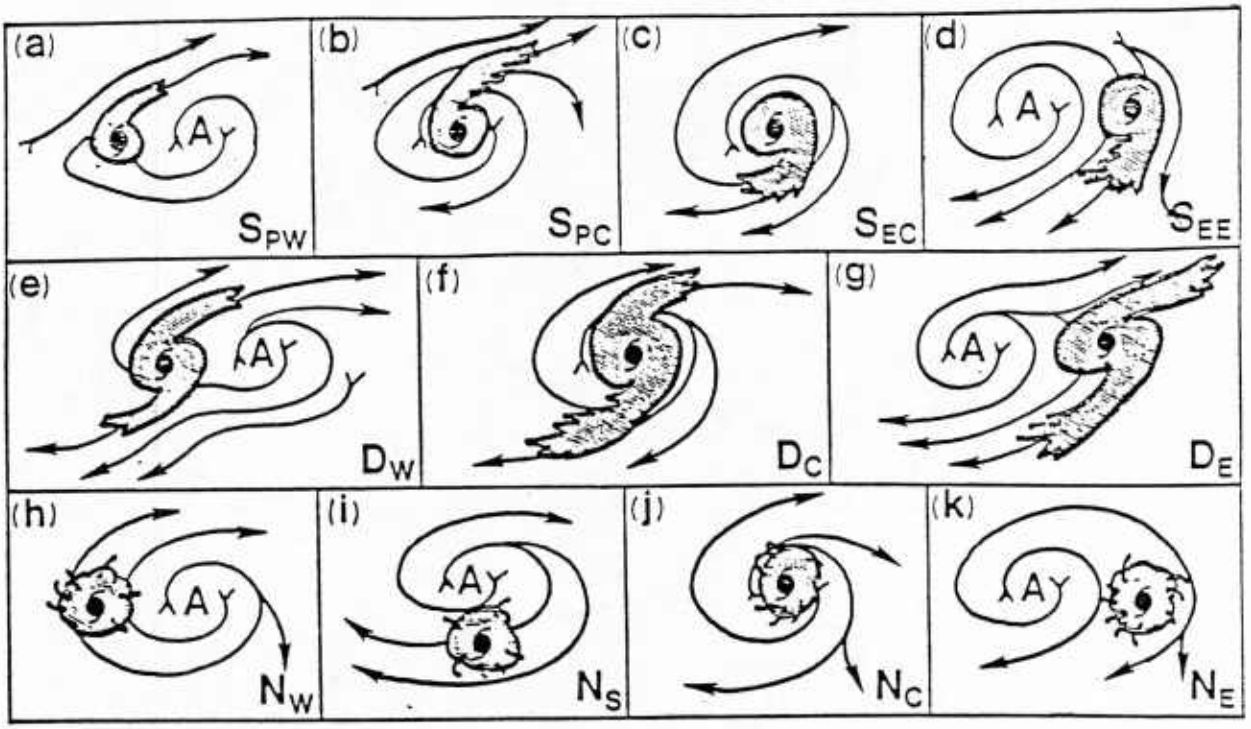

Fig. 55. Variety of outflow patterns associated with tropical cyclone intensification (from Chen and Gray, 1984).

to these systems). The same averaging was performed and is shown in Fig. 56 (diagram b). The results inside 3° radius are not reliable and have not been shown. Note how similar these two profiles are. The circulation about TC 17-79 is very much like that of the three minimal northwest Pacific typhoons. We can also make a comparison with the 10-year northwestern Pacific typhoon rawinsonde composite of Frank (1977), shown in diagram c of this figure. This latter rawinsonde composite result is for all northwest Pacific tropical cyclones of typhoon intensity ($\geq$ 65 knots) or greater. These were of considerably stronger intensity than the average of our seven N.I.O. cases.

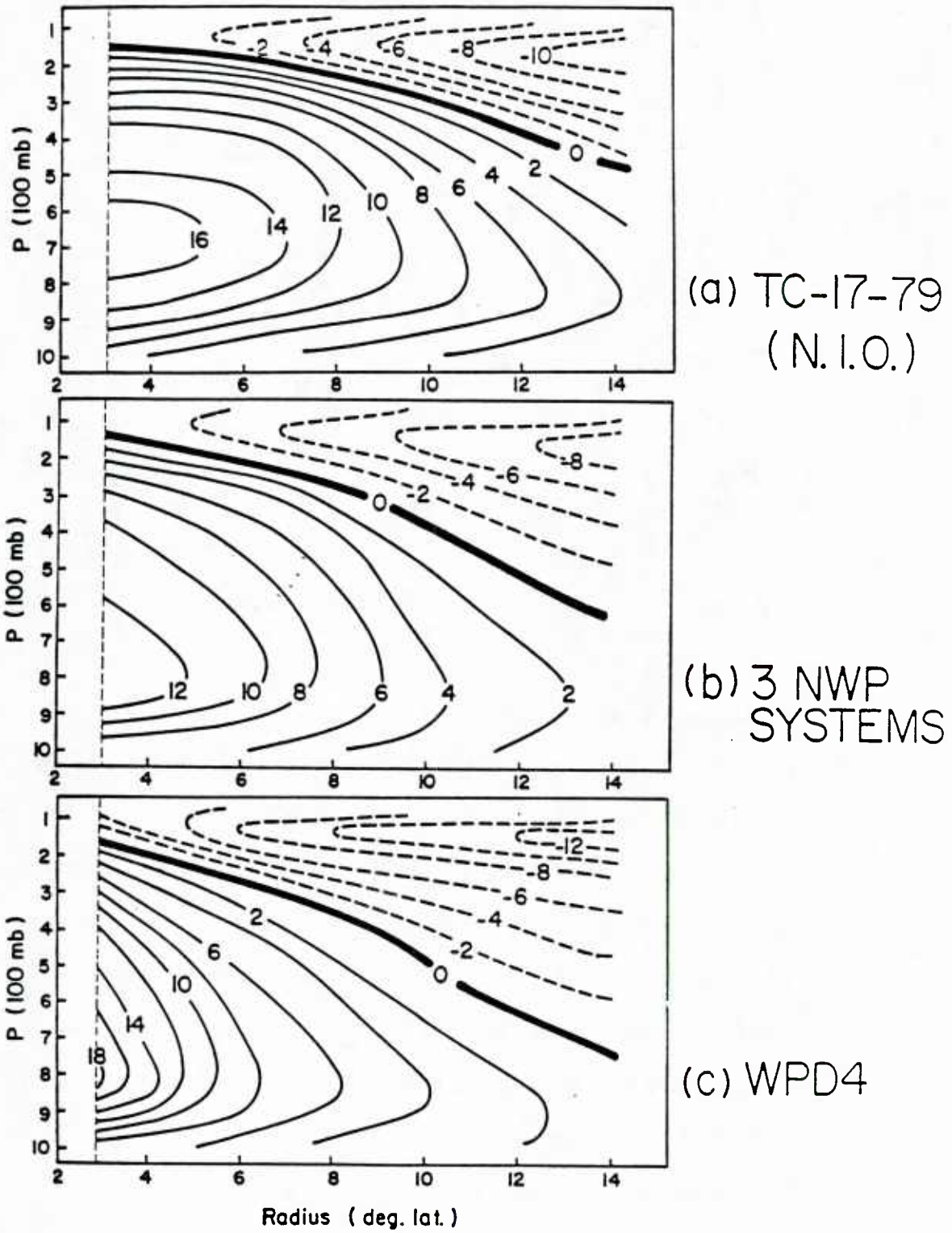

Fig. 56. Diagram a: vertical cross section of tangential wind averaged at three time periods right before the tropical cyclone N.I.O. TC 17-79 attained its maximum intensity. Diagram b: average of three northwest Pacific minimal typhoons during the FGGE year. Diagram c: the 10-year northwest Pacific typhoon rawinsonde composite of Frank (1977).

It is interesting to see that the average results for the three weak typhoon cases and the 10-year typhoon composite closely resemble the three time-period composite of TC 17-79. Although results in all three cases are similar, there are some differences. TC 17-79 appears to have a stronger outer circulation as compared to those of northwest Pacific systems. We believe this to be due to the stronger equatorial monsoon trough that is present in the N.I.O. as compared with the Pacific. We also find that the outer circulation of N.I.O. systems (TC 17-79, TC 18-79, TC 23-79, and TC 25-79) was generally stronger than that of most individual Pacific systems. The outer radius low-level cyclonic circulation also extends over a greater vertical extent for these four N.I.O. systems. Cyclonic winds extend up to 300-400 mb in the N.I.O. systems and even higher on their equatorial sides. It appears that N.I.O. tropical cyclones experience a stronger equatorward monsoonal influence and have a stronger large-scale surrounding low-level cyclonic circulation than similar tropical cyclones of the northwestern Pacific and the Atlantic. N.I.O. systems that do experience a more poleward than equatorwards cyclonic wind influence (as occurs in the late autumn periods of November and December) generally have a weaker, shallower and less well-defined low-level cyclonic circulation.

Maximum Intensity of N.I.O. Tropical Cyclones. Since the tropical cyclones in the N.I.O. form in relatively small semi-enclosed ocean basins, these systems generally have shorter lifetimes compared to those in the other ocean basins -- especially to the tropical cyclones of the northwest Pacific and north Atlantic ocean basins. There is a much higher probability that N.I.O. cyclones will move inland before

favorable large-scale conditions have sufficient time to initiate a substantial intensification. As discussed by Sadler and Gidley (1973), most N.I.O. systems dissipate due to landfall. Almost none take on extra-tropical characteristics. This is one of the major reasons that less than one-third of N.I.O. tropical cyclones reach typhoon intensity. (In the northwest Pacific and the Atlantic, roughly 60-70 percent of the tropical cyclones that form reach typhoon intensity.) Only a few N.I.O. systems are weakened or die due to being sheared off by strong baroclinic westerly wind patterns as often occurs at more polar latitudes in the other ocean basins.

Another reason for the weaker tropical cyclones in the N.I.O. is the lack of a TUTT (Tropical Upper Tropospheric Trough), which is almost always present in the northwest Pacific during summer and often present in the Atlantic during the summer season. Many researchers (Sadler, 1978; Holliday and Thompson, 1979) have emphasized the importance of the TUTT in initiating both the formation and the intensification of tropical cyclones through the development of favorable upper tropospheric poleward outflow channels. Because the TUTT is a mid-oceanic and primarily a mid-summer phenomenon it is not to be expected that it would be present during the spring and autumn transitional seasons when N.I.O. cyclones occur. The Asian continent to the north is also an inhibiting factor to the development of this oceanic upper trough system..

7.3 Characteristics of Motion of N.I.O. Tropical Cyclones

We have described the tracks of FGGE year N.I.O. cyclones in section 4. FGGE year N.I.O. cyclones mostly moved on a northwesterly track except for TC 18-79 which went straight northward. TC 17-79 had

an erratic and looping track due the passage of an upper-level trough to its north. The average northwestward track for these FGGE year systems is the result of the prevailing easterly steering current. N.I.O. systems typically do not recurve or have much of an easterly track component because they occur at a lower latitude and move over land and die before they have a chance to be caught up in the westerly circulation. The Himalayan Mountain Chain also helps protect the N.I.O. from the influences of strong and deep westerly currents which, if they were to impinge on these storm systems, would recurve them to the east.

The average speed of motion of these FGGE-year cyclones was about 8-10 kts. This speed is comparable to those of northwest Pacific tropical cyclones before they recurve but slower than Atlantic cyclones moving in the trade winds. Sadler and Gidley (1973) state that North Indian tropical cyclones move slower compared to the cyclones of the western Pacific. But Sadler and Gidley do not distinguish between the motion of northwest Pacific storms before and after they recurve. It is also to be noted that the variations of speed among different N.I.O. cyclones is much less than those of northwestern Pacific or western Atlantic systems. N.I.O. tropical cyclones occur over a smaller areal domain than do Pacific and Atlantic cyclones. They encounter fewer changes in their steering flow components. By contrast, tropical cyclones in the northwest Pacific occur over a very wide areal domain and throughout most of the year. Pacific systems thus encounter a greater variety of large-scale general circulation patterns. Consequently, the track and speed variability of Pacific cyclones is also greater.

Matsumoto (1984) has recently developed a new 1-3 day TC

statistical track prediction scheme for the Atlantic, northwest Pacific and N.I.O. This scheme has shown itself, in early testing, to be very skillful. This is the only statistical scheme that has been developed in the N.I.O. which combines synoptic, persistence, and steering flow parameters. Matsumoto found that his prediction errors in the N.I.O. are 10-20% smaller than in the northwest Pacific and Atlantic. This is attributed to the generally slower motion of N.I.O. cyclones. Matsumoto also found that persistence is a better predictor in the N.I.O. and steering and synoptic data less skillful predictors in comparison with the northwest Pacific and the Atlantic. It is planned that the new statistical scheme undergoes good testing to determine its feasibility as an operational forecast aid.

8. ACKNOWLEDGEMENTS

This research has been supported by the Naval Environmental Prediction Research Facility (NEPRF) under the encouragement of Samson Brand (Grant No. N00228-83-3122). We have utilized the computing facilities of the National Center for Atmospheric Research (NCAR) for ECMWF data analysis from the NSF Grant No. ATM-82-14041. NCAR is supported by the National Science Foundation.

We would like to thank Captain Roger Edson for a critical review of this manuscript and to Cindy Schrandt, Patti Nimmo and Barbara Brumit for very competent support in manuscript preparation.

9. REFERENCES

Arnold, C. P., 1977: Tropical cyclone cloud and intensity relationships. Dept. of Atmos. Sci. Paper No. 277, Colo. State Univ., Ft. Collins, CO, 154 pp.

Askue, C., 1984: Varying structure and intensity change characteristics of four western north Pacific tropical cyclones. Dept. of Atmos. Sci., M.S. Thesis, Colo. State Univ., Ft. Collins, CO, 97 pp.

Askue, C. and C. S. Lee, 1984: A study of the genesis and intensification of two 1979 northwest Pacific supertyphoons. Paper presented at the 15th Technical Conference on Hurricanes and Tropical Meteorology, January 9-13, Miami, Florida, 243-248.

Bansal, R. K. and R. K. Datta, 1972: Certain aspects for intensification of tropical storms over Indian Ocean area. Indian J. Meteo. Geophys., 23, 4, 503-506.

Chen, L. and W. M. Gray, 1984: Global view of the upper level outflow patterns associated with tropical cyclone intensity changes during FGGE. Paper presented at the 15th Technical Conference on Hurricanes and Tropical Meteorology, January 9-13, Miami, Florida, 224-231.

DeAngelis, D., 1979: Hurricane alley. Mariners Weather Log, 23, 322-325.

DeAngelis, D., 1980a: Hurricane alley. Mariners Weather Log, 24, 24-28.

DeAngelis, D., 1980b: Hurricane alley. Mariners Weather Log, 24, 107-110.

DeAngelis, D., 1980c: Hurricane alley. Mariners Weather Log, 24, 424-429.

Dvorak, V. F., 1975: Tropical cyclone intensity analysis and forecasting from satellite imagery. Mon. Wea. Rev., 103, 420-430.

Frank, W. M., 1977: The structure and energetics of the tropical cyclone, I: Storm structure. Mon. Wea. Rev. 105, 1119-1135.

Gray, W. M., 1968: Global view of the origin of tropical disturbances and storms. Mon. Wea. Rev., 96, 669-700.

Gray, W. M., 1975: Tropical cyclone genesis. Dept. of Atmos. Sci. Paper No. 234, Colo. State Univ., Ft. Collins, CO, 121 pp.

Gray, W. M., 1979: Hurricanes: their formation, structure and likely role in the tropical circulation. Supplement to Meteorology Over the Tropical Oceans. Published by RMS, James Glaisher House, Grenville Place, Bracknell, Berkshire, RG 12 1BX, D. B. Shaw, ed., 155-218.

Holland, G. J., 1984: On the climatology and structure of tropical cyclones in the Australian/southwest Pacific region, I: Data and tropical storms. Aust. Met. Mag., Vol 32, 1, 1-16.

Holland, G. J., 1984: On the climatology and structure of tropical cyclones in the Australian/southwest Pacific region, II: Hurricanes. Aust. Met. Mag., Vol. 32, 1, 17-32.

Holland, G. J., 1984: On the climatology and structure of tropical cyclones in the Australian/southwest Pacific region, III: Major hurricanes. Aust. Met. Mag., Vol 32, 1, 33-46.

Holland, G. J. and R. T. Merrill, 1984: On the dynamics of tropical cyclone structural changes. Quart. J. Roy. Meteor. Soc., 110, 723-745.

Holliday, C. H. and A. H. Thompson, 1979: Climatological characteristics of rapidly intensifying typhoons. Mon. Wea. Rev., 107, 1022-1034.

Joint Typhoon Warning Center, 1979: Annual Typhoon Report. NAVOCEAN-COMCEN/JTWC. Guam, 191 pp.

Keen, R. A., 1982: The role of cross-equatorial tropical cyclone pairs in the southern oscillation. Mon. Wea. Rev., 110, 1405-1416.

Krishnamurti, T. N., P. Greiman, Y. Ramanathan, R. Pasch and P. Ardanuy, 1980: Quick look summer MONEX atlas. Part I: Saudi Arabia Phase. FSU Report No. 80-4, 71 pp.

Krishnamurti, T. N., P. Ardanuy, Y. Ramanathan, and R. Pasch, 1981: On the onset vortex of the summer monsoon. Mon. Wea. Rev., 109, 2, 344-363.

Lee, C. S., 1984: Large-scale influences on individual cases of tropical cyclone genesis during the FGGE year. Paper presented at the 15th Technical Conference on Hurricanes and Tropical Meteorology, January 9-13, Miami, Florida, 281-288.

Love, G., 1982: The role of the general circulation in western Pacific tropical cyclone genesis. Dept. of Atmos. Sci., Paper No. 340, Colo. State Univ., Ft. Collins, CO 80523, 215 pp.

Matsumoto, C., 1984: A statistical method for one- to three-day tropical cyclone track prediction. Dept. of Atmos. Sci. Ph.D. Dissertation, Colo. State Univ., Ft. Collins, CO, 200 pp.

McBride, J. L., 1981: Observational analysis of tropical cyclone formation, Part III. Budget Analysis. J. Atmos. Sci., 38, 1117-1131.

McBride, J. L. and R. Zehr, 1981: Observational analysis of tropical cyclone formation, Part II. Comparison of non-developing versus developing systems. J. Atmos. Sci., 38, 1132-1151.

Mooley, D. A., 1980: Severe cyclonic storms in the Bay of Bengal, 1877-1977. Mon. Wea. Rev., 108, 1647-1655.

Sadler, J. C., 1978: Mid-season typhoon development and intensity changes and the tropical upper tropospheric trough. Mon. Wea. Rev., 106, 1137-1152.

Sadler, J. C. and R. E. Gidley, 1973: Tropical cyclones of the North Indian Ocean. ENVPREDRSCHFAC Tech. Paper No. 2-73, Naval Postgraduate School, Monterey, CA, 58 pp.

Saha, K., F. Sanders, and J. Shukla, 1981: Westward propagating predecessors of monsoon depressions. Mon. Wea. Rev., 109, 2, 330-343.

Weatherford, C. and W. M. Gray, 1984: Relating typhoon intensity to outer 1-3° radius circulation as measured by reconnaissance aircraft. Paper presented at the 15th Technical Conference on Hurricanes and Tropical Meteorology, January 9-13, Miami, Florida, 238-242.

Xu, J. and W. M. Gray, 1982: Environmental circulations associated with tropical cyclones experiencing fast, slow and looping motion. Dept. of Atmos. Sci. Paper No. 346, Colo. State Univ., Ft. Collins, CO 80523, 111 pp.

DISTRIBUTION

COMSEVENTHFLT
ATTN: FLT METEOROLOGIST
FPO SAN FRANCISCO 96601-6003

COMSEVENTHFLT
ATTN: NSAP SCIENCE ADVISOR
BOX 167
FPO SEATTLE 98762

COMSIXTHFLT
ATTN: FLT METEOROLOGIST
FPO NEW YORK 09501-6002

COMMANDER
MIDDLE EAST FORCE
FPO NEW YORK 09501-6008

COMMANDER
AMPHIBIOUS GROUP 1
ATTN: METEOROLOGICAL OFFICER
FPO SAN FRANCISCO 96601

COMMANDING OFFICER
USS CORAL SEA (CV-43)
ATTN: MET. OFFICER, OA DIV.
FPO NEW YORK 09550-2720

COMMANDING OFFICER
USS SARATOGA (CV-60)
ATTN: MET. OFFICER, OA DIV
FPO MIAMI 34078-2740

COMMANDING OFFICER
USS CONSTELLATION (CV-64)
ATTN: MET. OFFICER, OA DIV
FPO SAN FRANCISCO 96635-2780

COMMANDING OFFICER
USS ENTERPRISE (CVN-65)
ATTN: MET. OFFICER, OA DIV.
FPO SAN FRANCISCO 96636-2810

COMMANDING OFFICER
USS KITTY HAWK (CV-63)
ATTN: MET. OFFICER, OA DIV.
FPO SAN FRANCISCO 96634-2770

COMMANDING OFFICER
USS MIDWAY (CV-41)
ATTN: MET. OFFICER, OA DIV.
FPO SAN FRANCISCO 96631-2710

COMMANDING OFFICER
USS RANGER (CV-61)
ATTN: MET. OFFICER, OA DIV.
FPO SAN FRANCISCO 96633-2750

COMMANDING OFFICER
USS CARL VINSON (CVN-70)
ATTN: MET. OFFICER, OA DIV.
FPO SAN FRANCISCO 96629-2840

COMMANDING OFFICER
USS NEW JERSEY (BB-62)
ATTN: MET. OFFICER, OA DIV.
FPO SAN FRANCISCO 96688-1110

COMMANDING OFFICER
USS BELLEAU WOOD (LHA-3)
ATTN: METEOROLOGICAL OFFICER
FPO SAN FRANCISCO 96623-1610

COMMANDING OFFICER
USS NEW ORLEANS (LPH-11)
ATTN: MET. OFFICER
FPO SAN FRANCISCO 96627-1650

COMMANDING OFFICER
USS OKINAWA (LPH-3)
ATTN: MET. OFFICER
FPO SAN FRANCISCO 96625-1630

COMMANDING OFFICER
USS PELELIU (LHA-5)
ATTN: MET. OFFICER
FPO SAN FRANCISCO 96624-1620

COMMANDING OFFICER
USS TARAWA (LHA-1)
ATTN: MET. OFFICER
FPO SAN FRANCISCO 96622-1600

COMMANDING OFFICER
USS TRIPOLI (LPH-10)
ATTN: METEOROLOGICAL OFFICER
FPO SAN FRANCISCO 96626-1645

OFFICER IN CHARGE
U.S. NAVOCEANCOMDET
FPO SAN FRANCISCO 96685-2905

COMMANDING OFFICER
NAVAL RESEARCH LAB
ATTN: LIBRARY, CODE 2620
WASHINGTON, DC 20390

COMMANDING OFFICER
NAVWESTOCEANCEN
BOX 113
PEARL HARBOR, HI 96860

COMMANDING OFFICER
U.S. NAVOCEANCOMCEN
BOX 12, COMNAVMARIANAS
FPO SAN FRANCISCO 96630-2926

DIRECTOR OF RESEARCH (2)
U.S. NAVAL ACADEMY
ANNAPOLIS, MD 21402

NAVAL POSTGRADUATE SCHOOL
METEOROLOGY DEPT.
MONTEREY, CA 93943

LIBRARY
NAVAL POSTGRADUATE SCHOOL
MONTEREY, CA 93943-5100

COMMANDER (2)
NAVAIRSYSCOM
ATTN: LIBRARY (AIR-723D)
WASHINGTON, DC 20361-0001

COMMANDER
NAVAIRSYSCOM (AIR-330)
WASHINGTON, DC 20361-0001

USAFETAC/TS
SCOTT AFB, IL 62225

AFGWC/DAPL
OFFUTT AFB, NE 68113

DIRECTOR (12)
DEFENSE TECH. INFORMATION
CENTER, CAMERON STATION
ALEXANDRIA, VA 22314

ACQUISITIONS SECT. IRDB-D823
LIBRARY & INFO. SERV., NOAA
6009 EXECUTIVE BLVD.
ROCKVILLE, MD 20852

DIRECTOR
NATIONAL HURRICANE CENTER
NOAA, GABLES ONE TOWER
1320 S. DIXIE HWY
CORAL GABLES, FL 33146

DIRECTOR
FEDERAL EMERGENCY MANAGEMENT
AGENCY (FEMA)
WASHINGTON, DC 20472

COLORADO STATE UNIV. (6)
ATMOSPHERIC SCIENCES DEPT.
ATTN: DR. WILLIAM GRAY
FORT COLLINS, CO 80523

UNIVERSITY OF HAWAII
METEOROLOGY DEPT.
2525 CORREA ROAD
HONOLULU, HI 96822

INSTITUTE FOR STORM RESEARCH
UNIVERSITY OF ST. THOMAS
3600 MT. VERNON
HOUSTON, TX 77006

SCIENCE APPLICATIONS
INTERNATIONAL CORP. (SAIC)
205 MONTECITO AVE.
MONTEREY, CA 93940

DIRECTOR, JTWC
BOX 17
FPO SAN FRANCISCO 96630

BUREAU OF METEOROLOGY
BOX 1289K, GPO
MELBOURNE, VIC, 3001
AUSTRALIA

DIRECTOR, INDIAN INST. OF
TROPICAL METEOROLOGY
RAMDURG HOUSE
PUNE 411-005, INDIA